5-2015

Assessing Mesoscale-Equivalent Temperature in Kentucky

Keri Younger
Western Kentucky University, keri.younger710@topper.wku.edu

ASSESSING MESOSCALE-EQUIVALENT TEMPERATURE IN KENTUCKY

A Thesis
Presented to
The Faculty of the Department of Geography and Geology
Western Kentucky University
Bowling Green, Kentucky

In Partial Fulfillment
of the Requirements for the Degree
Master of Science

By
Keri Younger

May 2015

ASSESSING MESO-SCALE EQUIVALENT
TEMPERATURE IN KENTUCKY

Date Recommended 03/24/15

Rezaul Mahmood, Director of Thesis

Gregory Goodrich

Xingang Fan

Joshua Durkee

Dean, Graduate Studies and Research 4-20-15 Date

Acknowledgements

This work has been supported by the Department of Geography and Geology, as well as the Graduate School at Western Kentucky University, in the form of the Graduate Student Research Fellowship. I greatly appreciate the opportunity to pursue my Master's degree at WKU.

I would like to recognize and thank the members of my thesis committee, and especially my advisor, Dr. Rezaul Mahmood, for their continued advice and guidance throughout this research process.

I would also like to acknowledge my family and many friends who have offered much love, support, and encouragement during my pursuit of higher education, particularly over these past two years so far from home. Finally, very special thanks to my fiancé, Byron Lowry, without whom this would not have been possible.

TABLE OF CONTENTS

CHAPTER 1: Introduction..... 1

CHAPTER 2: Background..... 3
2.1 Global LULCCs and associated climate impact..... 4
2.1.1 Biogeophysical..... 4
2.1.2 Biogeochemical..... 5
2.2 Regional and local LULCCs and associated climate impact..... 6
2.2.1 Near-surface mesoscale environment..... 6
2.3 Temperature as a metric for climate change..... 7
2.4 Problem statement and hypothesis..... 9

CHAPTER 3: Data and Methodology..... 11
3.1 Data..... 11
3.2 Mesonet site selection..... 14
3.3 Methodology..... 16

CHAPTER 4: Results and Discussions..... 19
4.1 Discussion of spring season analysis..... 22
4.2 Discussion of summer season analysis..... 31
4.3 Discussion of fall season analysis..... 39
4.4 Discussion of winter season analysis..... 41
4.5 Synoptic influence on daily heat content..... 43

CHAPTER 5: Conclusions..... 51

References..... 54
Appendix..... 60

LIST OF FIGURES

Figure 3.1.1 Locations of the current Kentucky Mesonet stations, those included in this analysis, and Kentucky ASOS sites..... 12
Figure 3.1.2 Equivalent temperature calculated to account for a pressure bias of -5 hPa to +5 hPa..... 13
Figure 3.2.1 Aerial photograph of the Marshall County mesonet station, clipped at a radius of 1.5 km..... 15
Figure 3.2.2 Locations of the mesonet stations included in this analysis overlain on the land cover/land use of Kentucky, as well as the climate division boundaries..... 16
Figure 4.0.1 Composite 5-year seasonal climatology of temperature (T), equivalent temperature (T_E) and specific humidity (q) for Kentucky from December, 2009, to November, 2014..... 20
Figure 4.0.2 Composite seasonal contribution of temperature and moisture to the magnitude of T_E for all study sites from December, 2009, to November, 2014..... 20
Figure 4.0.3 Composite seasonal climatology of temperature (T), equivalent temperature (T_E) and specific humidity (q) for study sites in the Western Climate Division from December, 2009, to November, 2014..... 21
Figure 4.0.4 Composite seasonal contribution of temperature and moisture to the magnitude of T_E for study sites in the Western climate division from December, 2009, to November, 2014..... 22
Figure 4.1.1 Boxplots showing the distribution of T_E values during spring for each year. This includes all spring data from every study station in the area..... 23
Figure 4.1.2 Histograms (bins = 30) showing the distribution of T_E values during spring for each year. This includes all spring data from every study station in the area..... 24
Figure 4.1.3 Boxplots showing the distribution of T_E values during spring for each climate division. This includes all spring data from every study station in each climate division..... 25
Figure 4.1.4 Daily mean temperature, equivalent temperature (T_E) and total daily precipitation for Warren County, 2014..... 27
Figure 4.1.5 Monthly average difference (T_E-T) for a selection of ten counties for 2010. Monthly PDSI and Z-Index values for long and short term drought in Kentucky also are shown..... 27
Figure 4.1.6 Average temperature differences (T_E-T) for Spring, 2010..... 29
Figure 4.1.7 Average temperature differences (T_E-T) for Spring, 2011..... 29
Figure 4.1.8 Average temperature differences (T_E-T) for Spring, 2012..... 30
Figure 4.1.9 Average temperature differences (T_E-T) for Spring, 2013..... 30
Figure 4.1.10 Average temperature differences (T_E-T) for Spring, 2014..... 31
Figure 4.2.1 Boxplots showing the distribution of T_E values during summer for each year. This includes all summer data from every study station in the area..... 32

Figure 4.2.2 Histograms (bins = 30) showing the distribution of T_E values during summer for each year. This includes all summer data from every study station in the area..... 33
Figure 4.2.3 Boxplots showing the distribution of T_E values during summer for each climate division. This includes all summer data from every study station in each climate division..... 34
Figure 4.2.4 Average temperature differences (T_E-T) for Summer, 2010..... 36
Figure 4.2.5 Average temperature differences (T_E-T) for Summer, 2011..... 37
Figure 4.2.6 Average temperature differences (T_E-T) for Summer, 2012..... 37
Figure 4.2.7 Average temperature differences (T_E-T) for Summer, 2013..... 38
Figure 4.2.8 Average temperature differences (T_E-T) for Summer, 2014..... 38
Figure 4.5.1 Daily mean temperature, equivalent temperature (T_E), and total precipitation for Fulton, Hardin, Fayette, and Campbell counties, 2010. Highlighted areas indicate simultaneous peaks and drops in T_E for each site..... 44
Figure 4.5.2 Daily mean equivalent temperature, total precipitation, and daily pressure deviation from seasonal normal for Fulton, Hardin, Fayette, and Campbell counties, 2011. Negative sigma values indicate anomalous low pressure; positive sigma values indicate anomalous high pressure..... 45
Figure 4.5.3 Daily mean equivalent temperature, total daily precipitation, and daily pressure deviation from seasonal normal for Fulton, Hardin, Fayette, and Campbell counties, 2014. Highlighted areas indicate example of inversely proportional values described in text..... 46
Figure 4.5.4 Archived surface analysis chart at 18z for two coupled days, January 30, 2013 (A), and February 1, 2013 (B). Part A depicts a day with a peak in T_E with anomalous low pressure. Part B depicts a day with a drop in T_E with anomalous high pressure..... 47
Figure 4.5.5 Composite graphics compiled with IDV, utilizing data from the NARR model. Black lines: 250mb winds; Red lines: Mean sea level pressure; Gray lines: Surface streamlines; Green lines: Precipitable water content for entire atmosphere. Part A depicts the average synoptic pattern on days with 'cool' T_E and anomalous high pressure. Part B depicts the average synoptic pattern on days with 'warm' T_E and anomalous low pressure..... 49
Figure A-1 Composite seasonal climatology of temperature (T), equivalent temperature (T_E) and specific humidity (q) for study sites in the Central Climate Division from December, 2009, to November, 2014..... 60
Figure A-2 Composite seasonal contribution of temperature and moisture to the magnitude of T_E for study sites in the Central Climate Division from December, 2009, to November, 2014..... 61
Figure A-3 Composite seasonal climatology of temperature (T), equivalent temperature (T_E) and specific humidity (q) for study sites in the Bluegrass Climate Division from December, 2009, to November, 2014... 61
Figure A-4 Composite seasonal contribution of temperature and moisture to the magnitude of T_E for study sites in the Bluegrass Climate Division from December, 2009, to November, 2014..... 62

Figure A-5 Composite seasonal climatology of temperature (T), equivalent temperature (T_E) and specific humidity (q) for study sites in the Eastern Climate Division from December, 2009, to November, 2014..... 62
Figure A-6 Composite seasonal contribution of temperature and moisture to the magnitude of T_E for study sites in the Eastern Climate Division from December, 2009, to November, 2014..... 63
Figure A-7 Monthly average difference (T_E-T) for a selection of ten counties for 2011. Monthly PDSI and Z-Index values for long and short term drought in Kentucky also are shown..... 64
Figure A-8 Monthly average difference (T_E-T) for a selection of ten counties for 2012. Monthly PDSI and Z-Index values for long and short term drought in Kentucky also are shown..... 65
Figure A-9 Monthly average difference (T_E-T) for a selection of ten counties for 2013. Monthly PDSI and Z-Index values for long and short term drought in Kentucky also are shown..... 66
Figure A-10 Monthly average difference (T_E-T) for a selection of ten counties for 2014. Monthly PDSI and Z-Index values for long and short term drought in Kentucky also are shown..... 67
Figure A-11 Boxplots showing the distribution of T_E values during fall for each year. This includes all fall data from every study station in the area..... 68
Figure A-12 Histograms (bins = 30) showing the distribution of T_E values during fall for each year. This includes all fall data from every study station in the area..... 69
Figure A-13 Boxplots showing the distribution of T_E values during fall for each climate division. This includes all fall data from every study station in each climate division..... 70
Figure A-14 Average temperature differences (T_E -T) for Fall, 2010..... 70
Figure A-15 Average temperature differences (T_E -T) for Fall, 2011..... 71
Figure A-16 Average temperature differences (T_E -T) for Fall, 2012..... 71
Figure A-17 Average temperature differences (T_E -T) for Fall, 2013..... 72
Figure A-18 Average temperature differences (T_E -T) for Fall, 2014..... 72
Figure A-19 Boxplots showing the distribution of T_E values during winter for each year. This includes all winter data from every study station in the area..... 73
Figure A-20 Histograms (bins = 30) showing the distribution of T_E values during winter for each year. This includes all winter data from every study station in the area..... 74
Figure A-21 Boxplots showing the distribution of T_E values during winter for each climate division. This includes all winter data from every study station in each climate division..... 75
Figure A-22 Average temperature differences (T_E -T) for Winter, 2010..... 75
Figure A-23 Average temperature differences (T_E -T) for Winter, 2011..... 76
Figure A-24 Average temperature differences (T_E -T) for Winter, 2012..... 76
Figure A-25 Average temperature differences (T_E -T) for Winter, 2013..... 77
Figure A-26 Average temperature differences (T_E -T) for Winter, 2014..... 77

LIST OF TABLES

Table 4.5.1 Ten days chosen for each case for inclusion in the composite graphics. Daily T_E and pressure standard deviations from seasonal normal and precipitation totals are shown for Hardin County (Central climate division)..... 50

ASSESSING MESOSCALE-EQUIVALENT TEMPERATURE IN KENTUCKY

Keri Younger May 2014 77 Pages

Directed by: Rezaul Mahmood, Gregory Goodrich, Joshua Durkee, and Xingang Fan

Department of Geography and Geology Western Kentucky University

The purpose of this research is to investigate mesoscale-equivalent temperatures (T_E) in Kentucky and potential land cover influences. Kentucky presents a unique opportunity to perform a study of this kind because of the observational infrastructure provided by the Kentucky Mesonet (www.kymesonet.org). This network maintains 65 research-grade, in-situ weather and climate observing stations across the Commonwealth. Equivalent temperatures were calculated utilizing high-quality observations from 33 of these stations. In addition, the Kentucky Mesonet offers higher spatial and temporal resolution than previous research on this topic. As expected, the differences (T_E-T) were greatest in summer (smallest in winter), with an average of 35 ºC (5 ºC). In general, the differences were found to be largest in the western climate division. This is attributed to poorly drained land and the mesonet stations' adjacency to agricultural land. These differences are smaller during periods of drought, signifying less influence of moisture. Additionally, an inverse relationship between T_E and pressure deviation on a daily time-scale was found, suggesting a synoptic influence on near-surface heat content.

CHAPTER 1

INTRODUCTION

Climate change has primarily been assessed using surface air temperature variability and trends. However, air temperature alone is an inadequate metric of the full near-surface heat content, as it does not account for the heat content changes associated with moisture content changes (Pielke et al., 2004). In fact, at the surface, an increase of 1 ºC in the dewpoint temperature produces the same change in heat content as an air temperature increase of 2.5 ºC (Pielke, 2001). This means that even if there is a 1 ºC increase in air temperature, if the dewpoint temperature simultaneously decreases by 1 ºC (typical during boundary layer mixing during diurnal heating), there will actually be a net reduction in the near surface heat content. This relationship between moisture and heat content has the greatest impact in warmer, moist environments, and has the least impact in a cooler, dry atmosphere (Pielke, 2001). The use of a moist enthalpy calculation, herein known as equivalent temperature (T_E), defined as $T_E = \frac{c_p T + L_v q}{c_p}$, allows for a comparison between air temperature and the full heat content of the near surface atmosphere.

In order to explore this relationship between moisture and heat content adequately, knowledge of land-atmosphere interactions is necessary. This diverse topic comprises moisture, heat, and gas exchanges between the land surface and atmosphere. Surface energy and moisture budgets incorporate the net radiative fluxes, including sensible and latent heat partitioning and soil heat flux, precipitation, evaporation and transpiration, runoff, and infiltration. These budgets are fundamentally interconnected,

with changes in any component of one budget affecting change in another.

Any land use/land cover change (LULCC) that considerably alters any of these properties can have a non-trivial impact on the climate system at global, regional, and local scales, which leads to why LULCC research is an important facet of understanding potential climate change (Mahmood et al., 2014). As explained in the following chapter, LULCCs can affect the heat and moisture budgets at the surface quite meaningfully. Since T_E is more sensitive to surface vegetation, via evapotranspiration, than temperature alone, it should represent near-surface atmospheric heat content more accurately.

This thesis evaluates atmospheric heat content using the more complete metric of T_E, as associated with predominant land cover classifications in Kentucky. The thesis hypothesis is that T_E would be higher than air temperature alone throughout the year, that the differences would be greatest during the growing season due to the influence of vegetation, and that the differences would vary based on surrounding land cover types. This was proposed based on the understanding that different land cover would have different magnitudes of impacts on the near-surface heat and moisture budgets. In particular, greater evapotranspiration rates were expected at stations located adjacent to agricultural lands, leading to a larger contribution of moisture to the calculated heat content. An analysis was completed on meso-scale variations of T_E over daily, seasonal, and annual time-scales over the past five years using data from the Kentucky Mesonet (2014).

CHAPTER 2

BACKGROUND

The properties of different surfaces critically influence the transfer processes between the land and atmosphere, thereby affecting the characteristics of the planetary boundary layer and associated meteorological phenomena (Oke, 1987; Nicholson, 1988). To give some credence to the range of these relationships, a few, non-exhaustive, examples could be: over non-vegetative land, the relationship between the surface albedo and the surface layer of soil moisture is negatively proportional (Idso et al., 1975); the geometry of leaves and canopy thickness influences the local fluxes of radiation (Dickinson, 1983); very wet soil and canopy temperatures impact the surface sensible heat flux and associated boundary layer properties (Segal et al., 1989); and stomatal resistance (which differs by species) regulates the exchange of water vapor and CO_2 between the plant and the atmosphere (Oke, 1987; Bloom, 2010). Understanding the significance of land-atmosphere interactions leads to why LULCC research is an important facet of understanding potential climate change. Any LULCC that alters any of the land-atmosphere variables has the potential to affect the climate system directly.

Until recently, atmospheric composition, primarily increasing CO_2, has dominated policy related quantification of human-induced global climate change. Research over the last decade, however, has shown that LULCCs have a significant impact on the climate system and should be considered in any discussion of evaluating climate change or subsequent mitigation strategies (Pielke et al., 2002; Feddema et al., 2005; NRC, 2005; Pielke et al., 2009; Mahmood et al., 2010; Pielke et al., 2011; Mahmood et al., 2014). This literature review discusses research efforts that describe significant LULCCs, their

effect on climate change at both global and regional scales, and temperature as a metric for quantifying these impacts.

2.1. Global LULCCs and associated climate impact

There are two categories typically used to describe LULCCs: biogeophysical mechanisms that alter physical surface properties such as albedo (the proportion of incident radiation reflected by a surface) and roughness, and biogeochemical mechanisms, most notably the influence on the carbon cycle and associated impact on the global concentration of atmospheric CO_2 (Pongratz et al., 2010). At the global scale, both of these mechanisms have been investigated.

2.1.1. Biogeophysical

Over the past three centuries, human activity has transformed the Earth's surface drastically through deforestation and afforestation, desertification, urbanization, and agricultural activities. Ramankutty and Foley (1999) quantified LULCCs related to agriculture by reconstructing historical cropland areas from 1700 to 1992. They estimated that, since 1700 CE, there has been a global net loss of 11.4 million km^2 of forests and woodlands and 6.7 million km^2 of savannas, grasslands, and steppes, of which about 6 million km^2 and 4.7 million km^2, respectively, has been lost since 1850. A more recent study by Ramankutty et al. (2008) estimated that, for the year 2000, the global area of cropland was at 15 million km^2, approximately 12% of the Earth's ice-free land. LULCCs are not limited to agricultural development, and only Antarctica, and parts of Siberia, Canada, the Amazon, and Congo have avoided large-scale modifications (Pielke et al., 2011). Worldwide transformations of land surfaces at this magnitude can alter fundamentally the surface-energy budget by changing the surface albedo. This change in

global radiative forcing may be analogous to that due to human-produced aerosols, certain greenhouse gases, and natural solar variation (Pielke et al., 2002). Modeling studies have shown that the global impact due to biogeophysical change is a net cooling (Claussen et al., 2001; Brovkin et al., 2004; Matthews et al., 2004; Pongratz et al., 2010).

2.1.2. Biogeochemical

The biogeophysical and the biogeochemical budgets are connected. Altering any one of these budgets alters all of them (Mahmood et al., 2014). The carbon budget accounts for all processes that act as sources or sinks for carbon to and from the atmosphere. Vegetation plays a key role in this budget through the assimilation of CO_2 into carbohydrates, the respiration of CO_2, and the release of CO_2 due to plant decay (Bloom, 2010; Mahmood et al., 2014). Therefore, a change in the amount, type, and location of actively growing plant biomass affects the amount of carbon in the atmosphere. The net flux of carbon from LULCCs from 1990 to 2010 accounted for 12.5% of global anthropogenic carbon emissions (Houghton et al., 2012). Modeling studies have shown that the global impact due to biogeochemical change is a net warming (Claussen et al., 2001; Brovkin et al., 2004; Matthews et al., 2004; Pongratz et al., 2010).

While it is generally accepted that there should be a global climate impact due to LULCC, determining exact effects is more challenging. There are a few substantial reasons for this. First, regional positive radiative forcing (warming effects) due to a decrease in albedo can be canceled by regional negative radiative forcing (cooling effects) due to an increase in albedo. Averaging these impacts in a global climate model make it difficult to detect a global signal (Feddema et al., 2005; Pielke et al., 2011; Mahmood et al., 2014). Furthermore, the impacts of LULCCs become relatively static

and behave more like trends over time once the change is complete, compared to other dynamic, cyclical global climate oscillations, making them challenging to quantify and predict (Pielke et al., 2011; Mahmood et al., 2014).

2.2. Regional and local LULCCs and associated climate impacts

On local and regional scales, the impacts of LULCCs are significant, apparent, and undeniable (Mahmood et al., 2014). These atmospheric feedbacks are widely variable and depend on geographic location as well as the pre-existing land use (Pielke et al. 2002) and they can manifest through temperature, moisture and wind speed (Mahmood et al., 2014). Temperature changes associated with local and regional LULCCs vary. Urbanization can cause varying degrees of net warming due to increased energy partitioning into sensible heat, known as the urban heat island effect (Oke, 1987), rainfed and irrigated agriculture has a substantial cooling effect on near-surface temperatures due to more energy partitioning into latent heat and increased evaporative cooling (Mahmood et al., 2006; Roy et al., 2007), and tropical deforestation causes a decrease in surface evapotranspiration and resultant increase in near-surface temperatures (Sampaio et al., 2007). Atmospheric moisture depends similarly on the type of land cover change and, in the case of some agricultural areas, there is tendency for an increase in convective cloud and precipitation development (Mahmood et al., 2014). The urban heat island effect also leads to an increase in rainfall, and the effects are likely located downwind of, as opposed to within, the city itself (Oke, 1987; Mahmood et al., 2014).

2.2.1. Near-surface mesoscale environment

Land cover attributes themselves can have a dramatic impact on the near-surface mesoscale environment. Enhanced vertical circulations have been observed along and

near the boundaries of heterogeneous vegetation cover (Weaver and Avissar, 2001; Ray et al., 2002; Carleton et al., 2008; Mahmood et al., 2014). McPherson et al. (2004) found that, along the winter wheat belt in Oklahoma, well-defined cooling and warming anomalies occurred during plant growth and after harvest, respectively. The diurnal cycle of dewpoint temperatures across the winter wheat belt was also studied and showed that the wheat fields created a moist anomaly during the growing season and a reverse effect following the harvest (Haugland and Crawford, 2005). Additionally, it was found that the average diurnal temperature and pressure differences across the wheat belt are consistent with an inland "sea breeze" circulation (Haugland and Crawford, 2005).

2.3. Temperature as a metric for climate change

Air temperature variability and trends have been one of the main approaches of quantifying climate change. While the above findings clearly specify direct correlations between LULCCs and changes in air temperature, air temperature alone may not be the best metric for measuring these changes. The results of numerous studies show that there has been substantial global warming over the past century (Jones et al., 1986; IPCC, 2001; 2007; 2013). As the atmosphere warms, water vapor capacity increases, as governed by the clausius-clapeyron relationship and physically observed in multiple studies (Santer et al., 2007; Wentz et al., 2007). Although an increase in atmospheric moisture is exponentially proportional to an increase in temperature, relatively few observational studies have analyzed the two variables simultaneously (Fall et al., 2010). There are a handful of recent studies that focus on moist enthalpy, or equivalent temperature (T_E), taking into account both the surface air temperature and specific humidity. This includes a global-scale study by Ribera et al. (2004) and

local/regional/continental-scale research by Pielke et al. (2004), Davey et al. (2006), Rogers et al. (2007), and Fall et al. (2010). T_E differs from other moisture parameters, such as virtual temperature, in that it uses specific heat to calculate the full heat content.

By itself, temperature is an inadequate measure of warming or cooling, and T_E offers the ability to account for the heat content changes associated with moisture content changes (Pielke et al., 2004). These studies found that, in general, overall patterns of T_E followed those of air temperature, but with higher values than air temperature itself, at the surface level. As discussed previously, land use and land cover can affect the heat and moisture budgets at the surface significantly. Since T_E is more sensitive to vegetation properties than air temperature alone, it should represent surface heat content more accurately. Therefore, it is useful not only to compare air temperature and T_E values, but also relate them to vegetation characteristics and land use/land cover. Of the papers discussed above, three examined the relationship between temperature and land cover. The differences between T and T_E were found to be more significant during the growing season, as well as in areas with higher surface evaporation and transpiration rates. These results indicated that T_E is a more appropriate metric for identifying regional heat content characteristics, especially in the context of land use and land cover.

Through this review, it is clear that LULCCs have a non-trivial effect on the climate system at both the global and regional scales. The increase in research performed in this area over the past decade has helped shift perceptions of human-caused climate change to a broader spectrum that includes many forcings, not solely limited to greenhouse gas emissions (NRC, 2005; Mahmood et al., 2010; Pielke et al., 2011; Mahmood et al., 2014). While there has been extensive research and modeling done of

LULCCs, further studies can be performed utilizing high-quality, in-situ observation networks to detect impact signals of LCCs more effectively (Mahmood et al., 2014). With regards to T_E, data from a high-resolution observation network can be analyzed to improve understanding of meso-climates and possible impacts on local heat content characteristics. Increased knowledge of how LULCCs link to the climate system at all spatial and temporal scales is necessary to model our climate system more accurately and to provide more precise predictions of the future.

2.4. Problem statement and hypothesis

LULCCs can affect significantly the heat and moisture budgets at the surface. Since T_E is more sensitive to surface vegetation properties than temperature alone, it should represent near-surface atmospheric heat content more accurately and, therefore, useful not only for comparing temperature and equivalent temperature, but also relating them to vegetation characteristics. A few studies have examined explicitly the relationships between both temperature and land cover. However, these studies were done at limited spatial and temporal resolutions, as compared to what is possible using data from the Kentucky Mesonet.

The purpose of this research is to provide a meso-scale assessment of T_E at daily, seasonal, and annual time scales over Kentucky. There is a unique opportunity to perform a study of this kind in Kentucky because of the high-quality weather and climate observation infrastructure provided by the Kentucky Mesonet (2014). This network consists of 65 surface stations across the Commonwealth and this research utilizes a subset of data from 33 stations. This offers higher spatial and temporal resolution compared to previous research. Results of this research should improve understanding of

how land use and land cover can affect meso-climates and near-surface heat content. These results could also be beneficial for areas located in a comparable climate division, with similar land-cover attributes that do not have a comprehensive mesonet to conduct research of this kind.

This thesis hypothesizes that the values for T_E will be higher than air temperature alone on warm, wet days, and T_E will be smallest on cool, dry days. Also, it is expected that these differences will be greatest during the growing season and will vary based on the type of vegetation cover at the site. Different land-cover types influence moisture availability through varying moisture storage capability and evapotranspiration rates. Thus, T_E can be used as a supplementary metric for evaluating near-surface heat content with respect to land-cover use (Fall et al., 2010). Additional research questions addressed include how extreme precipitation periods (drought and flooding) impact T_E distributions and how synoptic patterns impact daily fluctuations in heat content.

CHAPTER 3

DATA AND METHODOLOGY

3.1. Data

The Kentucky Mesonet (2014) encompasses 65 automated in-situ surface observation stations across the Commonwealth. All stations directly measure and record five-minute air temperature, relative humidity, precipitation, solar radiation, wind speed, and wind direction, and calculate the dewpoint temperature. For this study, hourly air temperature and dewpoint temperature values are used, and they are arithmetic averages of the reported five-minute data. The hourly pressure data used for this analysis were obtained from the nearest Automated Surface Observation Station (ASOS) archived by the Midwest Regional Climate Center (MRCC, 2014). Figure 3.1.1 shows the locations of all Kentucky Mesonet stations, the sites included in this research, and the ASOSs within Kentucky. ASOS locations in neighboring states were used as the source of pressure data if they were located closest to the chosen mesonet site.

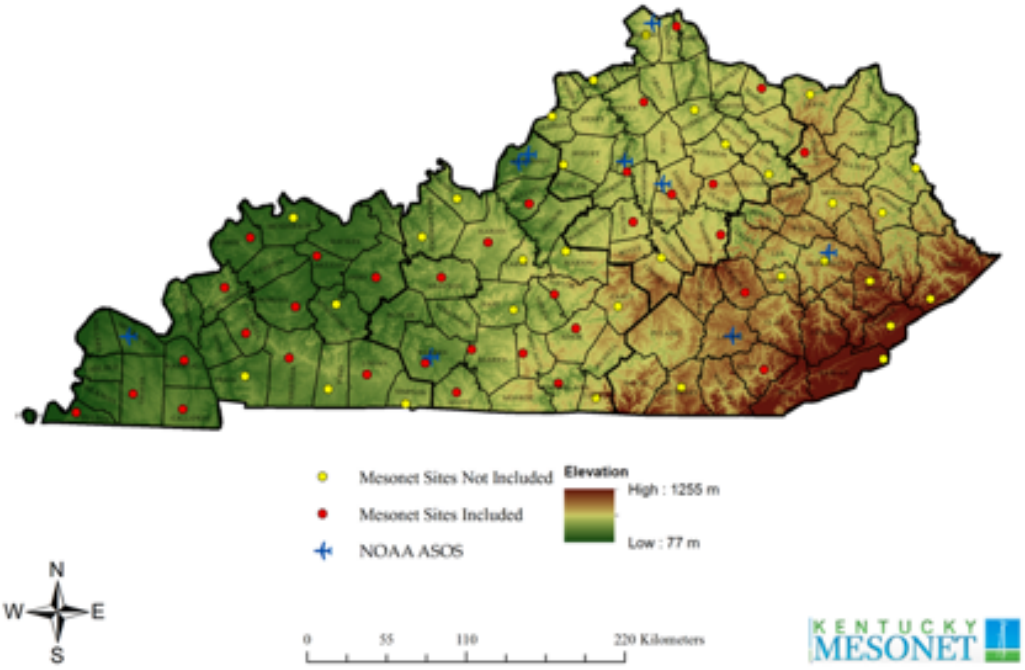

Figure 3.1.1. Locations of the current Kentucky Mesonet stations, those included in this analysis, and Kentucky ASOS sites. Elevation is represented in meters. Source: Kentucky Mesonet (2014).

Since there is not an ASOS site at every mesonet location, pressure was estimated. There were two possible options available to estimate pressure. The first option was to apply a spatial statistical interpolation method (such as kriging) to produce pressure estimates at each grid point in the study area. The second option was to use pressure data from the nearest ASOS. Both methods would introduce small biases. Through observation of three months of data at multiple sites (n = 2,184 hours), it was determined that differences in pressure values across the state are well within a 10 hPa range. To quantify possible errors from using the nearest ASOS for data, a pressure sensitivity test was performed. For one time step at the Warren County mesonet, T_E was recalculated accounting for a 10 hPa pressure bias. With everything else held constant, pressure was changed systematically in 1 hPa increments from 1012.58 hPa to 1022.58

hPa (actual pressure: 1017.58). This resulted in an error range of 0.035ºC in T_E. The results of this approach are shown in Figure 3.1.2. The Warren County mesonet site was chosen for this test because an ASOS is located nearby to validate the estimated error. Since pressure does not vary much at the meso-scale (except under severe weather conditions), it is acceptable to use pressure data from nearby ASOS stations. In addition, this sensitivity analysis shows that even if large errors get introduced due to using pressure from a non-local source, impacts on the T_E calculation would be minimal.

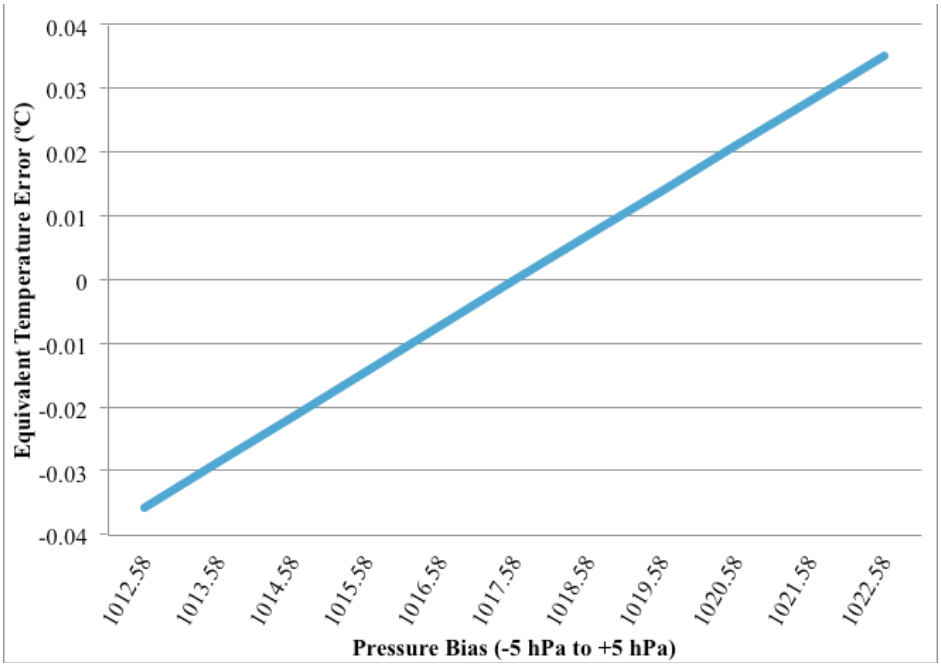

Figure 3.1.2. Equivalent temperature calculated to account for a pressure bias of -5 hPa to +5 hPa. Warren County mesonet 2011-12-01 00:00 CST. Source: Kentucky Mesonet (2014).

To help explain anomalous observations in T_E patterns, two drought indices were considered: Palmer Z-Index and Palmer Drought Severity Index (PDSI). The Z-Index quantifies short-term moisture departure from climatological normals based on monthly conditions with no consideration for previous deficits or surpluses of moisture (NCDC, 2013). This index responds rapidly to current weather conditions, and may reflect short-

term wet periods during extended droughts, and vice versa. The PDSI identifies long-term drought based on dominant, recurring circulation patterns and is calculated using both current and prior monthly weather patterns (NCDC, 2013). Data for both of these indices were accessed from the MRCC (2014) archive for each climate division.

3.2. Mesonet site selection

The site selection was based on three criteria: location, predominant land cover, and the length of time series. Kentucky can be categorized into four distinct climate divisions (western, central, bluegrass, and eastern), as defined by the National Climatic Data Center (NCDC, 2015). The sites were selected to represent the most diverse range of dominant land covers as possible. Aerial photos from 2012 at a 1m resolution were acquired from the National Agriculture Imagery Program (NAIP). These digital images were taken across the continental U.S. during the agricultural growing seasons (Kentucky Statewide, 2012). Aerial photographs for Kentucky are available from the Kentucky Geography Network archive (KGN, 2012). Photographs were then buffered and clipped around each chosen station at a 1.5 km radius to depict the dominant surrounding land cover. An example of one such aerial photo is presented in Figure 3.2.1. Additionally, each station within the study area can be classified based on its land use/land cover. These data were taken from the 2011 National Land Cover Database, a "national land cover product created by the Multi-Resolution Land Characteristics (MRLC) Consortium" (Jin et al., 2013, 160). Figure 3.2.2 shows the locations of each mesonet station chosen for analysis and the underlying land cover. Finally, all sites selected were installed by at least 1 December, 2009, allowing for a five-year data series. While this is relatively a short time series for typical climatic studies, the results of this research

should provide valuable information about heat content variations at the meso-scale and various time-scales, and serve as a basis for continuing research, utilizing Kentucky Mesonet data.

Figure 3.2.1. Aerial photograph of the Marshall County mesonet station, clipped at a radius of 1.5 km. Source: KGN (2012).

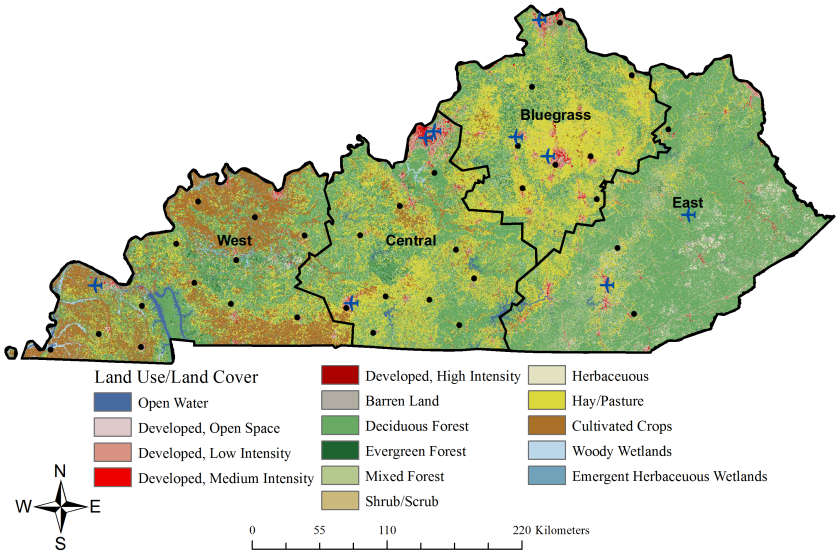

Figure 3.2.2. Locations of the mesonet stations included in this analysis overlain on the land cover/land use of Kentucky, as well as the climate division boundaries. Source: Kentucky Mesonet (2014).

3.3. Methodology

Moist enthalpy, or heat content, is expressed as:

$$H = c_p T + L_v q$$

where c_p is the isobaric specific heat of air (1005 $Jkg^{-1}K^{-1}$), T is the air temperature (K), L_v is the latent heat of vaporization ($2.5x10^6$ Jkg^{-1}), and q is the specific humidity (Pielke et al., 2004). Moist enthalpy has units of Joules per kilogram, so, to enable comparison with air temperature, equivalent temperature in Kelvin is calculated by

$$T_E = \frac{H}{c_p}$$

Since the products available from the mesonet do not include a direct measure for specific humidity (q), it is calculated from the dewpoint temperature (T_d) and the vapor pressure of the air (e), using Bolton's (1980) empirical relationship:

$$e = 6.112\exp\left[\frac{17.67T_d}{T_d + 243.5}\right]$$

From this, q is calculated as

$$q = \frac{0.622e}{P - 0.37e}$$

where P is the station pressure in hPa, obtained from the nearest ASOS (Rogers et al., 2007).

Data for each of the 33 locations were analyzed on hourly, daily, monthly, seasonal, and annual timescales. T_E was calculated at hourly time steps for each station from 1 December, 2009, through 30 November, 2014, and then aggregated to different timescales. Seasons were defined as follows: Winter – December, January, February; Spring – March, April, May; Summer – June, July, August; and Fall – September, October, November. Averaging the hourly values for each day allowed daily comparisons between air temperature and T_E, presented yearly and seasonally for each station. To represent and compare the distribution of T_E values graphically, yearly boxplots, grouped by season, were made for all stations. Additionally, boxplots per climate division were made and grouped seasonally. The format is a standard box and whisker plot, depicting the median, first and third quartiles, and the maximum and minimum values. Values are drawn as outliers if they are larger than $q_3 + w(q_3 - q_1)$ or smaller than $q_1 - w(q_3 - q_1)$, where q_1 and q_3 are the first and third quartiles, and w is the maximum whisker length. The maximum whisker length was set to 1.5, which corresponds to approximately +/-2.7σ for a normally distributed dataset.

Results from this thesis suggest that the influence of varying land covers on the magnitude of T_E are more apparent on monthly and seasonal time scales, while daily

fluctuations of T_E are more closely linked to synoptic forcings. A selection of ten stations, hereafter referred to by the county in which they are located - Calloway (1), Fulton (1), Ohio (1), Bullitt (2), Hardin (2), Warren (2), Campbell (3), Fayette (3), Owen (3), and Knox (4) - were used to identify individual daily cases of large and small temperature differences (T_E-T) to assess synoptic influences on T_E. These stations were chosen to represent geographical diversity of the region, as well as varying land covers. Daily synoptic weather maps were accessed from the National Centers for Environmental Prediction, Weather Prediction Center archive (NCEP, 2014). Daily precipitation totals for each county were accessed from the Kentucky Mesonet (2014) archives. Results of these analyses are discussed in the following chapter.

CHAPTER 4

RESULTS AND DISCUSSIONS

The seasonal climatology of T, T_E, and specific humidity (q) are shown in Figure 4.0.1. As expected, both T and T_E follow similar seasonal patterns, warmer in the summer and cooler in the winter, with T_E values larger than T throughout the year. During winter, when specific humidity was at its lowest, the differences between T_E and T were also the smallest (0.97 ºC on 28 January, 2014). During summer, when humidity was at its highest, differences between T_E and T were also the largest (59.70 ºC on 12 July, 2011). T mostly represented the magnitude of T_E, with moisture contributing a small percentage of heat content (Figure 4.0.2). Summer had the maximum contribution from moisture with 10.53%, and winter had the minimum contribution from moisture with 3.16%. However, it is also evident that even a small contribution from moisture has a great impact on T_E. For example, in the summer a moisture content of 10.53% or 14.14 g kg^{-1} leads to a T_E of 59.33 ºC in comparison to the air temperature of 24.16 ºC.

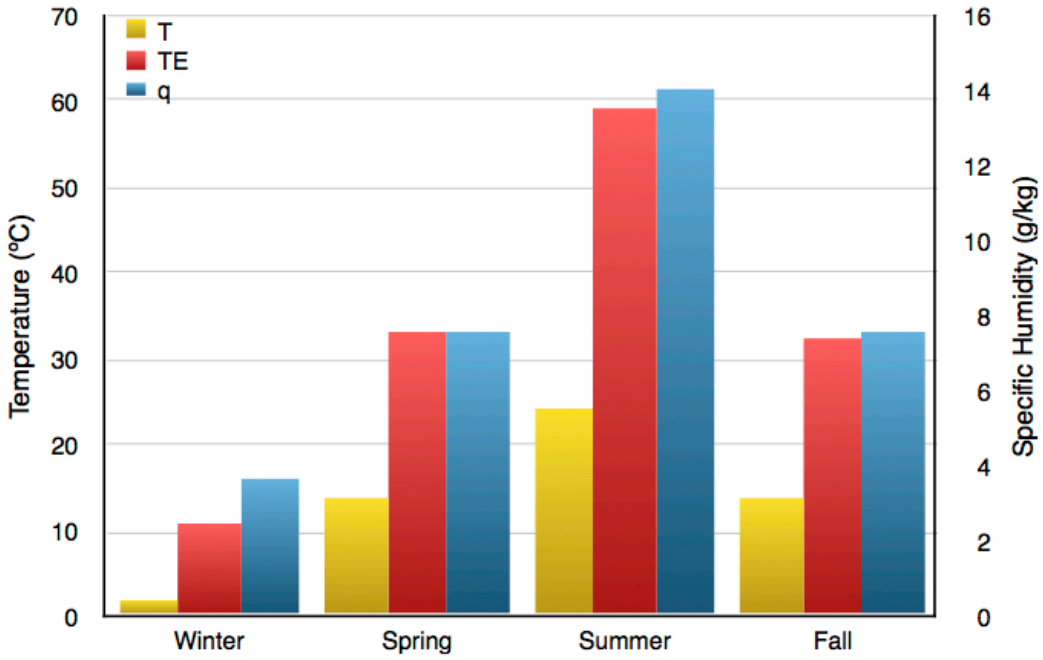

Figure 4.0.1. Composite 5-year seasonal climatology of temperature (T), equivalent temperature (T_E) and specific humidity (q) for Kentucky from December, 2009, to November, 2014.

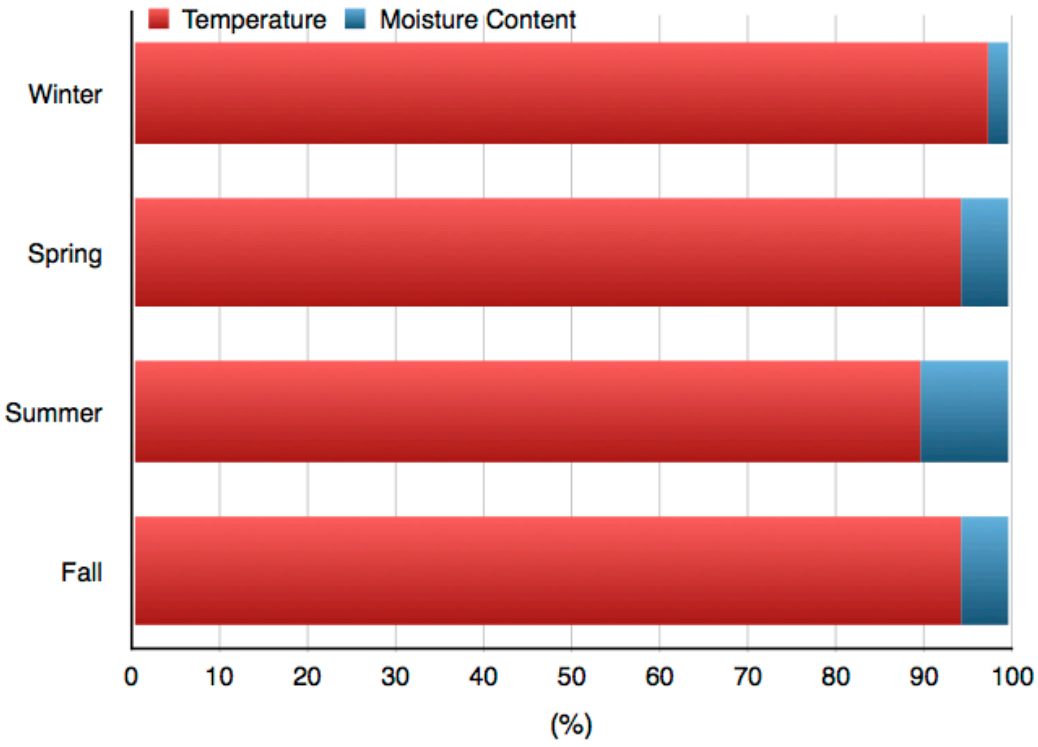

Figure 4.0.2. Composite seasonal contribution of temperature and moisture to the magnitude of T_E for all study sites from December, 2009, to November, 2014.

Seasonal averages were also calculated for each climate division: Western (1), Central (2), Bluegrass (3) and Eastern (4); only the Western division is shown, as results were comparable for each division (Figures 4.0.3 and 4.0.4). Averaging over each climate division produced similar results to the full composite averages over the entire study area. The Western climate division had the highest average specific humidities and the highest moisture contributions to T_E during spring and summer, the Eastern climate division had the highest values for fall, and the Central climate division had the highest values for winter. The Western division is predominantly cultivated crops, and the results suggest that increased evapotranspiration during the growing season influenced the higher values in spring and summer.

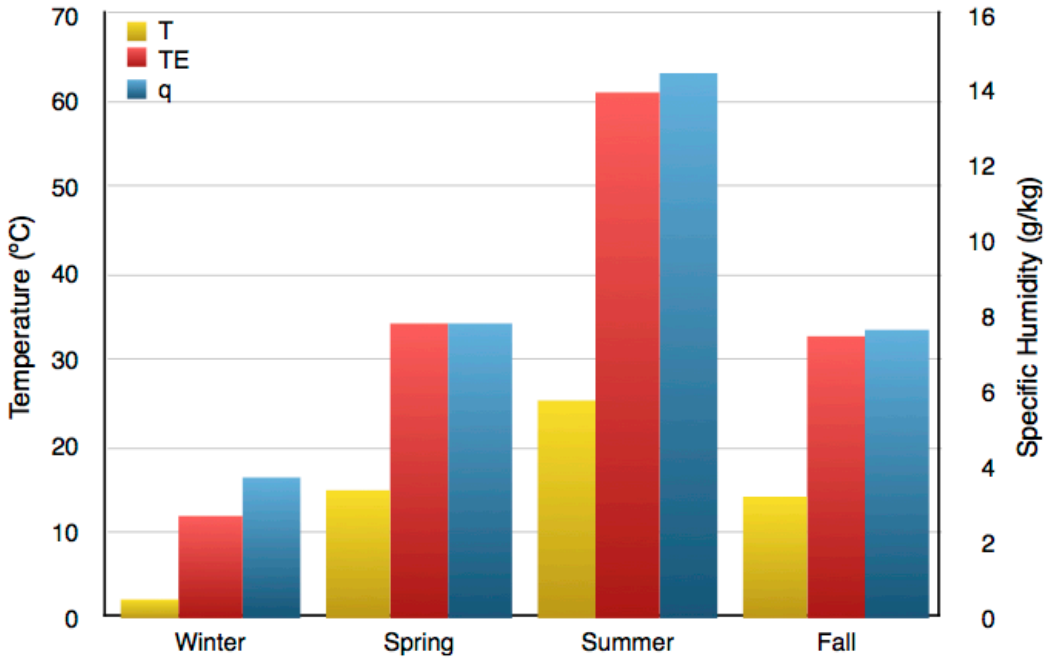

Figure 4.0.3. Composite seasonal climatology of temperature (T), equivalent temperature (T_E) and specific humidity (q) for study sites in the Western Climate Division from December, 2009, to November, 2014.

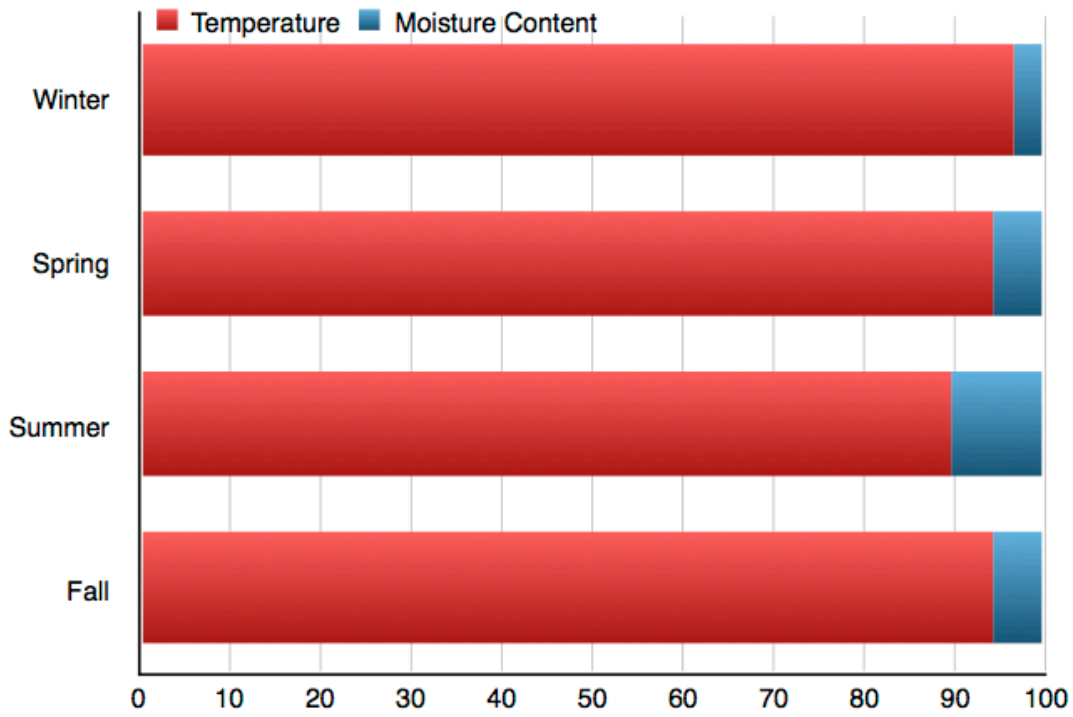

Figure 4.0.4. Composite seasonal contribution of temperature and moisture to the magnitude of T_E for study sites in the Western climate division from December, 2009, to November, 2014.

4.1 Discussion of spring season analysis

The seasonal distribution of T_E values is shown in Figure 4.1.1 for spring of each year for the entire study area. Median values and the distributions about the median were nearly the same for 2010 and 2011. In 2012, the median was highest at 39.68 ºC, compared to 31 ºC for the preceding years and 29 ºC for the following years, and also had the smallest interquartile range. Additionally, Spring 2012 was the only year to have a negatively skewed distribution, as represented by a skewness value of -0.2425. Spring had the most symmetric distributions when compared to the other seasons, with positive skewness values for 2010, 2011, 2013, and 2014 of 0.1409, 0.2602, 0.1978 and 0.1107, respectively. These distribution patterns were also apparent in the spring histograms (Figure 4.1.2). To examine the normalness of the T_E distribution further, a one-sample

Kolmogorov-Smirnov (K-S) test was performed. Although skewness values were small, the spring distributions of T_E were not statistically normal at a 5% significance level. The maximum T_E, 75.73 ºC, occurred on 30 May, 2011, while the minimum T_E, -14.08 ºC, occurred on 04 March, 2014.

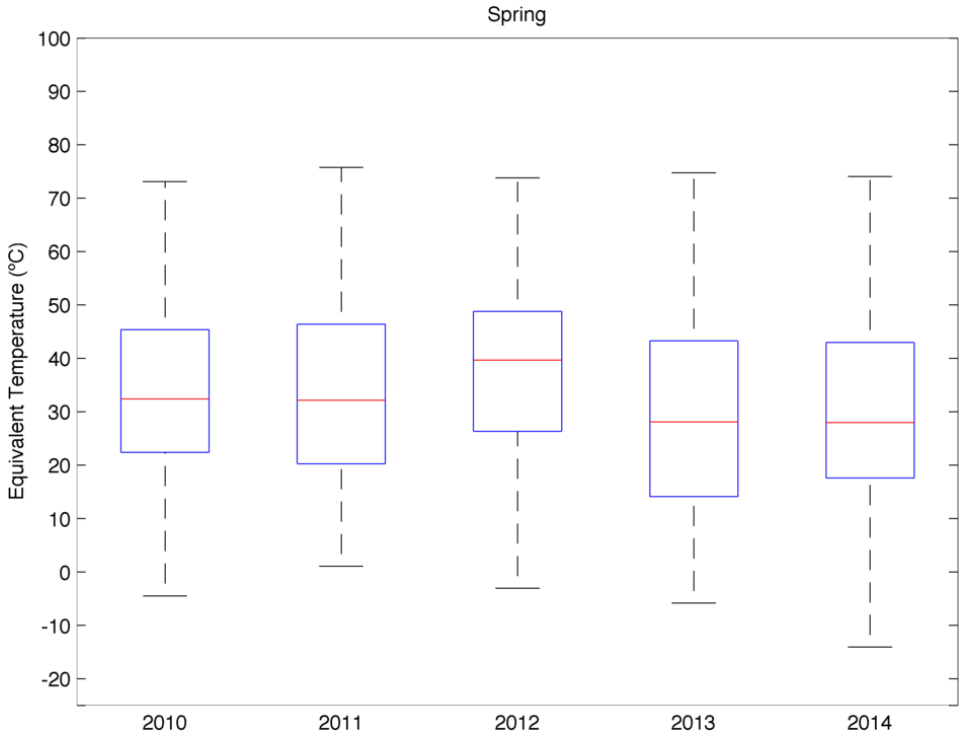

Figure 4.1.1. Boxplots showing the distribution of T_E values during spring for each year. This includes all spring data from every study station in the area.

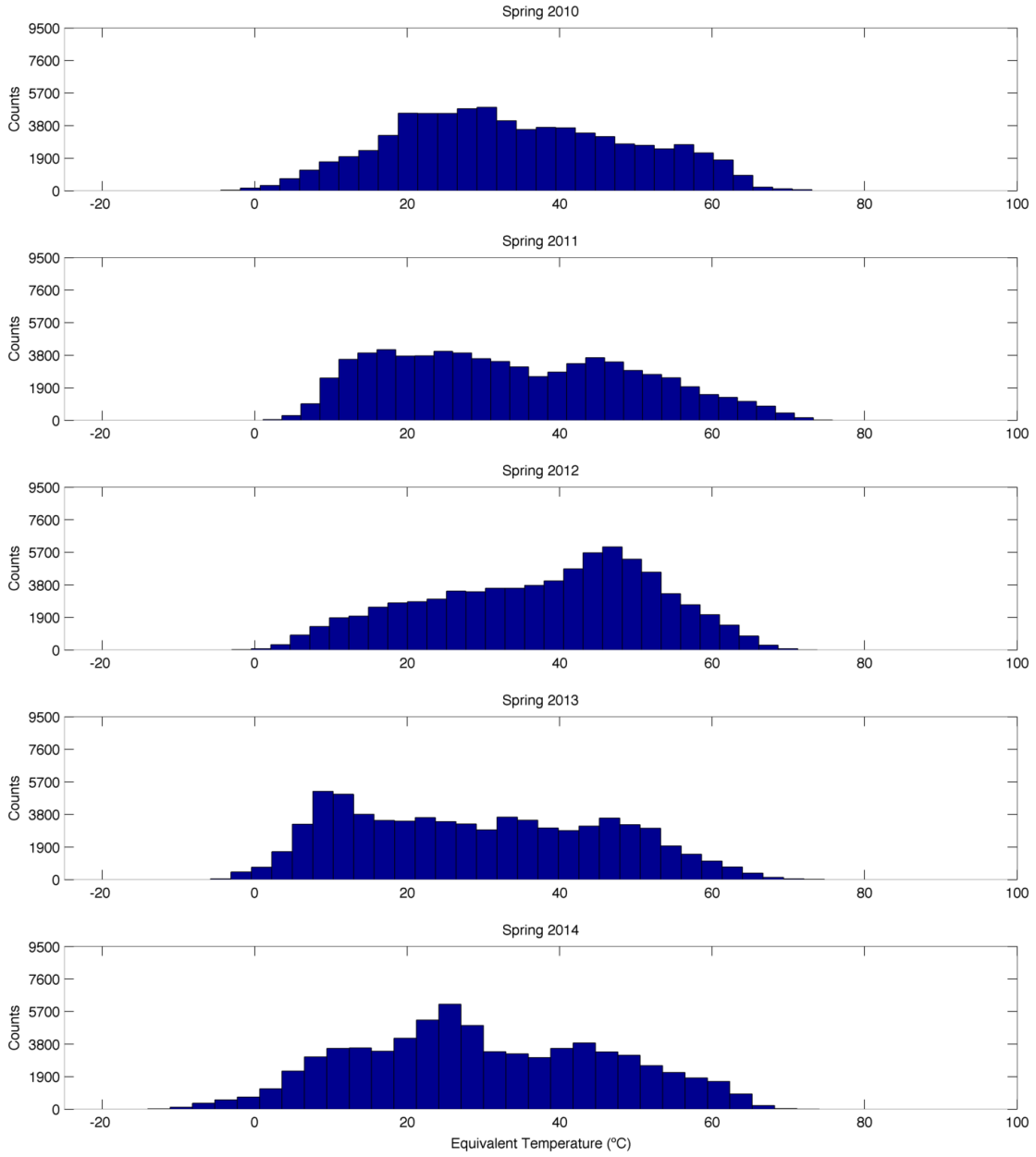

Figure 4.1.2. Histograms (bins = 30) showing the distribution of T_E values during spring for each year. This includes all spring data from every study station in the area.

A similar analysis was completed for the four climate divisions of Kentucky (Figure 4.1.3). All climate divisions exhibited similar T_E distributions. The Western division is broadly characterized by wetlands along the Mississippi and Ohio Rivers, cultivated cropland, forest, coal mines, and oil and gas production. The Central division

represents the most diverse range of land cover and land use, ranging from forest, cultivated cropland, pasture and hay land, and mining activities, to recreation/tourism, military reservations, and numerous urban-suburban areas. This division had the warmest maximum and minimum T_Es. The Bluegrass division is broadly characterized by pasture and hay land, forest and expanding urban and sub-urban development. The Eastern division is characterized by varied forest, pastureland, and extensive logging, coal mines, and oil and gas production. Without the enhanced evapotranspiration from extensive croplands found in the other climate divisions, as well as the higher elevation, a cooler and less varied T_E distribution was expected, but not observed. The Bluegrass division had the coolest maximum and minimum T_Es.

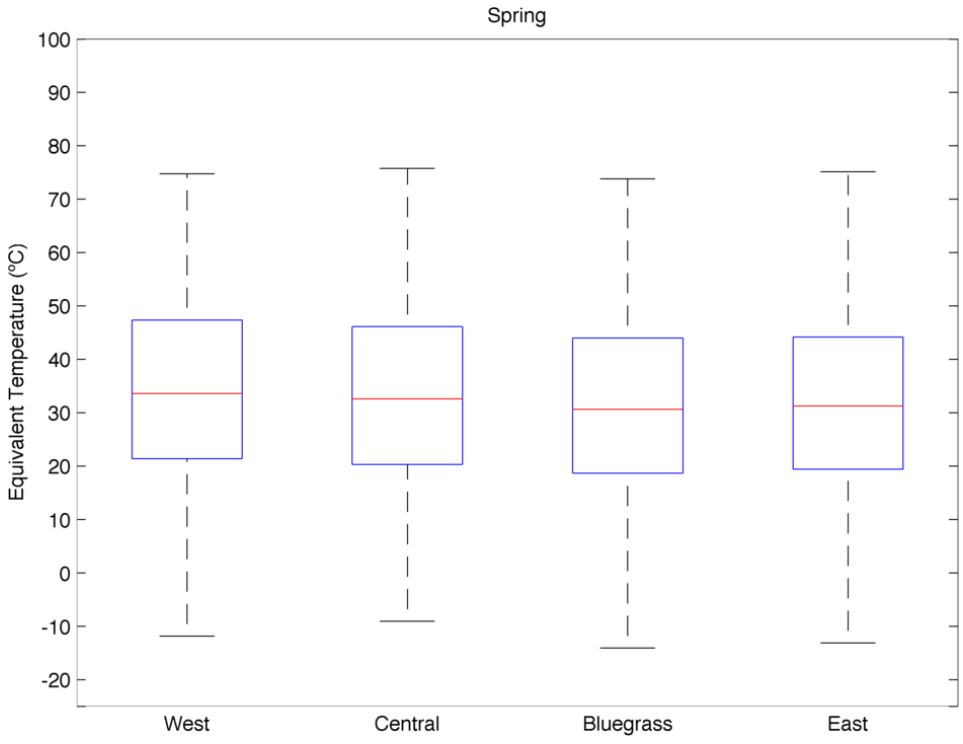

Figure 4.1.3. Boxplots showing the distribution of T_E values during spring for each climate division. This includes all spring data from every study station in each climate division.

Daily averages of T_E and T were calculated for each station; only Warren County 2014 is shown (Figure 4.1.4). During the spring, both T and T_E begin cool and steadily increase approaching summer. Fluctuations in T_E closely followed those of T. This observation was expected as T_E magnitude is directly related to air temperature. Small differences are noted at the beginning of spring, and begin to increase as the season progressed. This was due to increasing temperatures, as well as increasing moisture availability, as spring is a wet season. To understand these observations further, the monthly average difference between T_E and T (T_E -T) for each station and month was calculated. A composite of the ten individual stations listed above is presented for 2010 (Figure 4.1.5). During the spring, difference values start at approximately 10 ºC in March and steadily increased to 30 ºC in May. Variation of these differences is small from station to station. The Kentucky Mesonet located in Fulton County (western-most county) had the largest differences during spring 2010 and 2011. The stations in Calloway and Warren counties had the largest differences during spring 2013 and 2014.

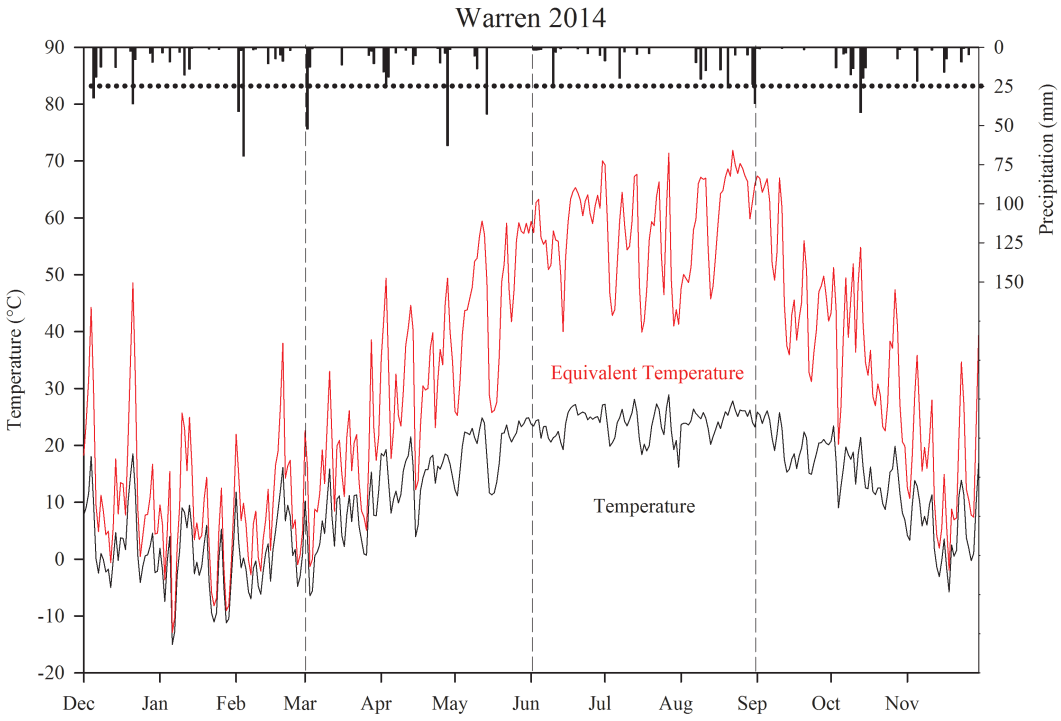

Figure 4.1.4. Daily mean temperature, equivalent temperature (T_E) and total daily precipitation for Warren County, 2014.

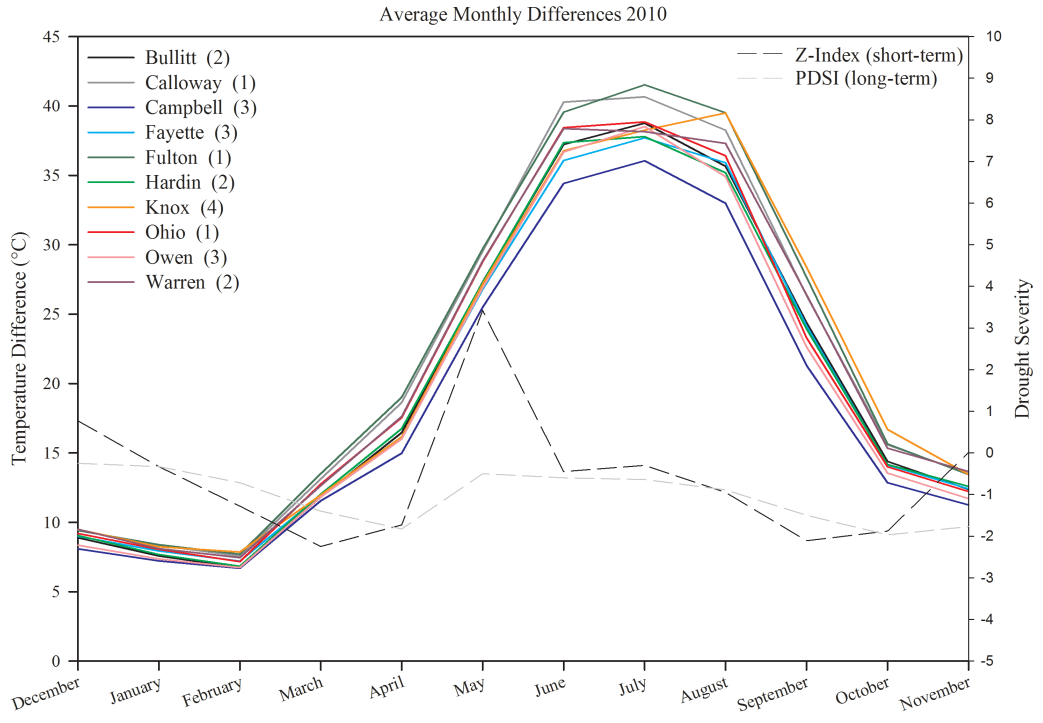

Figure 4.1.5. Monthly average difference (T_E-T) for a selection of ten counties for 2010. Monthly PDSI and Z-Index values for long and short term drought in Kentucky also are shown.

Spatial patterns of differences between T_E and T for spring in Kentucky are presented in Figures 4.1.6 to 4.1.10. Western Kentucky exhibited larger differences when compared to the rest of the state throughout the study period. The land in this region is poorly drained with wetlands, allowing for increased moisture available to the lower atmosphere. Additionally, the majority of stations in this region are adjacent to agricultural land with crops that begin growing in late spring. Stations in Campbell (3), Mason (3), and Jackson (4) counties consistently had the smallest differences each year. The reason for this is not currently known. Spring 2010 and 2011 generally had similar differences across the state, with 2011 having slightly larger differences for stations located in Caldwell (1), Hopkins (1), Warren (2), Barren (2), Cumberland (2), Mason (3), and Jackson (4) counties. A drought began developing in western Kentucky in spring 2012 and intensified throughout the summer (USDM, 2012). The Palmer Drought Severity Index (PDSI) for Kentucky in May, 2012, was -1.9, indicating drought conditions throughout the state (MRCC, 2014). This drought was most intense in the Western climate division, with a PDSI of -3.36 in May, 2012 (MRCC, 2014). Despite drought conditions, spring 2012 had the largest differences. This suggests that there was moisture available in the atmosphere that was not realized in precipitation. The spring seasons of 2013 and 2014 had the smallest differences.

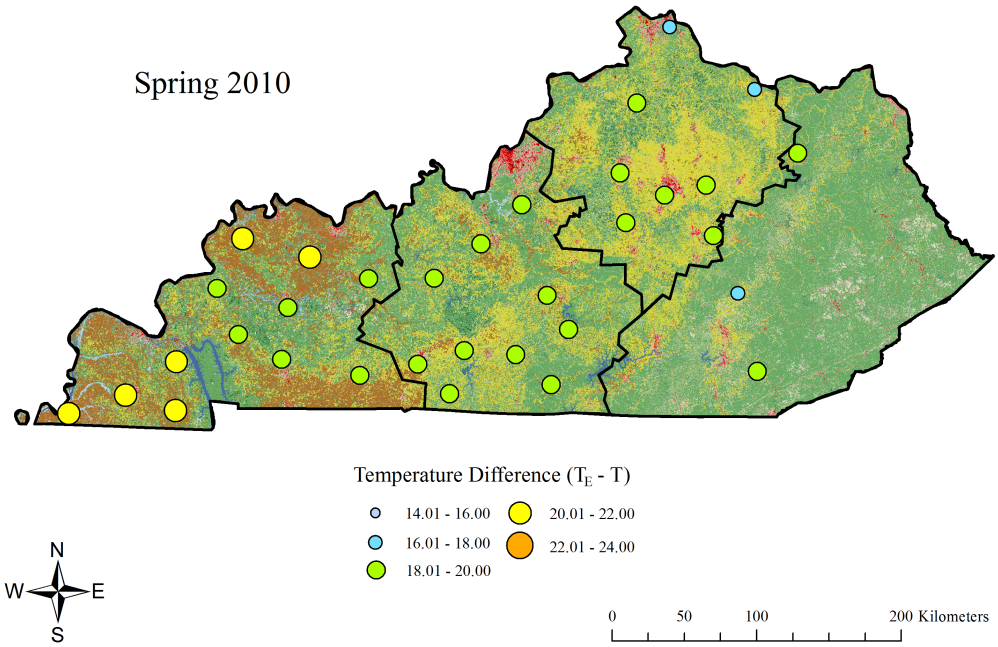

Figure 4.1.6. Average temperature differences (T_E-T) for Spring, 2010.

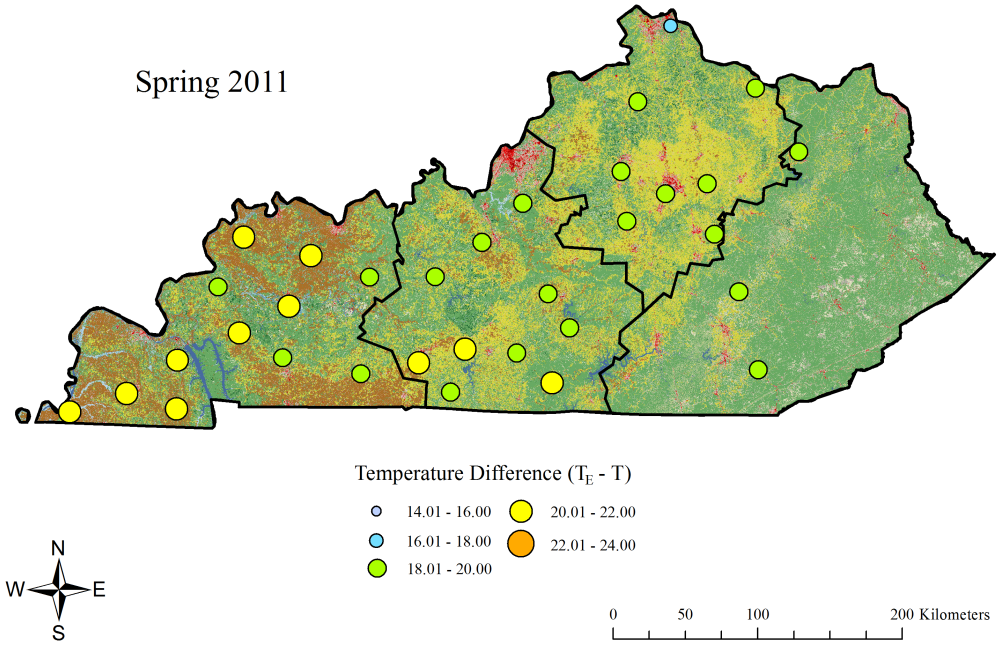

Figure 4.1.7. Average temperature differences (T_E-T) for Spring, 2011.

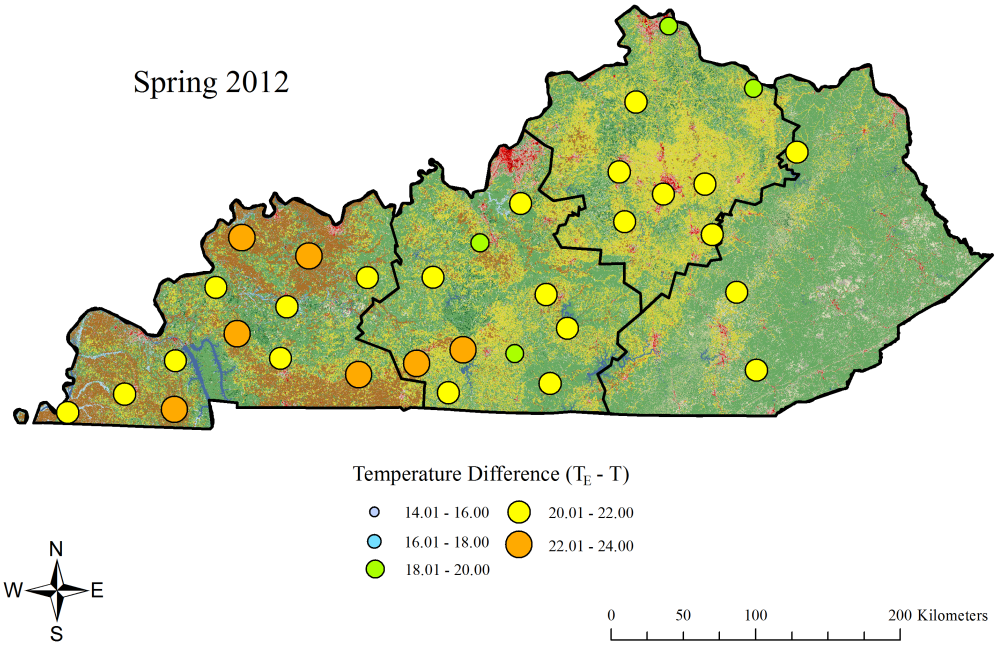

Figure 4.1.8. Average temperature differences (T_E-T) for Spring, 2012.

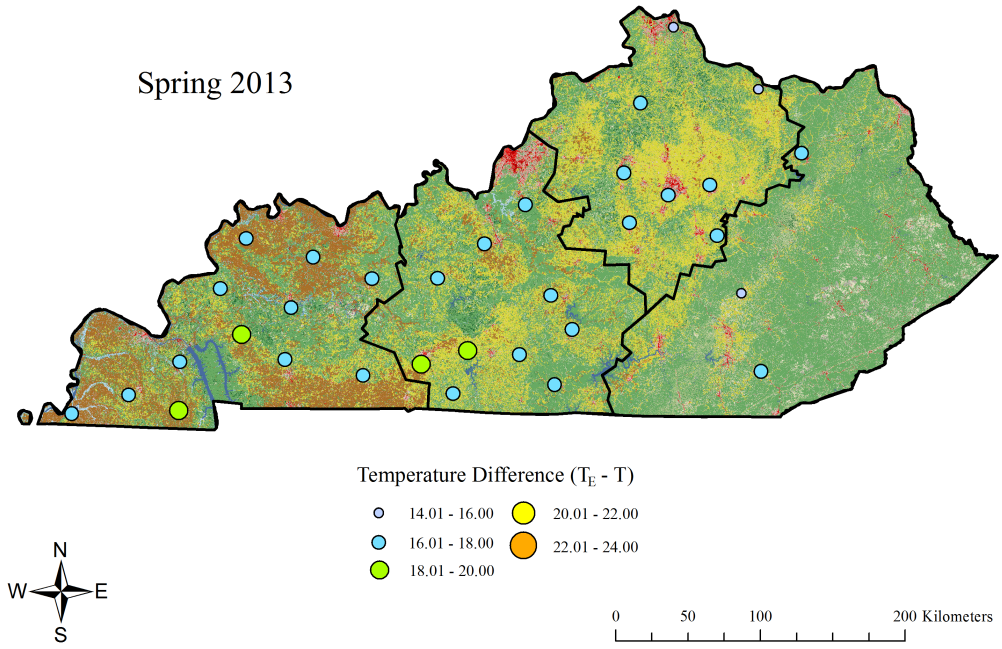

Figure 4.1.9. Average temperature differences (T_E-T) for Spring, 2013.

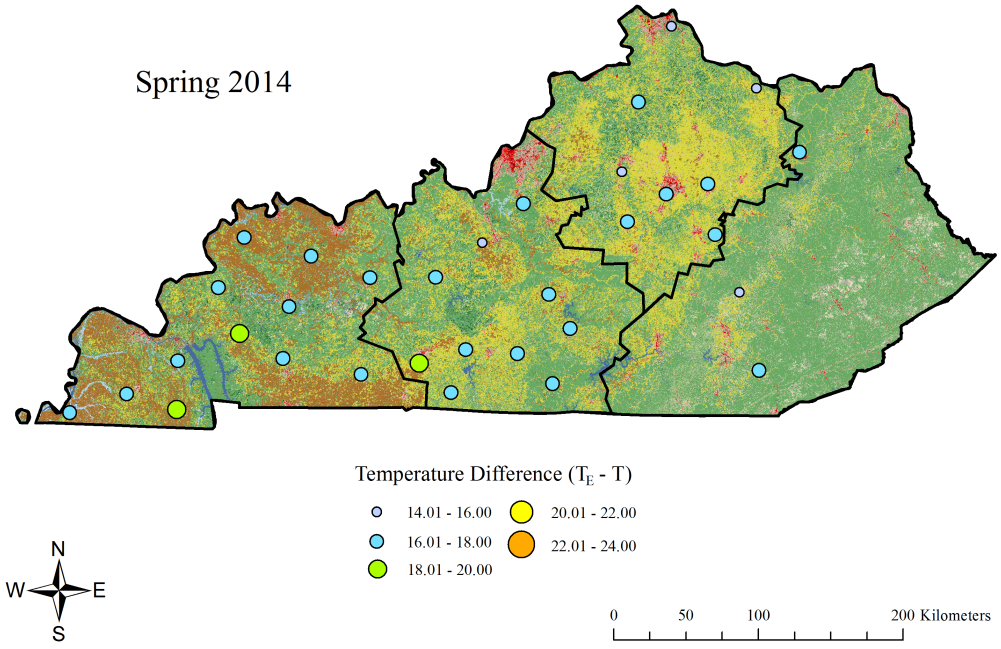

Figure 4.1.10. Average temperature differences (T_E-T) for Spring, 2014.

4.2 Discussion of summer season analysis

The seasonal distribution of T_E values is shown in Figure 4.2.1 for summer of each year. The range of T_E values in the summertime were approximately 60 ºC, as compared to 80 ºC in the spring. This is consistent with a smaller range of temperatures in summer compared to the transition seasons, spring and fall. Median values and the distributions about the median for each year were generally similar during summer. Summer of 2012 had the 'coolest' median, maximum and minimum T_Es. These low T_Es can be attributed to the drought Kentucky experienced during 2012 (discussed later in this section). Each year had many outliers (outside 2.7 σ of the median), especially on the cool side, caused by anomalously cool days due to cold frontal passages at the beginning and end of the season. The maximum T_E, 93.24 ºC, occurred on 12 July, 2011, while the minimum T_E, 21.76 ºC, occurred on 2 June, 2012. All of the yearly datasets for summer

were negatively skewed. This asymmetric distribution was also apparent in the summer histograms (Figure 4.2.2). The summer distributions of T_E were not statistically normal at a 5% significance level based on the one-sided K-S test.

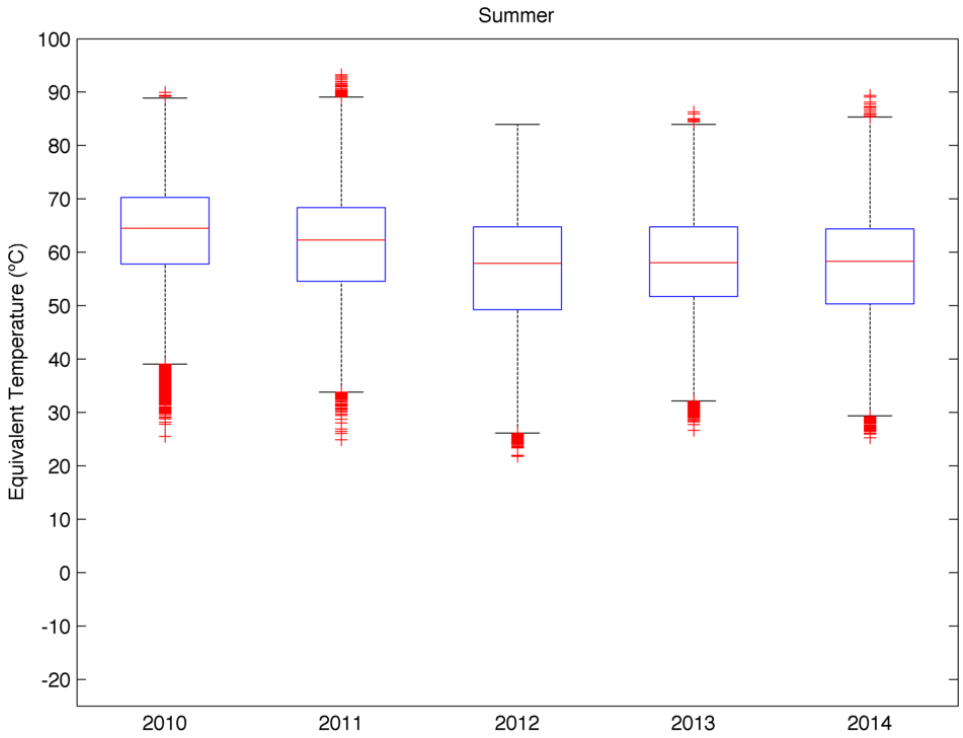

Figure 4.2.1. Boxplots showing the distribution of T_E values during summer for each year. This includes all summer data from every study station in the area.

A similar analysis was completed for the four climate divisions (Figure 4.2.3). Based on the overall temporal distribution of data, all climate divisions had generally similar T_E distributions for summer. The Western division had the largest range of T_E values at 71.23 ºC, while the Eastern division had the smallest at 64.04 ºC. While all divisions had outliers (values at least 2.7 σ from the median), the Central division had the highest count. The diverse range of land cover and land use described in the previous section may explain these extreme T_Es.

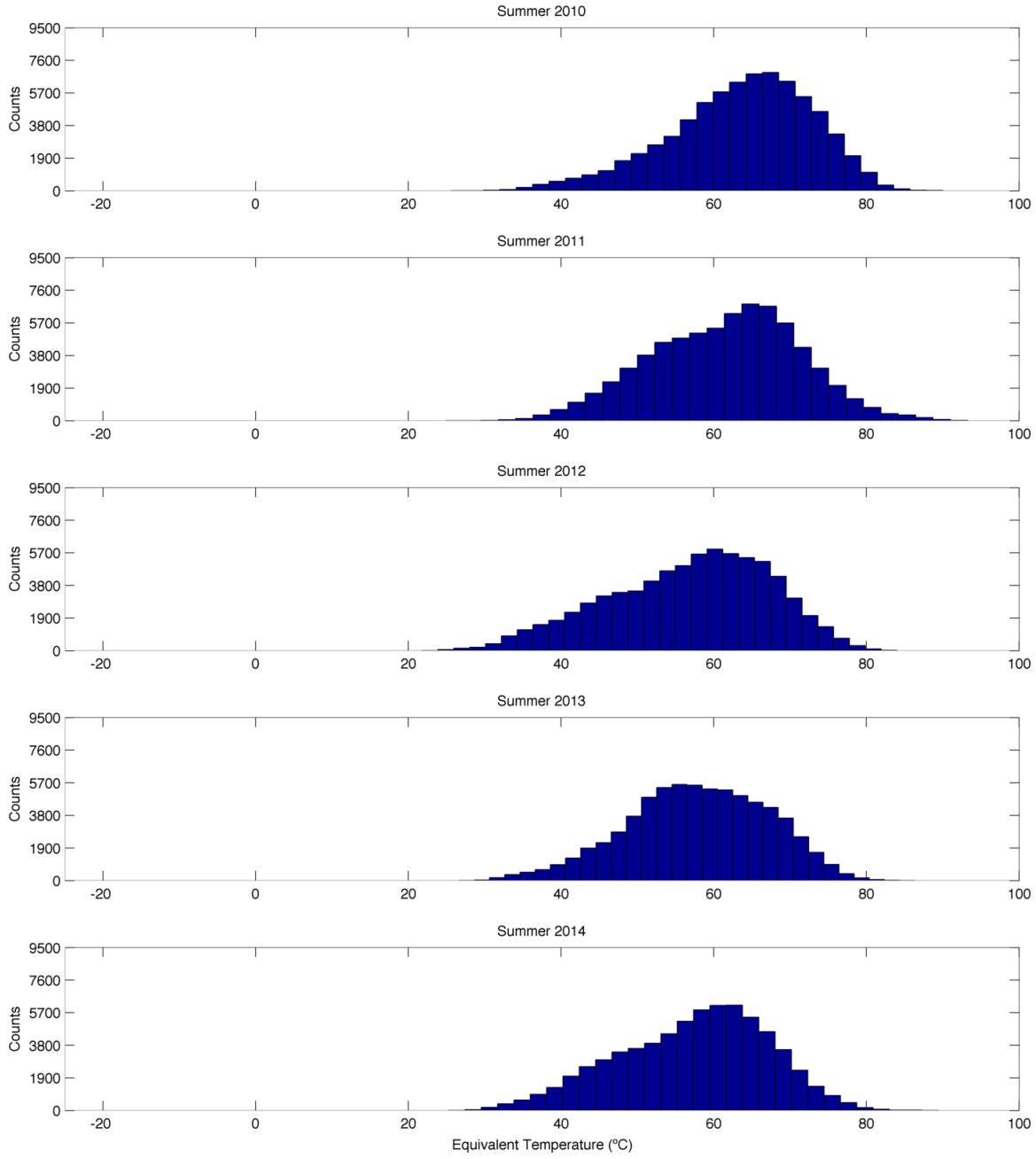

Figure 4.2.2. Histograms (bins = 30) showing the distribution of T_E values during summer for each year. This includes all summer data from every study station in the area.

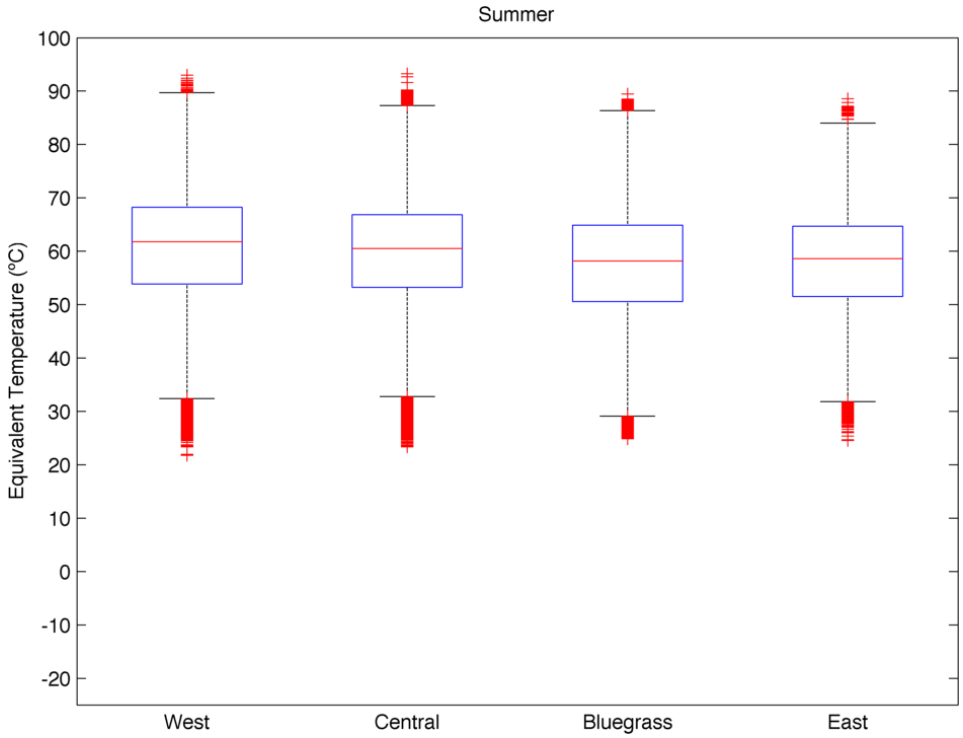

Figure 4.2.3. Boxplots showing the distribution of T_E values during summer for each climate division. This includes all summer data from every study station in each climate division.

Average daily T_E was higher than air temperature throughout the year, with the greatest differences occurring during the summer season (Figure 4.2.4). In all seasons except summer, the fluctuations in T_E followed closely with those of T. Compared to daily T_E, T did not vary as much throughout the summer, so large variations in T_E could be attributed to moisture content changes and the heightened exchange of moisture between the land and atmosphere due to actively growing plants. During the peak of summer, the average monthly differences (T_E-T) were approximately 40 ºC for most years, compared to as low as 5 ºC during winter (Figures A-7 to A-10). Of the ten stations identified previously, Fulton County had the largest differences for summers 2010 and 2011, Warren County had the largest differences for summers 2012 and 2013, and Calloway County had the largest differences for summer 2014. The mesonet station in

Campbell County (northern-most county) consistently had the smallest differences throughout summer for each year. This station is located near a wheat field, and is surrounded by deciduous forest. Average monthly differences throughout Kentucky peaked in July for all years except 2013 and 2014. July 2014 exhibited differences of 2-7 ºC less than June and August, 2014. These smaller values are most pronounced at the stations in the Western climate division (Calloway, Fulton, and Ohio). A short-term drought is evident using the Palmer Z-Index in western Kentucky for July, 2014, with values of 0.7, -1.72 and 1.32 for June, July, and August, 2014, respectively (MRCC, 2014). This short-term dryness is likely to have contributed to the smaller T_E values observed at these stations, and the resultant smaller differences.

Spatial patterns of differences between T_E and T in Kentucky (Figures 4.2.4 to 4.2.8) were also analyzed for summer. In general, differences were largest in the cultivated croplands of western and central Kentucky. This suggests that as summer is the growing season for Kentucky, increased near-surface moisture associated with evapotranspiration from crops influenced these larger differences. As observed in the monthly average differences for summer, the mesonet station in Campbell County consistently had small values. The summers of 2010 and 2011 exhibited the largest differences, while the differences were smallest during the summer of 2012. The summer of 2011 was relatively wet throughout all of Kentucky, with a PDSI value of 3.85 for June (MRCC, 2014). Wet conditions across Kentucky contributed to the larger differences observed during the summer of 2011. Western Kentucky developed a severe drought during late spring and summer 2012, culminating in an exceptional drought, the highest intensity assigned by the U.S. Drought Monitor, by early July (USDM, 2012).

This long-term drought is evident in the western climate division's cumulative PDSI value of -20.07 during spring and summer 2012 (MRCC, 2014). As the summer progressed, the drought expanded east to the rest of Kentucky, reaching severe conditions in central Kentucky (cumulative PDSI of -11.29) by the end of August (USDM, 2012). This drought was an extension of the historical 2012 Central Great Plains drought, which rivaled the conditions observed during the Dust Bowl of the 1930s (Hoerling et al., 2014). Exceptionally dry and hot conditions across the Commonwealth during this summer contributed to the smaller differences between T_E and T (small contribution of moisture).

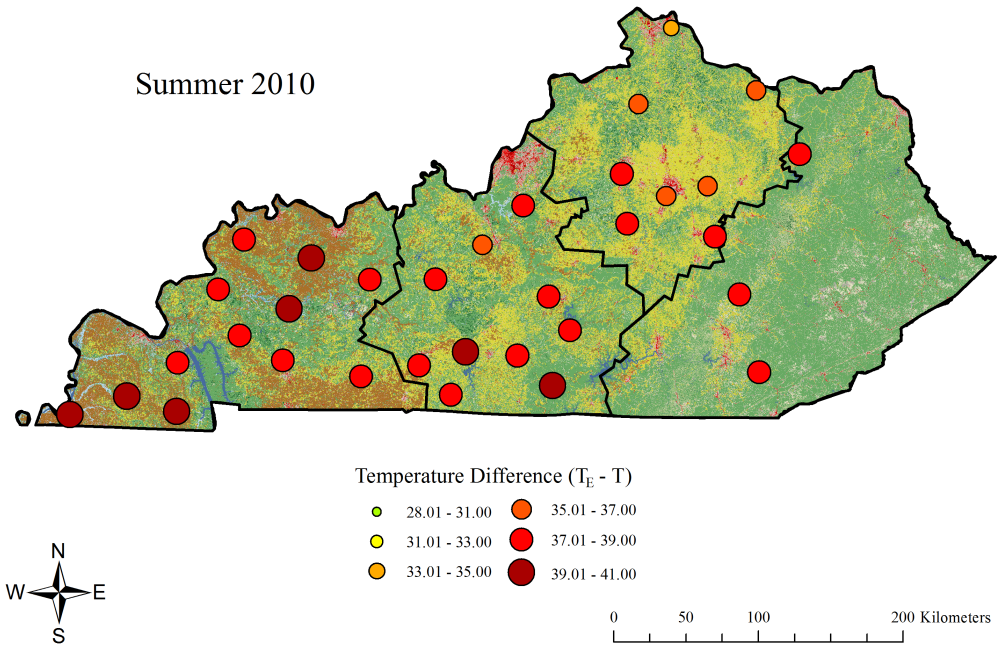

Figure 4.2.4. Average temperature differences (T_E-T) for Summer, 2010.

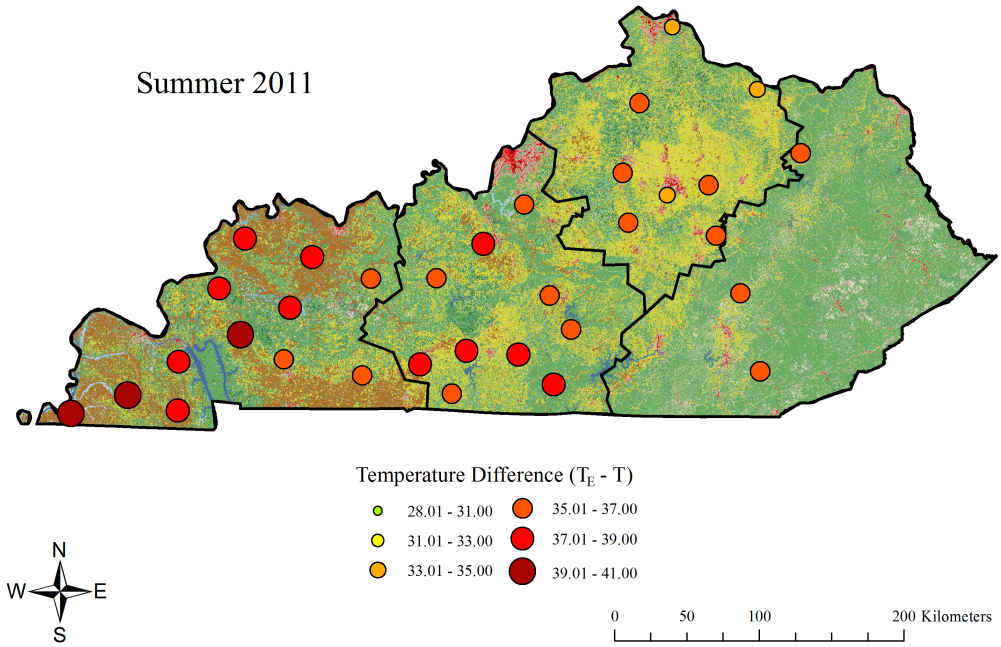

Figure 4.2.5. Average temperature differences (T_E-T) for Summer, 2011.

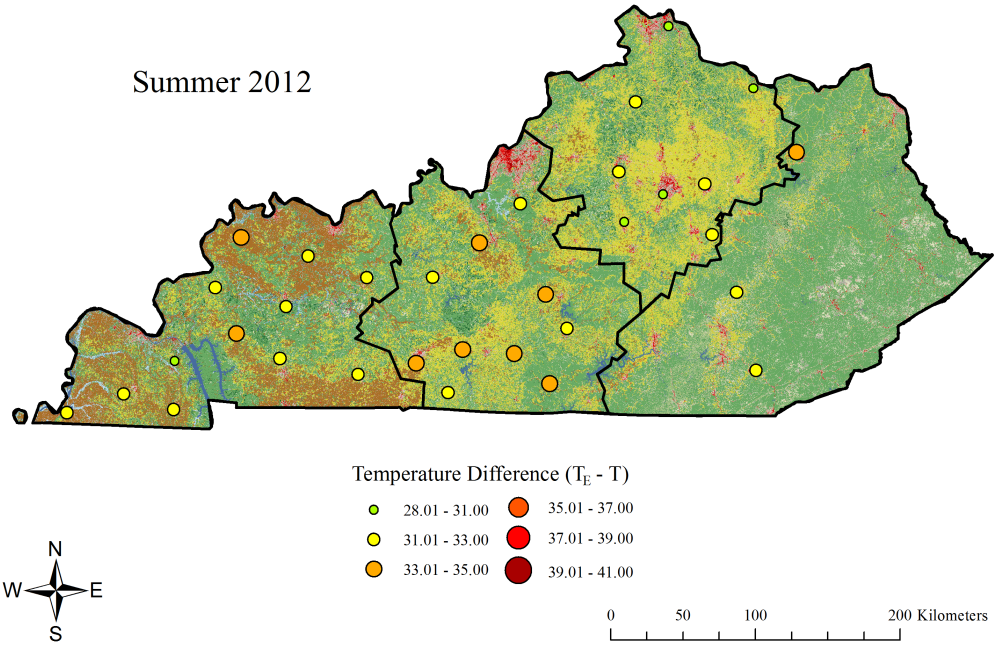

Figure 4.2.6. Average temperature differences (T_E-T) for Summer, 2012.

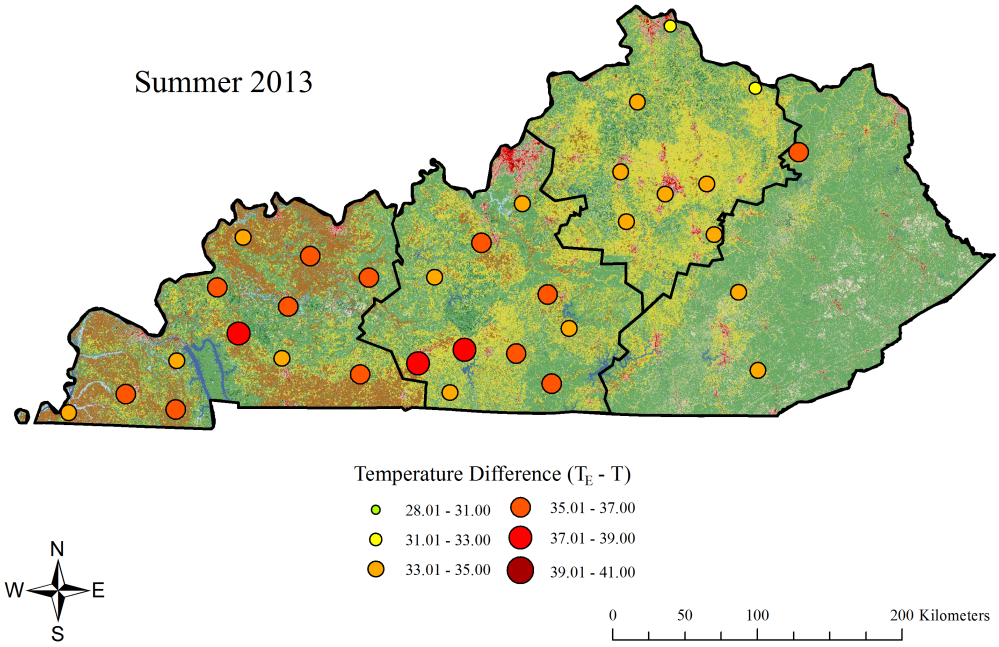

Figure 4.2.7. Average temperature differences (T_E-T) for Summer, 2013.

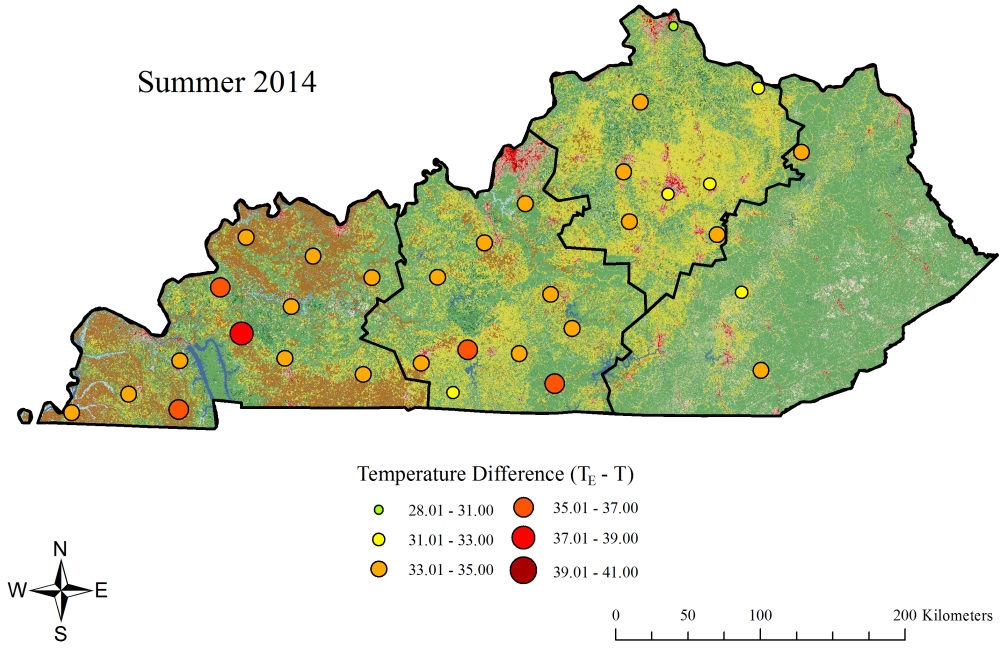

Figure 4.2.8. Average temperature differences (T_E-T) for Summer, 2014.

4.3 Discussion of fall season analysis

The seasonal distribution of T_E values is shown in Figure A-11 for fall of each year. Fall 2010 had the smallest range of T_Es (78.12 ºC), coolest maximum (76.69 ºC), and warmest minimum (-1.43 ºC). The largest range and interquartile of T_E values was Fall 2013, with the maximum T_E, 80.92 ºC, occurring on 10 September, 2013. Additionally, the 2013 T_E distribution represented the only negatively skewed fall dataset, with a skewness value of -0.0270. Similar to spring, fall had relatively small skewness values of 0.2720, 0.1766, 0.4364 and 0.0524 for 2010, 2011, 2012 and 2014, respectively. These distributions are additionally shown in the fall histograms (Figure A-12). The fall distributions of T_E were also not statistically normal at a 5% significance level based on the one-sided K-S test.

This analysis was also completed for the four climate divisions (Figure A-13). Fall had similar median T_Es and interquartile ranges for the climate divisions as what was observed in spring. The maximum and minimum T_Es were observed to be slightly warmer in fall than in spring. The Western division had the largest range of T_E, while the Bluegrass and Eastern divisions had similar T_E distributions.

During the fall, daily averages of T and T_E begin warm and steadily decrease approaching winter. Similar to spring, fall daily fluctuations in T_E closely followed those of T (Figure 4.1.4). Larger average monthly differences (T_E-T) were observed at the beginning of fall (approximately 25 ºC in September), and decreased as the season progressed (approximately 12 ºC in November). This can be attributed to decreasing temperatures and moisture availability, as cold, dry air masses began to move through

Kentucky. Of the ten stations identified previously, the Knox County station had the largest differences for fall 2010 and 2011, while the Calloway, Warren, and Fulton County stations had the largest differences for Fall 2012, 2013, and 2014 (Figures A-7 to A-10). Similar to what was observed during the summer seasons, the mesonet station in Campbell County (northern-most county) consistently had the smallest differences throughout fall for each year.

Spatial patterns of differences between T_E and T in Kentucky were also analyzed for fall (Figures A-14 to A-18). Generally, differences were largest in western and south-central Kentucky. Fall exhibited similar spatial patterns as spring, but with smaller magnitudes, due to fall being a dry season in Kentucky compared to spring. During fall 2010, differences were smallest throughout Kentucky as a drought developed. PDSI values for Kentucky were -1.5, -1.97 and -1.77 for September, October, and November 2010, respectively (MRCC, 2014). The largest fall differences were observed in 2013 across the state; the Calloway and Caldwell County stations had the largest differences in 2013. In 2011, the differences were nearly identical at all stations, except for two counties: Rowan and Adair counties had the largest and smallest average differences, respectively, in fall 2011. Differences were most varied across the state during fall, 2014. Small differences were observed at the Caldwell, Hopkins and Christian County stations in western Kentucky, as well as at the Campbell and Mason county stations in the Bluegrass division. Larger differences were observed throughout south-central Kentucky. As expected, fall had a geographic spread of differences that were generally similar to spring season. The lower values in fall could be due to the lower evapotranspiration rates following early fall harvest.

4.4 Discussion of winter season analysis

The seasonal distribution of T_E values is shown in Figure A-19 for winter of each year. Winters of 2010, 2011, and 2014 had comparable values for the median, approximately 7 ºC. The range of T_Es was largest for winter 2014, and the minimum T_E (-24.24 ºC) occurred on 22 January, 2014. Each year had a large number of outliers (outside 2.7 σ of the median), especially on the warm side, caused by anomalously warm days due to warm frontal passages at the beginning and end of the season. The bulk of the winter T_E distribution in 2012 and 2013 was, on average, 5-10 ºC warmer than other years. Winter 2013 had the warmest T_E value (56.0726 ºC), which occurred on 12 January, 2013. The winter seasons had the most asymmetric distributions of T_E compared to the other seasons, as indicated by the large number of outliers. All winter seasons exhibited positively skewed distributions, with skewness values ranging from 0.5395 in 2010 to 0.9304 in 2011, and were not statistically normal at a 5% significance level based on the one-sided K-S test. Winter histograms are presented in Figure A-20.

This analysis was also completed for the four climate divisions (Figure A-21). Each climate division had similar T_E distributions. The central division had the warmest median (10.02 ºC) and the largest range of T_Es (76.39 ºC). Unlike the other seasons, winter had many outliers on the warm side in all climate divisions due to warm frontal passages. Winter had similar T_E distribution patterns as summer, with a relatively small range of values, when compared to the spring and fall seasons.

As expected, daily averages of T and T_E were the coolest during the winter season. Consistent with what was observed in spring and fall, daily fluctuations in T_E in

the winter closely followed those of T (Figure 4.1.4). Differences (T_E-T) were relatively similar throughout the season, reaching minimum values in January 2011, 2012, and 2014 and in February 2010 and 2013 (Figure 4.1.5). This was a contrast to the transition seasons of spring and fall, as differences throughout those seasons drastically increase and decrease, respectively. The largest differences occurred at the Knox County station for the winters of 2010 and 2014, at the Fulton County station in winter 2011, and at the Warren County station for the winters of 2012 and 2013. As in other seasons, the smallest winter differences occurred at the Campbell County station for all years.

Spatial patterns of differences between T_E and T in Kentucky were analyzed for winter (Figures A-22 to A-26). As expected, the temperature differences were smallest in the winter, with a range of only 6-12 ºC. In general, the differences were largest throughout southern Kentucky, however it is important to note that with such a small range of differences, 'largest' is a relative term. The winters of 2010 and 2014 had the smallest differences across the state, with slightly higher values in 2010. The differences were also small in 2011; however, the stations in McLean and Fulton Counties in the Western climate division had differences that were 1-3 ºC larger than the rest of the state. The winters of 2012 and 2013 exhibited similar differences, and were 2-5 ºC warmer across the state than other years. Mason County was an exception to this observation in 2013, with a smaller difference of 8.5 ºC compared to differences of 10-12 ºC throughout the rest of Kentucky during these two winters. The Mason County site is located adjacent to a wheat field.

4.5 Synoptic influence on daily heat content

The results of this thesis suggest that the influence of land cover and land surface condition (e.g., moistness) is more visible for seasonal-scale modulation of T_E and the difference between T_E and T. On the other hand, synoptic-scale influence is more apparent for rapid daily time-scale changes in T_E and subsequent difference between T_E and T. Hence, all seasons exhibited similar synoptic patterns on days with large and small differences between T_E and T.

Data for each of the ten locations (west to east: Fulton, Calloway, Ohio, Warren, Hardin, Bullitt, Fayette, Owen, Campbell, and Knox counties) were analyzed on a daily timescale. T_E was calculated at hourly time steps for each station from 1 December, 2009, through 30 November, 2014, and then aggregated to a daily average. For each day, the standard pressure deviation from normal was calculated to aid in identification of frontal passages. Only a selection of figures is presented in this section, as results from each year and station were comparable.

Daily averages of T_E and T were calculated for each station and year (Figure 4.5.1). Fluctuations in T_E closely followed those of T for all sites. This observation was expected as T_E magnitude is directly related to air temperature. Small differences (T_E-T) are noted in winter, and steadily increase through spring approaching the summer season. This was due to increasing temperatures, as well as increasing moisture availability. Differences peak during summer, and then steadily decrease through fall, approaching winter. If differing land covers can cause the daily fluctuations in heat content it was expected that these sites would exhibit different patterns in T_E. However, this was not

observed. Relative peaks and drops in T_E were observed on the same days at each site, as highlighted in Figure 4.5.1. While varying vegetation characteristics did not cause the actual fluctuations, they did have an impact on the magnitude of the peaks and drops. For example, the peak that occurred in late January approached 35 ºC at Fulton County, but remained below 30 ºC at the other three sites. Additionally, the Fulton County station had a drop in T_E of approximately 20 ºC in early July, compared to a 30 ºC drop observed at the other sites.

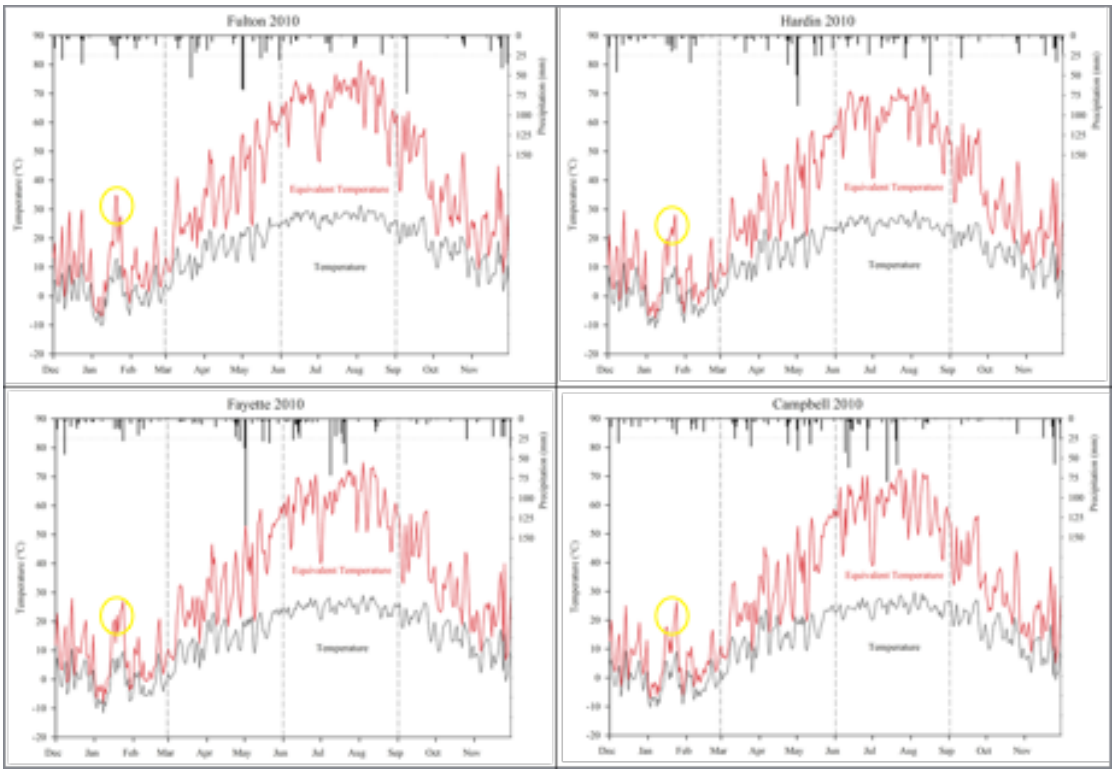

Figure 4.5.1. Daily mean temperature, equivalent temperature (T_E), and total precipitation for Fulton, Hardin, Fayette, and Campbell counties, 2010. Highlighted areas indicate simultaneous peaks and drops in T_E for each site.

Daily averages of T_E were then compared to the daily pressure deviation from seasonal normal to identify the impact of synoptic patterns on daily heat content (Figure 4.5.2). Generally, it was observed that on days with anomalous low pressure, equivalent

temperatures were at a relative maximum. Additionally, these days were associated with measured precipitation at the site. Conversely, days with anomalous high pressure were coupled with relative minimums in T_E and zero precipitation. An inverse relationship between T_E and pressure deviation was found for all seasons, although the relationship is more strongly correlated in winter and spring with coefficient values r = -0.56 and r = -0.31, respectively.

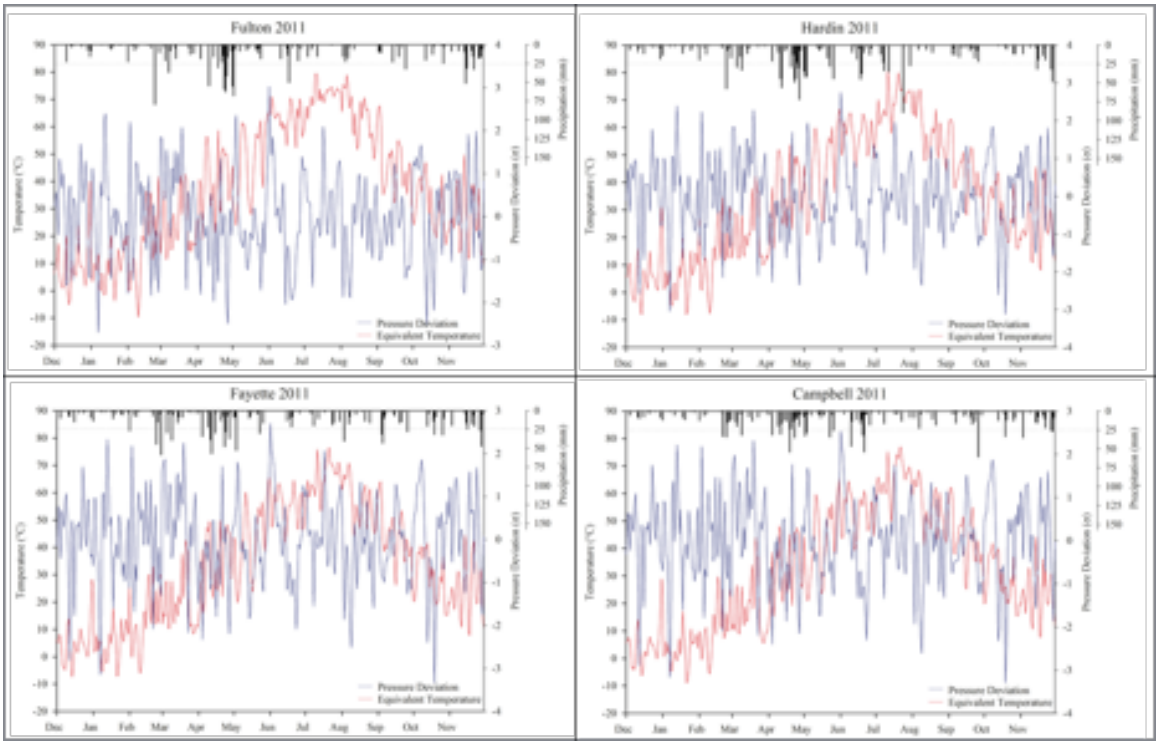

Figure 4.5.2. Daily mean equivalent temperature, total precipitation, and daily pressure deviation from seasonal normal for Fulton, Hardin, Fayette, and Campbell counties, 2011. Negative sigma values indicate anomalous low pressure; positive sigma values indicate anomalous high pressure.

This inverse relationship confirms that daily fluctuations in heat content can be attributed to the passage of synoptic systems, observed most clearly in the winter and spring seasons (Figure 4.5.3). To demonstrate, archived surface analysis charts at 18z were used to identify the probable cause of the peak in T_E on 30 January, 2013, and

subsequent minimum on 1 February, 2013 (Figure 4.5.4) (WPC, 2013). On 30 January a low-pressure system was centered over southern Lake Michigan, with a secondary low located on the south-central border of Kentucky. A cold front associated with the northern low approached Kentucky, and passed through the state by 03z on 31 January. The average differences between T_E and T on this day were 25.1 ºC, 23.8 ºC, 21.9 ºC, and 21.4 ºC in Fulton, Hardin, Fayette, and Knox counties, respectively. The precipitation measured at each of these stations was 18.29 mm, 37.34 mm, 26.42 mm, and 57.66 mm, respectively. Following the passage of the frontal system, a relatively strong surface high-pressure center (1034 hPa) moved in on 1 February, 2013. The average temperature differences on this day at each site were 3.5 ºC, 3.2 ºC, 2.9 ºC, and 4.4 ºC, respectively.

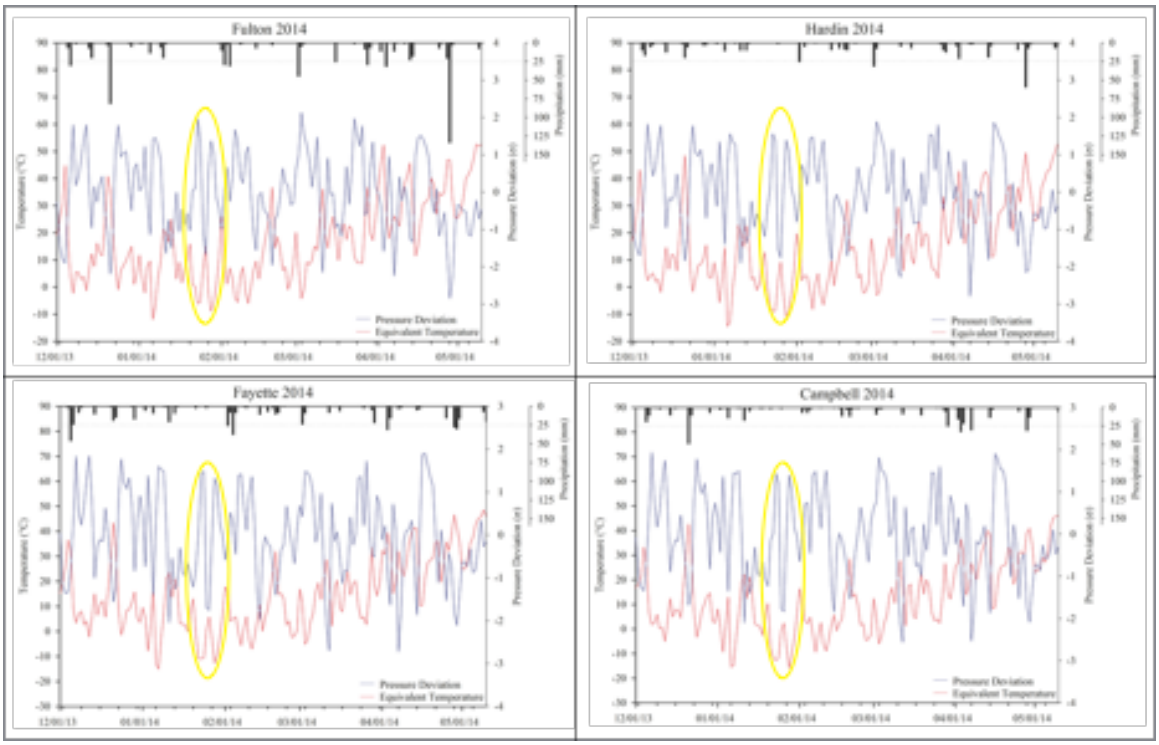

Figure 4.5.3. Daily mean equivalent temperature, total daily precipitation, and daily pressure deviation from seasonal normal for Fulton, Hardin, Fayette, and Campbell counties, 2014. Highlighted areas indicate example of inversely proportional values described in text.

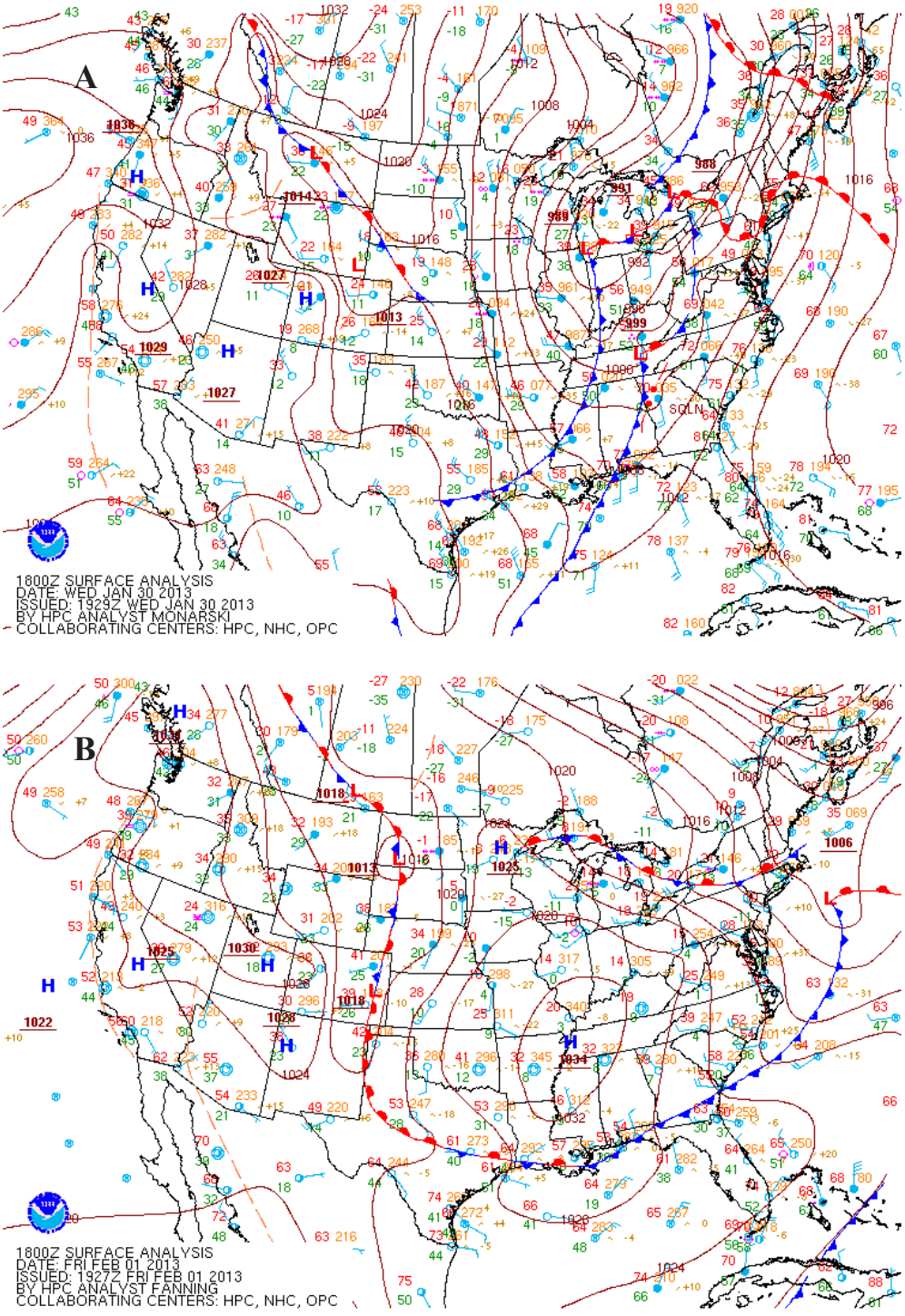

Figure 4.5.4. Archived surface analysis chart at 18z for two coupled days, January 30, 2013 (A), and February 1, 2013 (B). Part A depicts a day with a peak in T_E with anomalous low pressure. Part B depicts a day with a drop in T_E with anomalous high pressure. Source: WPC (2013).

Composite graphics were created to determine if the synoptic patterns discussed above were coupled similarly with maximum and minimum T_E values throughout the winter and spring (Figure 4.5.5). These graphics were compiled with the Integrated Data Viewer (IDV), utilizing data from the North American Regional Reanalysis (Murray et al., 2003; Mesinger et al., 2006). The NARR model has a horizontal resolution of 32 km and a vertical resolution of 45 layers, with output data available for 8 times daily at 29 levels (Mesinger et al., 2006). Ten days during the period December 1 to May 10 were chosen to compile each graphic; data was accessed for 18z on each day (Table 4.5.1). The days selected had equal to or greater than one standard deviation above or below seasonal normal for both T_E and pressure. Days were also selected to represent every year and month equally during the period to minimize temporal biases.

Table 4.5.1. Ten days chosen for each case for inclusion in the composite graphics. Daily T_E and pressure standard deviations from seasonal normal and precipitation totals are shown for Hardin County (Central climate division).

'Cool' T_E				'Warm' T_E			
Date	T_E σ	P σ	Precip (mm)	Date	T_E σ	P σ	Precip (mm)
03/06/2010	-1.76	2.04	0.00	12/02/2009	1.54	-2.09	13.97
05/09/2010	-0.88	1.84	0.00	01/24/2010	2.34	-2.59	16.76
12/10/2011	-1.34	1.92	0.00	05/02/2010	1.54	-1.45	3.46
01/13/2011	-1.11	2.39	0.00	04/19/2011	1.32	-1.26	1.02 (28.45 next day)
01/03/2012	-1.94	1.30	0.00	01/11/2012	1.16	-2.56	14.99
03/10/2012	-1.90	2.90	0.00	02/23/2012	1.81	-3.08	4.57
02/01/2013	-1.73	1.39	0.00	01/30/2013	1.37	-2.87	37.34
04/03/2013	-1.14	1.70	0.00	12/21/2013	3.52	-1.84	45.97
02/07/2014	-1.36	1.48	0.00	03/28/2014	0.22	-0.47	8.64
04/16/2014	-1.14	1.86	0.00	04/28/2014	1.23	-2.14	61.72

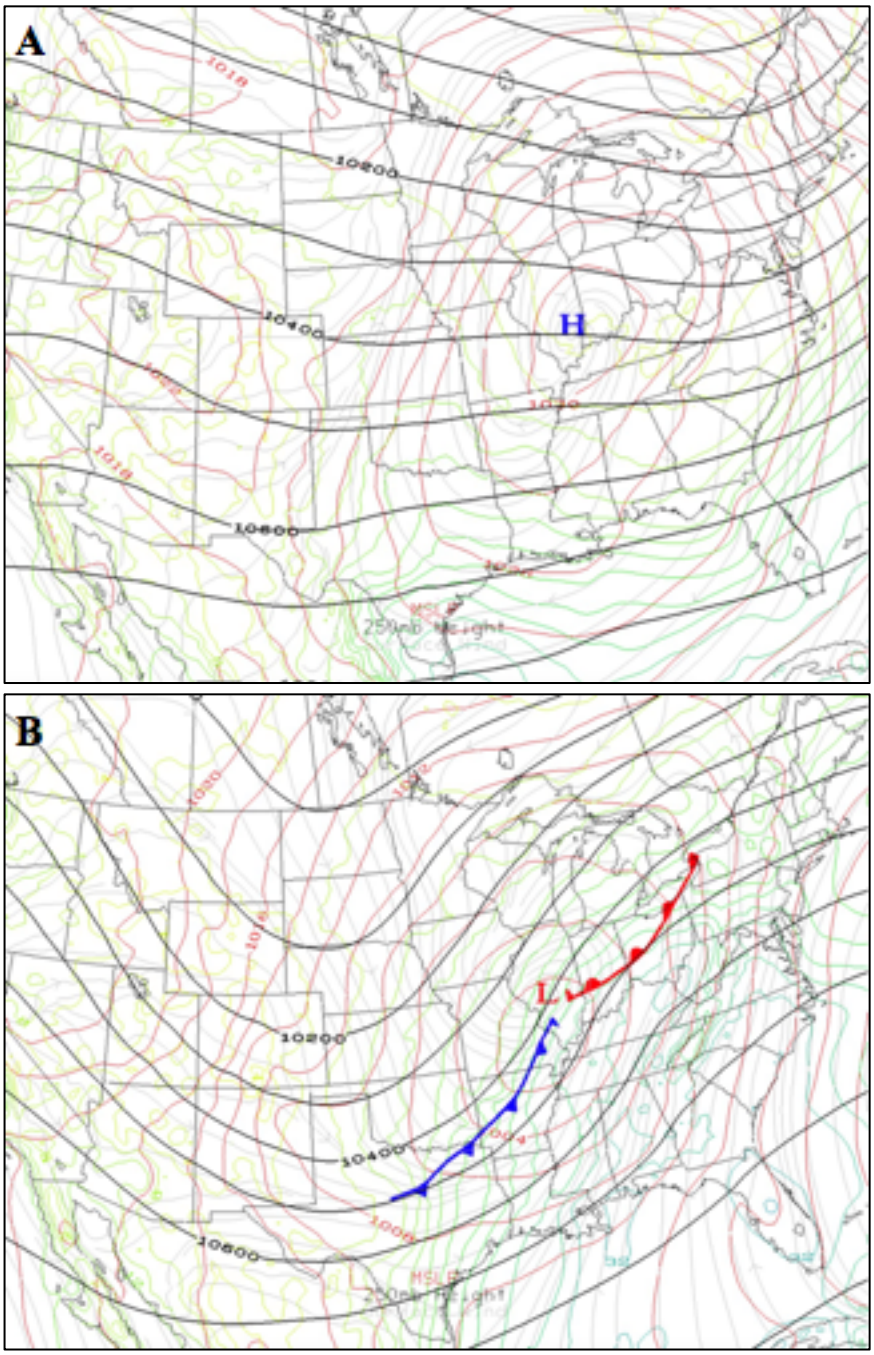

Figure 4.5.5. Composite graphics compiled with IDV, utilizing data from the NARR model. Black lines: 250mb winds; Red lines: Mean sea level pressure; Gray lines: Surface streamlines; Green lines: Precipitable water content for entire atmosphere. Part A depicts the average synoptic pattern on days with 'cool' T_E and anomalous high pressure. Part B depicts the average synoptic pattern on days with 'warm' T_E and anomalous low pressure.

On days with 'cooler' T_E and anomalous high pressure (Figure 4.5.5A), the average synoptic pattern observed has Kentucky on the backside of a 250mb trough, with convergence aloft associated with it. A surface high pressure dominates the area, with predominantly northerly winds across the state, and very little moisture present throughout the atmosphere. This observation is consistent with the knowledge of surface high pressure coupled to dry, cooler air immediately following the passage of a cold front, which should coincide with minimum heat content due to the absence of available moisture. Days with 'warmer' T_E and anomalous low pressure (Figure 4.5.5B) were synoptically characterized by a 250mb trough over the plains, placing Kentucky generally in an area of divergence aloft. A low-pressure system was, on average, located to the northwest of Kentucky, with an approaching cold front. This configuration places Kentucky in the warm sector, with south-southwesterly winds and significant moisture advection associated with the front. This allows T_E values to be at a relative maximum due to warmer temperatures (preceding the cold front) and increased contribution from moisture. This observation again is consistent with the conceptual understanding that heat content will be greatest on days with warm temperatures and heightened moisture availability.

CHAPTER 5

CONCLUSION

Over the last decade there has been an increased amount of research conducted on the role of land use/land cover on the climate system, ranging from local to global scales. This body of research indicates substantial relationships between land use/land cover and the impacts on near-surface air temperature and moisture content. However, there have been relatively few investigations on the heat content of the near-surface atmosphere, specifically as it relates to land cover. The use of air temperature alone to describe heat content is not an adequate measure of heating or cooling, as it does not account for near-surface moisture. Equivalent temperature (T_E) is a more appropriate metric for analyzing the near-surface heat content as it accounts for both the sensible air temperature and moisture. This research sought to provide a meso-scale climatological assessment of TE at daily, seasonal, and annual time-scales in Kentucky, as well as how predominant land use/land cover impacts the near-surface heat content in Kentucky.

Throughout Kentucky, both T and T_E follow similar seasonal patterns, warmer in the summer and cooler in the winter, with T_E values larger than T throughout the year. The differences between T_E and T were smallest during winter (greatest during summer), when specific humidity was at its lowest (highest). While T mostly represented the magnitude of T_E, even a small moisture contribution (e.g., 10.53% or 14.14 g kg^{-1}) had an impact on T_E (59.3 ºC). Although each climate division exhibited similar patterns, the Western climate division was found to have the greatest average specific humidities and the highest moisture contributions to T_E during spring and summer. Temperature differences (T_E –T) were also generally largest in western Kentucky. This division is

poorly drained, allowing for greater moisture availability to the near-surface atmosphere. Additionally, the Kentucky Mesonet stations in this area are located adjacent to cultivated cropland and it's suggested the increased evapotranspiration during the growing season influenced the greater difference values in spring and summer. The mesonet station in Campbell County persistently exhibited the smallest temperature differences throughout each month and year. The reasons for this are still under investigation. Heat content was greatest in the summer seasons, with differences between T_E and T approaching 50 ºC in some locations. Conversely, it was at a minimum in the winter seasons, with differences as low as 5 ºC. Periods of extreme precipitation also impacted the average heat content. An exceptional drought developed in Kentucky throughout the summer of 2012, and expanded eastward, reaching severe conditions in central Kentucky by the end of July (USDM, 2012). Compared to other years, summer 2012 had the smallest temperature differences, which were attributed to the extreme dry and hot conditions across the Commonwealth (small contribution of moisture). The 2011 summer exhibited large differences, and was relatively wet in Kentucky, with a PDSI value of 3.85 (MRCC, 2014).

Results of this study suggest that the influence of land cover and land surface condition (e.g., moistness) is more apparent on the seasonal-scale modulation of T_E, and synoptic patterns are more apparent at the daily time-scale, although land cover may affect the magnitude of the daily fluctuations. An inverse relationship between T_E and pressure deviation was found for all seasons, although the relationship is more strongly correlated in winter and spring, with coefficient values $r = -0.56$ and $r = -0.31$, respectively. During winter and early spring, it was observed that days with 'cooler' T_E

and anomalous high pressure were associated synoptically with convergence aloft, surface high pressure, predominantly northerly winds, and little-to-no moisture throughout the atmosphere. On the contrary, days with 'warmer' T_E and anomalous low pressure were synoptically characterized by a trough over the Plains, leading to divergence aloft near Kentucky. Generally, a low-pressure system was located to the northwest, with an approaching cold front, placing Kentucky in the warm sector. Winds at the surface were out of the south-southwest, with moisture advection into the state associated with the cold front. These observations were consistent with the conceptual understanding of the coupled effect of air temperature and moisture on the near-surface heat content, supporting the conclusion that daily fluctuations in T_E are more closely related to synoptic-scale circulation than vegetation characteristics.

Future research priorities ought to analyze the microclimates of a selection of Kentucky mesonet sites in more detail to identify possible causes of the inter-annual variation in T_E observed that could not be explained by broad land-cover classification. These could include a trend analysis of air temperature, T_E and Lq (moisture contribution), soil analyses of each site, as well as additional factors that may impact the near-surface heat content such as the local wind and solar radiation variability. Additionally, the influence on the near-surface moisture budget and resultant T_E of poor versus well-drained epikarst and karst regions throughout Kentucky should be investigated. Furthermore, the correlation of T_E ranges to different air mass types ought to be studied.

REFERENCES

Bloom, A,J., 2010. *Global Climate Change: Convergence of Disciplines*. Sunderland, MA: Sinauer Associates, Inc:

Bolton, D., 1980. The computation of equivalent potential temperature. *Monthly Weather Review* **108**: 1046-1053.

Brovkin, V., Sitch, S., Werner, V.B., Claussen, M., Bauer, E., Cramer, W., 2004. Role of land cover changes for atmospheric CO2 increase and climate change during the last 150 years. *Global Change Biology* **10**: 1253–1266.

Carleton, A.M., Travis, D.J., Adegoke, J.O., Arnold, D.L., Curran, S., 2008. Synoptic circulation and land surface influences on convection in the Midwest U.S. "Corn Belt" during the summers of 1999 and 2000b. Part II: role of vegetation boundaries. *Journal of Climate* **21**: 3617–3641.

Claussen, M., Brovkin, V., Ganopolski, A., 2001. Biogeophysical versus biogeochemical feedbacks of large-scale land cover change. *Geophysical Research Letters* **28**: 1011–1014.

Davey, C.A., Pielke, R.A. Sr., Gallo, K.P., 2006. Differences between nearsurface equivalent temperature and temperature trends for the eastern United States: equivalent temperature as an alternative measure of heat content. *Global and Planetary Change* **54**: 19–32.

Dickinson R.E., 1983. Land surface processes and climate-surface albedos and energy balance. *Advances in Geophysics* **25:** 305-353.

Fall, S., Diffenbaugh, N.S., Niyogi, D., Pielke, R.A. Sr., Rochon, G., 2010. Temperature and equivalent temperature over the United States (1979-2005). *International Journal of Climatology* **30**: 2045-2054.

Feddema, J.J., Oleson, K.W., Bonan, G.B., Mearns, L.O., Buja, L.E., Meehl, G.A., Washington, W.M., 2005. The importance of land-cover change in simulating future climates. *Science* **310:** 1674-1678.

Haugland, M.J., Crawford, K.C., 2005. The diurnal cycle of land-atmosphere interactions across Oklahoma's winter wheat belt. *Monthly Weather Review* **133**: 120-130.

Hoerling, M., Eischeid, J., Kumar, A., Leung, R., Mariotti, K., Mo, K., Schubert, S., Seager, R., 2014. Causes and predictability of the 2012 Great Plains drought. *Bulletin of the American Meteorology Society* **95**: 269-282.

Houghton, R.A., House, J.I., Pongratz, J., van der Werf, G.R., DeFries, R.S., Hansen, M.C., Le Quere, C., Ramankutty, N., 2012. Carbon emissions from land use and land-cover change. *Biogeosciences* **9**: 5125-5142.

Idso, S.B., Jackson, R.D., Reginato, R.J., Kimball, B.A., Nakayama, F.S., 1975. The dependence of bare soil albedo on soil water content. *Journal of Applied Meteorology* **14**: 109-113.

IPCC (Intergovernmental Panel on Climate Change), 2001. Climate Change 2001. Synthesis Report. *Contribution of Working Groups I, II, and III to the Third Assessment Report of the Intergovernmental Panel on Climate Change* Watson RT and the Core Writing Team (eds.). Cambridge, MA: Cambridge University Press:

IPCC (Intergovernmental Panel on Climate Change), 2007. Climate Change 2007. Synthesis Report. *Contribution of Working Groups I, II and III to the Fourth Assessment Report of the Intergovernmental Panel on Climate Change* Pachauri RK and Reisinger A and the Core Writing Team (eds.). Geneva, Switzerland: IPCC.

IPCC (Intergovernmental Panel on Climate Change), 2013. Climate Change 2013. Summary for policymakers. *Working Group I Contribution to the Fifth Assessment Report of the Intergovernmental Panel on Climate Change*, Core Writing Team (eds.). Stockholm, Sweden: IPCC.

Jin, S., Yang, L., Danielson, P., Homer, C., Fry, J., and Xian, G., 2013. A comprehensive change detection method for updating the National Land Cover Database to circa 2011. *Remote Sensing of Environment* **132**: 159 – 175.

Jones, P.D., Raper, S.C.B., Bradley, R.S., Diaz, H.F., Kelly, P.M., Wigley, T.M.L., 1986. Northern hemisphere surface air temperature variations: 1851-1984. *Journal of Climate and Applied Meteorology* **25**: 161-179.

Kentucky Mesonet, 2014. *Summary Data*. Bowling Green, KY: Kentucky Mesonet. Online at: http://www.kymesonet.org.

KGN (Kentucky Geography Network), 2012. *Kentucky Statewide 1 Meter Aerial Imagery*. Frankfort, KY: KGN. Retrieved April 14, 2014, from http://kygisserver.ky.gov/geoportal/catalog/search/resource/details.page?uuid=%7BAEEB6F93-CB84-4C06-904C-F4B69079B493%7D

KYMN (Kentucky Mesonet), 2014. *Monthly Climatological Summary*. Bowling Green, KY: Kentucky Mesonet. Retrieved September 18, 2014, from http://www.kymesonet.org/historical_data.php

Mahmood, R., Pielke, R.A. Sr., Hubbard, K.G., Niyogi, D., Bonan, G., Lawrence, P., McNider, R., McAlpine, C., Etter, A., Gameda, S., Qian, B., Carleton, A., Beltran-Przekurat, A., Chase, T., Quintanar, A.I., Adegoke, J.O., Vezhapparambu, S., Conner, G., Asefi, S., Sertel, E., Legates, D.R., Wu, Y., Hale, R., Frauenfeld, O.N., Watts, A., Shepherd, M., Mitra, C., Anantharaj, V.G., Fall, S., Lund, R., Nordfelt, A., Blanken, P., Du, J., Chang, H-I., Leeper, R., Nair, U.S., Dobler, S., Deo, R., Syktus, J.. 2010. Impacts of land use land cover change on climate and future research priorities. *Bulletin of the American Meteorological Society* **91**: 37–46.

Mahmood, R., Pielke, R.A. Sr., Hubbard, K.G., Niyogi, D., Dirmeyer, P.A., McAlpine, C., Carleton, A.M., Hale, R., Gameda, S., Beltran-Przekurat, A., Baker, B., McNider, R., Legates, D.R., Shepherd, M., Du, J., Blanken, P.D., Frauenfeld, O.W., Nair, U.S., Fall, S., 2014. Land cover changes and their biogeophysical effects on climate. *International Journal of Climatology* **34**: 929–953.

Matthews, H.D., Weaver, A.J., Meissner, K.J., Gillett, N.P., Eby, M., 2004. Natural and anthropogenic climate change: incorporating historical land cover change, vegetation dynamics and the global carbon cycle. *Climate Dynamics* **22**: 461–479.

McPherson, R.A., Stensrud, D.J., Crawford, K.C., 2004. The impact of Oklahoma's winter wheat belt on the mesoscale environment. *Monthly Weather Review* **132**: 405-421.

Mesinger, F., DiMego, G., Kalnay, E., Mitchell, K., Shafran, P. C., Ebisuzaki, W., Joviç, D., Woollen, J., Rogers, E., Berbery, E.H., Ek, M.B., Fan, Y., Grumbine, R., Higgins, W., Li, H., Lin, Y., Manikin, G., Parrish, D., Shi, W., 2006. North American regional reanalysis. *Bulletin of the American Meteorological Society*, 87(3): 343-360.

MRCC (Midwest Regional Climate Center), 2014. *State and Climate Division Data - Monthly by Year*. Urbana-Champaign, IL: MDCC. Retrieved September 18, 2014, from http://mrcc.isws.illinois.edu/CLIMATE/nClimDiv/STCD_ monthly1.jsp

Murray, D., McWhirter, J., Wier, S., Emmerson, S., 2003. *The Integrated Data Viewer: a Web-enabled application for scientific analysis and visualization*. Paper presented at the 19th International Conference on IIPS for Meteorology, Oceanography and Hydrology, February 13, Long Beach, CA.

NCDC (National Climatic Data Center), 2013. *US Palmer Drought Indices*. Asheville, NC: NCDC. Retrieved September 18, 2014, from http://www.ncdc.noaa.gov/oa/climate/research/prelim/drought/palmer.html

NCDC (National Climatic Data Center), 2015. *US Climate Divisions*. Asheville, NC: NCDC. Retrieved March 6, 2015, from http://www.ncdc.noaa.gov/monitoring-references/maps/us-climate-divisions.php

NCEP (National Centers for Environmental Prediction), 2014. *Daily Weather Map*. College Park, MD: NCEP. Retrieved September 18, 2014, from http://www.hpc.ncep.noaa.gov/dailywxmap/

Nicholson, S.E., 1988. Land surface atmosphere interaction. *Progress in Physical Geography* **12**: 36-65.

NRC (National Research Council), 2005. *Radiative Forcing of Climate Change: Expanding the Concept and Addressing Uncertainties*. Washington, D.C.: The National Academies Press.

Oke, T.R., 1987. *Boundary Layer Climates*, 2nd edn. New York, NY: Routledge.

Pielke, R.A. Sr., 2001. Influence of the spatial distribution of vegetation and soils on the prediction of cumulus convective rainfall. *Reviews of Geophysics* **39**: 151-177.

Pielke, R.A. Sr., Davey, C., Morgan, J., 2004. Assessing "global warming" with surface heat content. *Eos Transactions* **85**: 210–211.

Pielke, R.A. Sr., Beven, K., Brasseur, G., Calvert, J., Chahine, M., Dickerson, R.R., Wood, E., 2009. Climate change: The need to consider human forcings besides greenhouse gases. *Eos, Transactions American Geophysical Union* **90**: 413.

Pielke, R.A. Sr., Marland, G., Betts, R.A., Chase, T.N., Eastman, J.L., Niles, J.O., Running, S.W., 2002. The influence of land-use change and landscape dynamics on the climate system: relevance to climate-change policy beyond the radiative effect of greenhouse gases. *Philosophical Transactions of the Royal Society of London. Series A: Mathematical, Physical and Engineering Sciences* **360**: 1705-1719.

Pielke, R.A., Pitman, A., Niyogi, D., Mahmood, R., McAlpine, C., Hossain, F., Klein Goldewijk, K., Nair, U., Betts, R., Fall, S., Reichstein, M., Kabat, P., de Noblet-Ducoudr´e, N., 2011. Land use/land cover changes and climate: modeling analysis and observational evidence. *WIREs Climate Change* **2**: 828–850.

Pongratz, J., Reick, C.H., Raddatz, T., Claussen, M., 2010. Biogeophysical versus biogeochemical climate response to historical anthropogenic land cover change. *Geophysical Research Letters* **37(8)**: L08702.

Ramankutty, N., Foley, J.A., 1999. Estimating historical changes in global land cover: croplands from 1700 to 1992. *Global Biogeochemical Cycles* **13**: 997–1027.

Ramankutty, N., Evan, A.T., Monfreda, C., Foley, J.A., 2008. Farming the planet: 1. Geographic distribution of global agricultural lands in the year 2000. *Global Biogeochemical Cycles* **22(1)**: GB1003.

Ray, D.K., Nair, U.S., Welch, R.M., Su, W., Kikuchi, T., 2002. *Influence of land use on the regional climate of Southwest Australia*. Paper presented at the 13th Symposium on Global Change and Climate Variations and 16th Conference on Hydrology, Orlando, FL, 13-17 January.

Ribera, P., Gallego, D., Gimeno, L., Pérez, J.F., García, R., Hernández, E., de la Torre, L., Nieto, R., Calvo, N., 2004. The use of equivalent temperature to analyze climate variability. *Studia Geophysica et Geodaetica* **48**: 459–468.

Rogers, J.C., Wang, S., Coleman, J.S.M., 2007. Evaluation of a long term (1882-2005) equivalent temperature time series. *Journal of Climate* **20**: 4476-4485.

Roy, S.S., Mahmood, R., Niyogi, D., Lei, M., Foster, S.A., Hubbard, K.G., Douglas, E., Pielke, R.A. Sr., 2007. Impacts of the agricultural Green Revolution–induced land use changes on air temperatures in India. *Journal of Geophysical Research: Atmospheres (1984–2012)* **112:** D21108**.**

Sampaio, G., Nobre, C.A., Costa, M.H., Satyamurty, P., Soares-Filho, B.S., Cardoso, M., 2007. Regional climate change over eastern Amazonia caused by pasture and soybean cropland expansion. *Geophysical Research Letters* **34**: L17709.

Santer, B.D., Mears, C., Wentz, F.J., Taylor, K.E., Gleckler, P.J., Wigley, T.M.L., Barnett, T.P., Boyle, J.S., Bruggermann, W., Gillett, N.P., Klein, S.A., Meehl, G.A., Nozawa, T., Pierce, D.W., Stott, P.A., Washington, W.M., Wehner, M.F., 2007. Identification of human-induced changes in atmospheric moisture content. *Proceedings of the National Academy of Sciences* **104**: 15248-15253.

Segal, M., Garratt, J.R., Kallos, G., Pielke, R.A. Sr., 1989. The impact of wet soil and canopy temperatures on daytime boundary-layer growth. *Journal of Atmospheric Science* **46**: 3673-3684.

USDM (United States Drought Monitor), 2012. *Drought Monitor Map Archive*. Lincoln, NE: USDM. Retrieved August 25, 2014, from http://droughtmonitor.unl.edu/MapsAndData/MapArchive.aspx

Weaver, C.P., Avissar, R., 2001. Atmospheric disturbances caused by human modification of the landscape. *Bulletin of the American Meteorological Society* **82**: 269–282.

Wentz, F.J., Ricciardulli, L., Hilburn, K., Mears, C., 2007. How much more rain will global warming bring? *Science* **317**: 233-235.

WPC (Weather Prediction Center), 2013. *Surface Analysis Archive*. College Park, MD: WPC. Retrieved October 11, 2014, from http://www.wpc.ncep.noaa.gov/archives/web_pages/sfc/sfc_archive_maps.php

Appendix

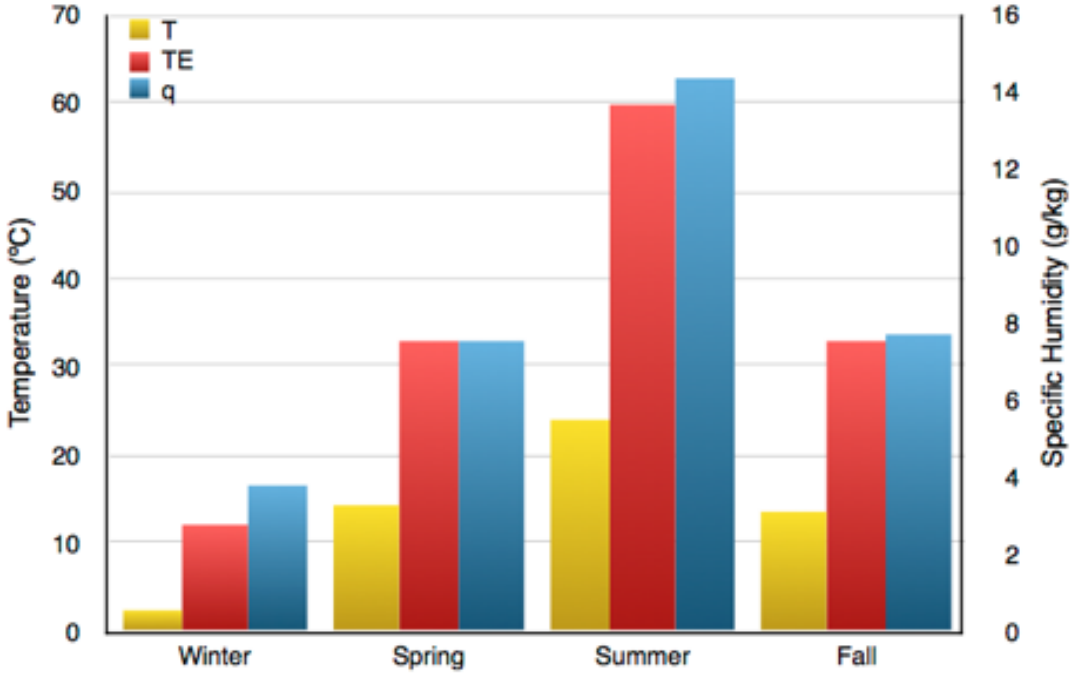

Figure A-1. Composite seasonal climatology of temperature (T), equivalent temperature (T_E) and specific humidity (q) for study sites in the Central Climate Division from December, 2009, to November, 2014.

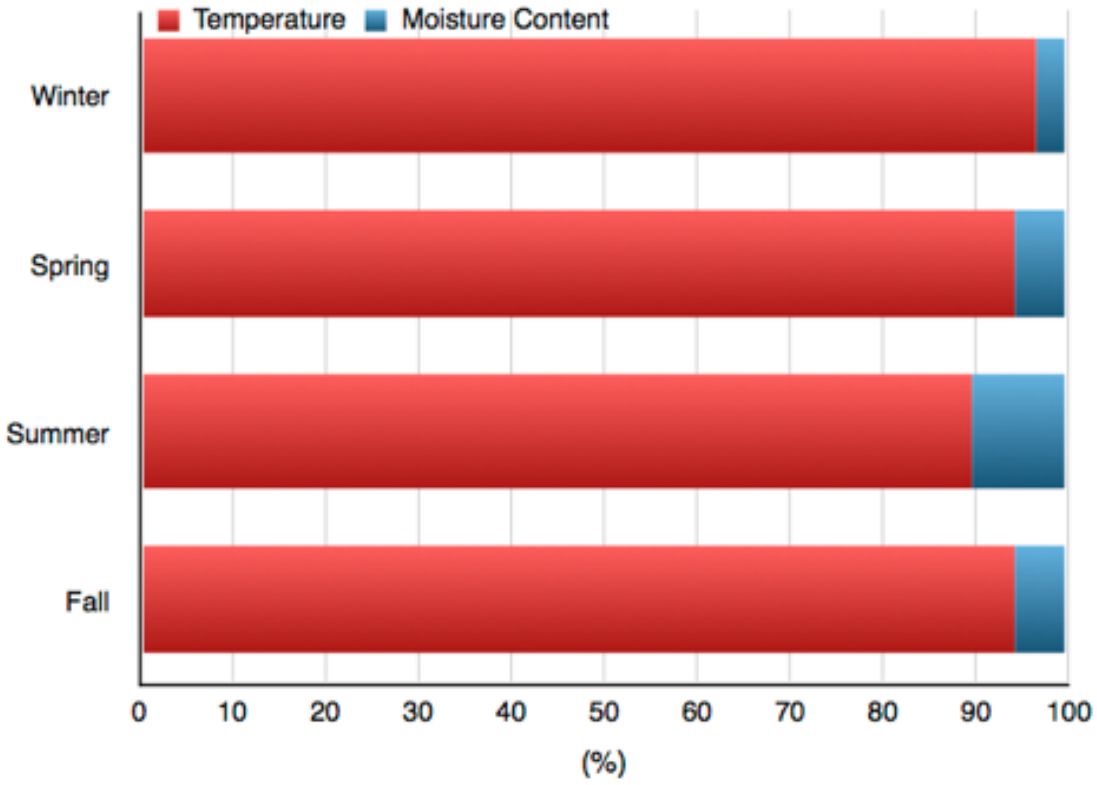

Figure A-2. Composite seasonal contribution of temperature and moisture to the magnitude of T_E for study sites in the Central Climate Division from December, 2009, to November, 2014.

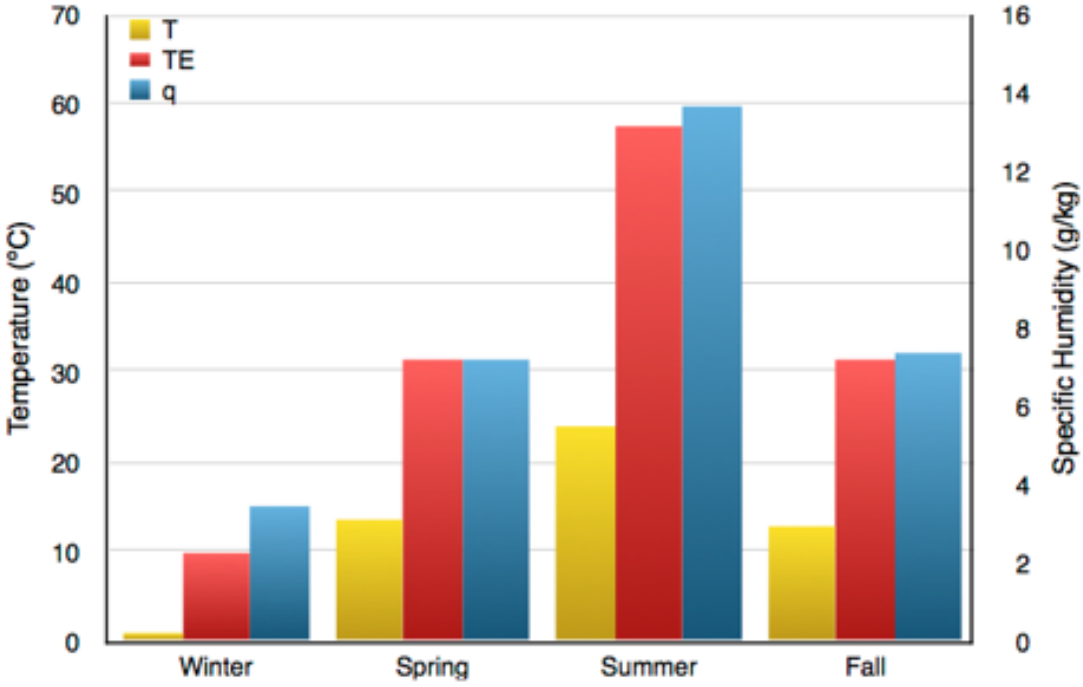

Figure A-3. Composite seasonal climatology of temperature (T), equivalent temperature (T_E) and specific humidity (q) for study sites in the Bluegrass Climate Division from December, 2009, to November, 2014.

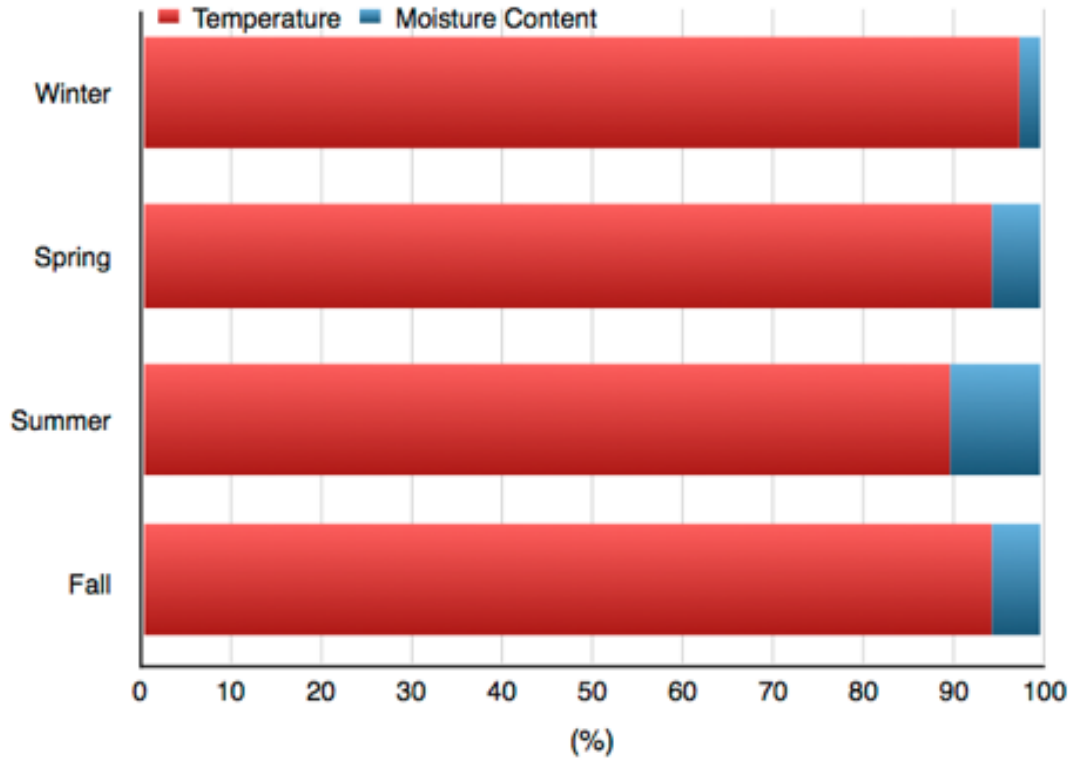

Figure A-4. Composite seasonal contribution of temperature and moisture to the magnitude of T_E for study sites in the Bluegrass Climate Division from December, 2009, to November, 2014.

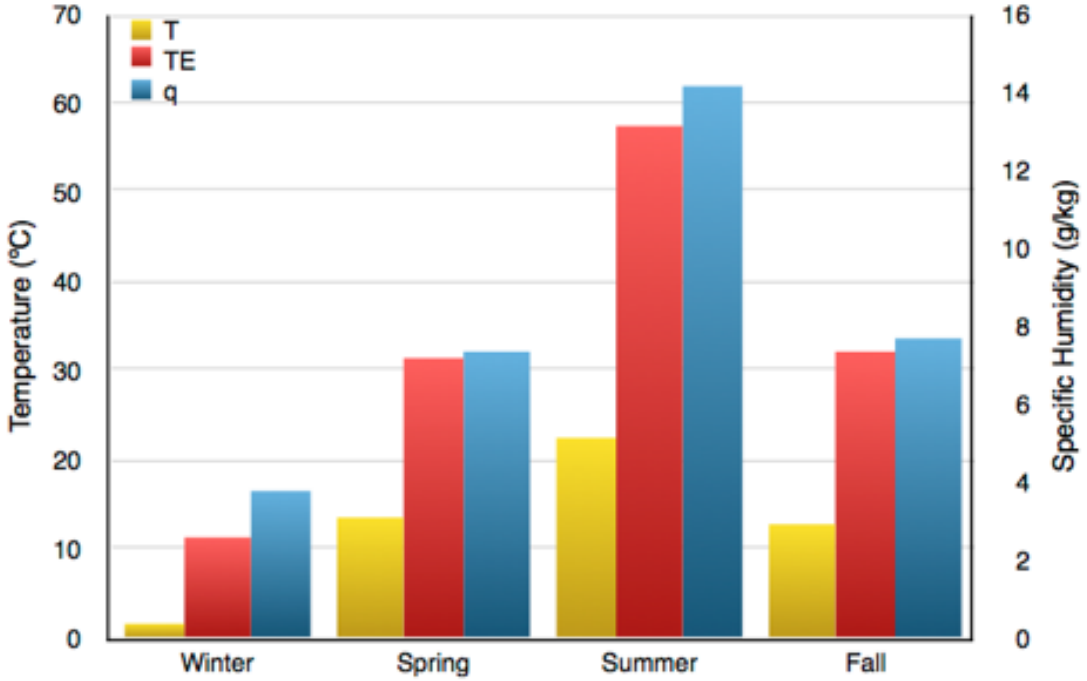

Figure A-5. Composite seasonal climatology of temperature (T), equivalent temperature (T_E) and specific humidity (q) for study sites in the Eastern Climate Division from December, 2009, to November, 2014.

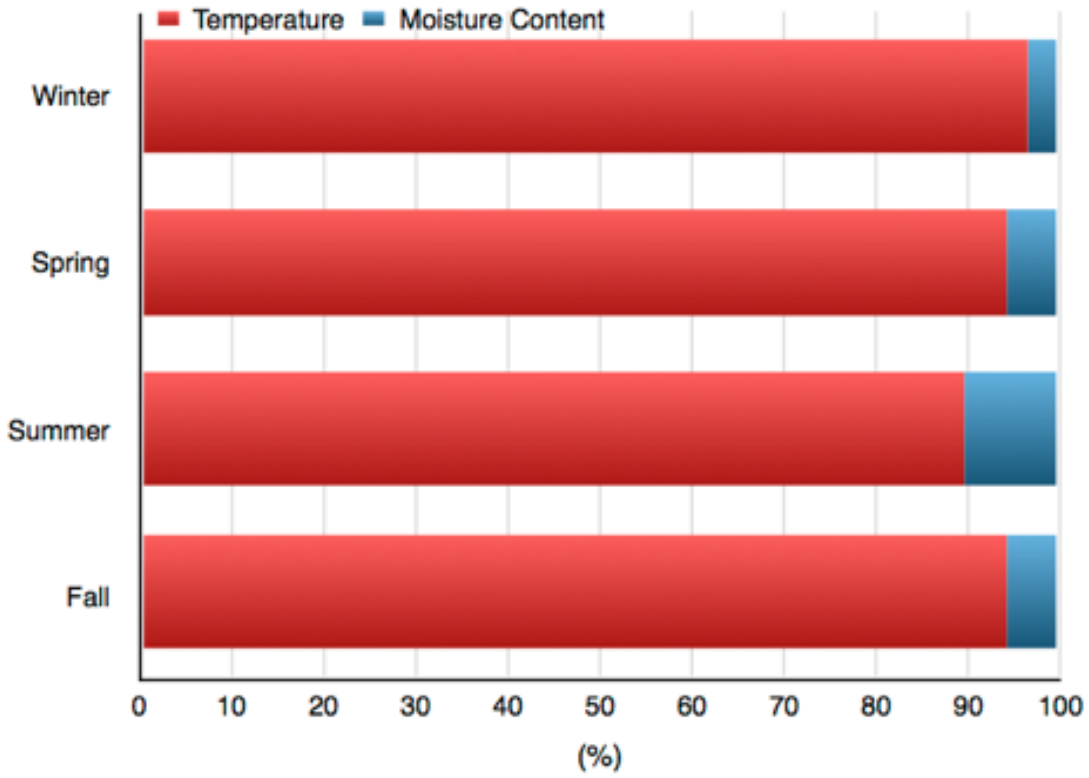

Figure A-6. Composite seasonal contribution of temperature and moisture to the magnitude of T_E for study sites in the Eastern Climate Division from December, 2009, to November, 2014.

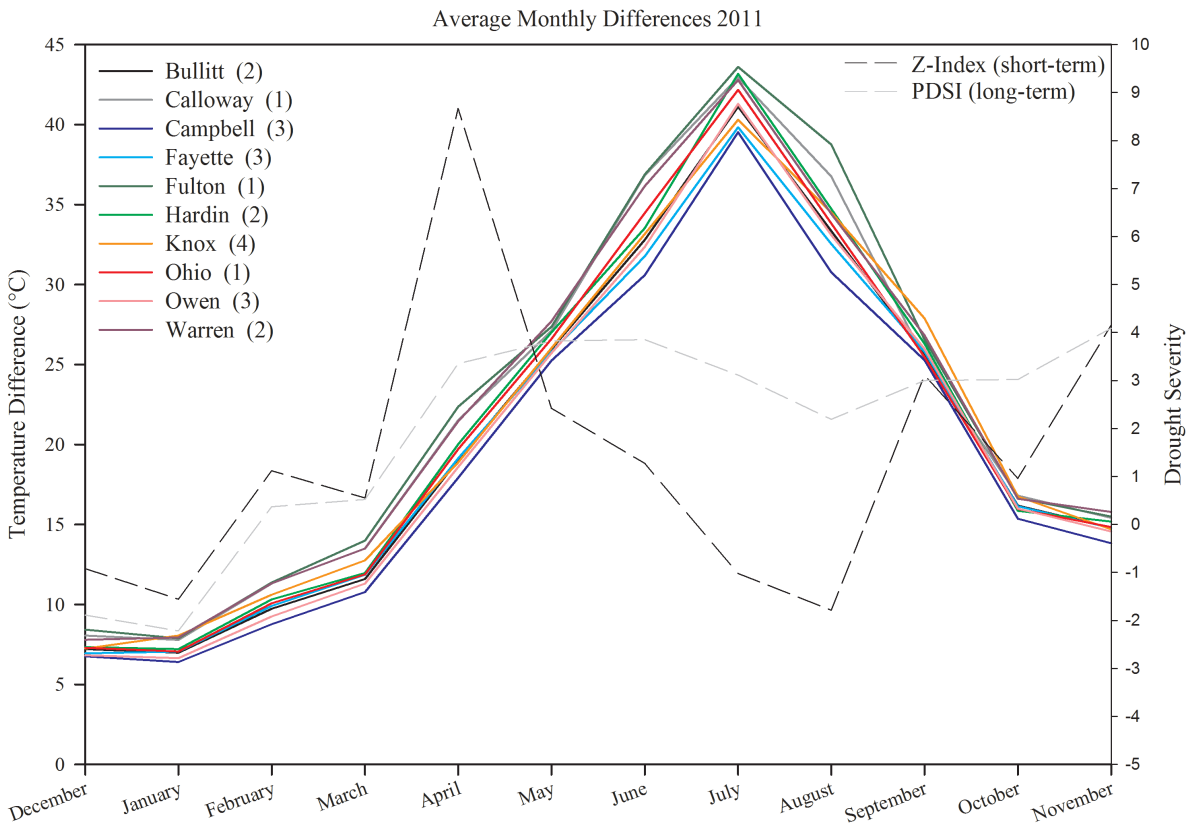

Figure A-7. Monthly average difference (T_E-T) for a selection of ten counties for 2011. Monthly PDSI and Z-Index values for long and short term drought in Kentucky also are shown.

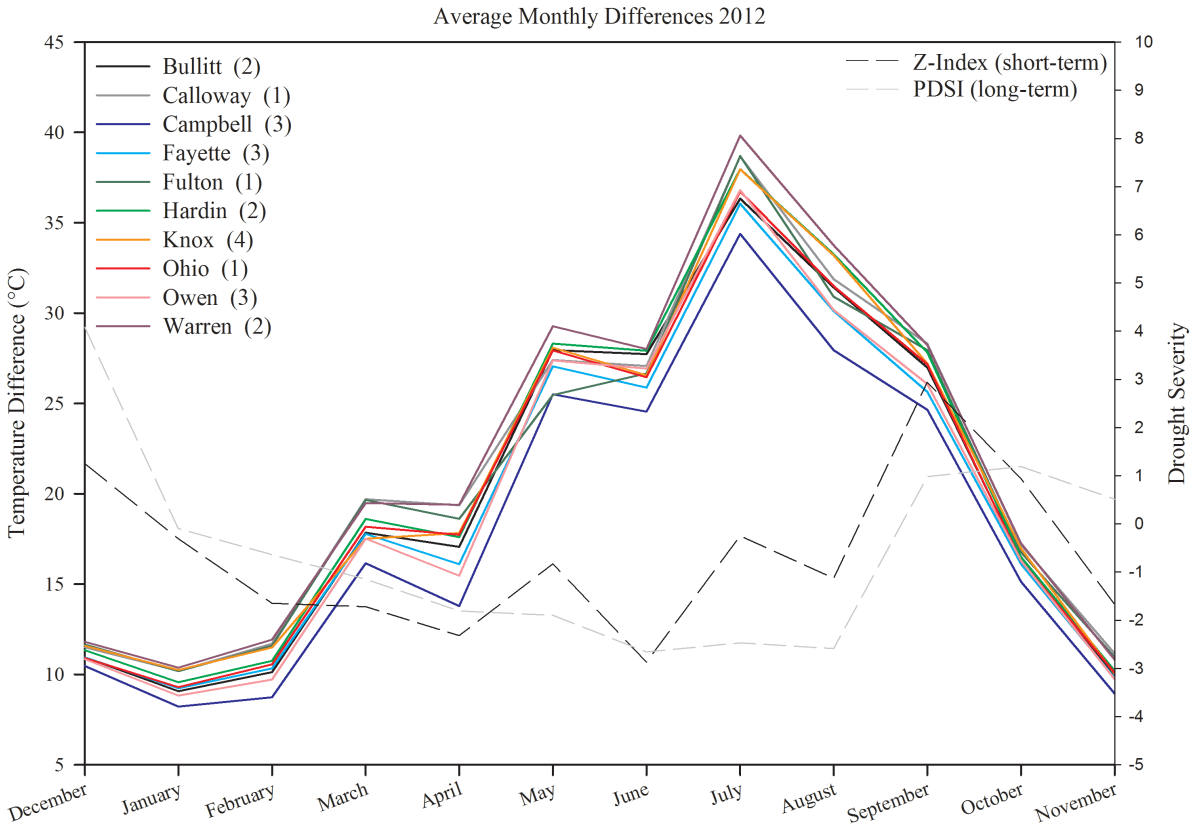

Figure A-8. Monthly average difference (T_E-T) for a selection of ten counties for 2012. Monthly PDSI and Z-Index values for long and short term drought in Kentucky also are shown.

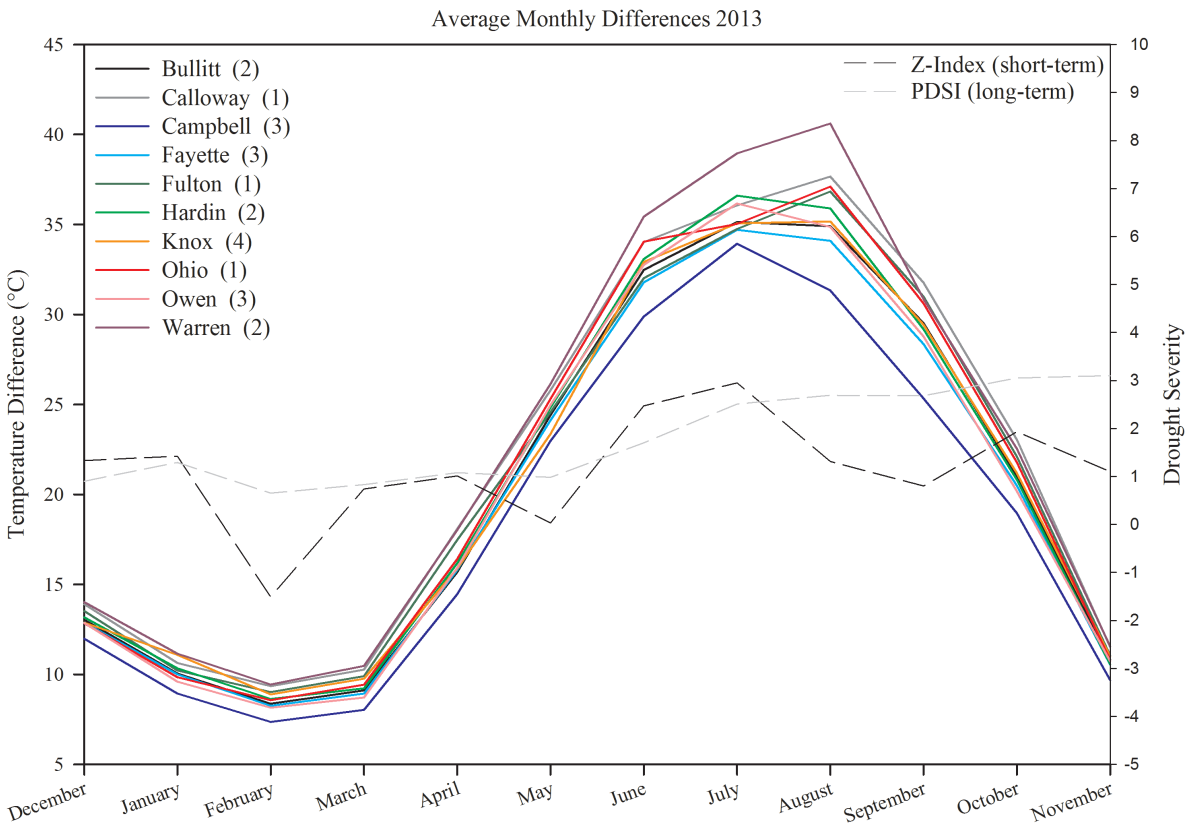

Figure A-9. Monthly average difference (T_E-T) for a selection of ten counties for 2013. Monthly PDSI and Z-Index values for long and short term drought in Kentucky also are shown.

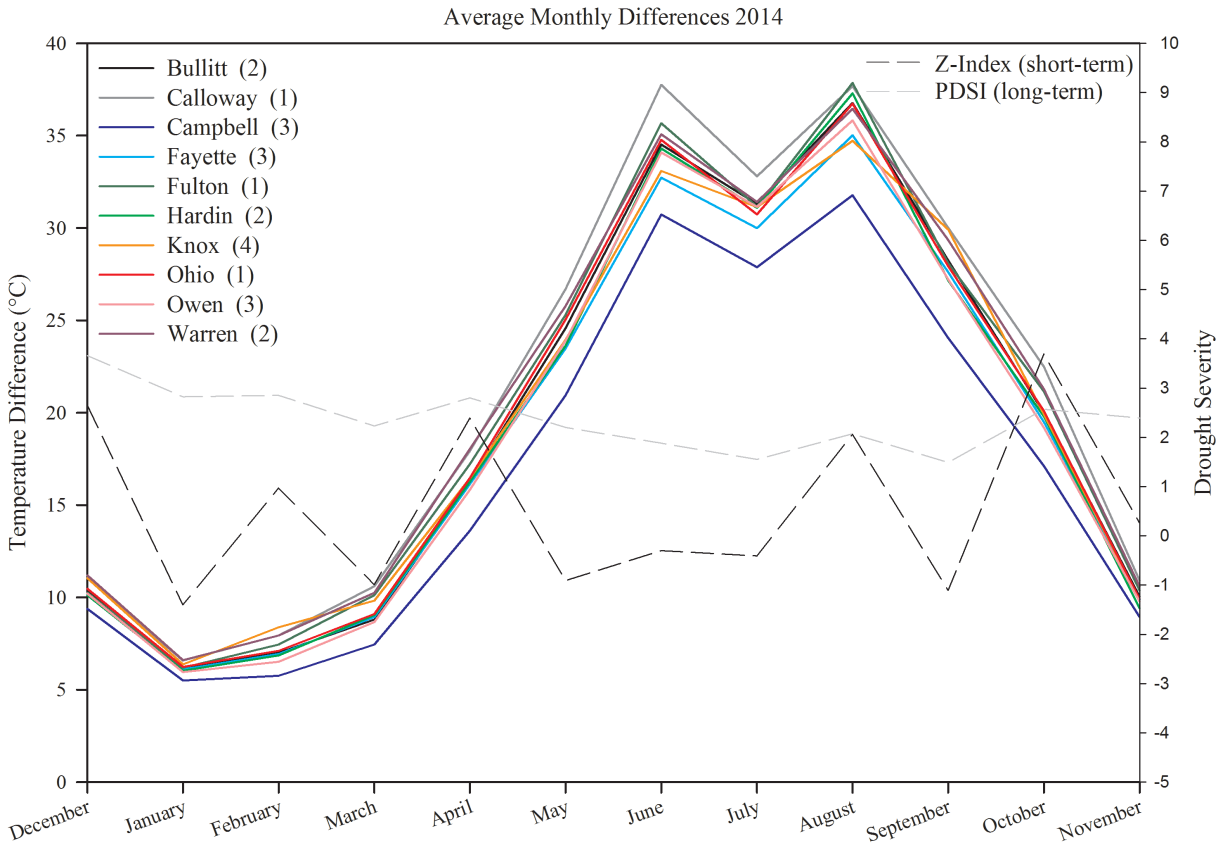

Figure A-10. Monthly average difference (T_E-T) for a selection of ten counties for 2014. Monthly PDSI and Z-Index values for long and short term drought in Kentucky also are shown.

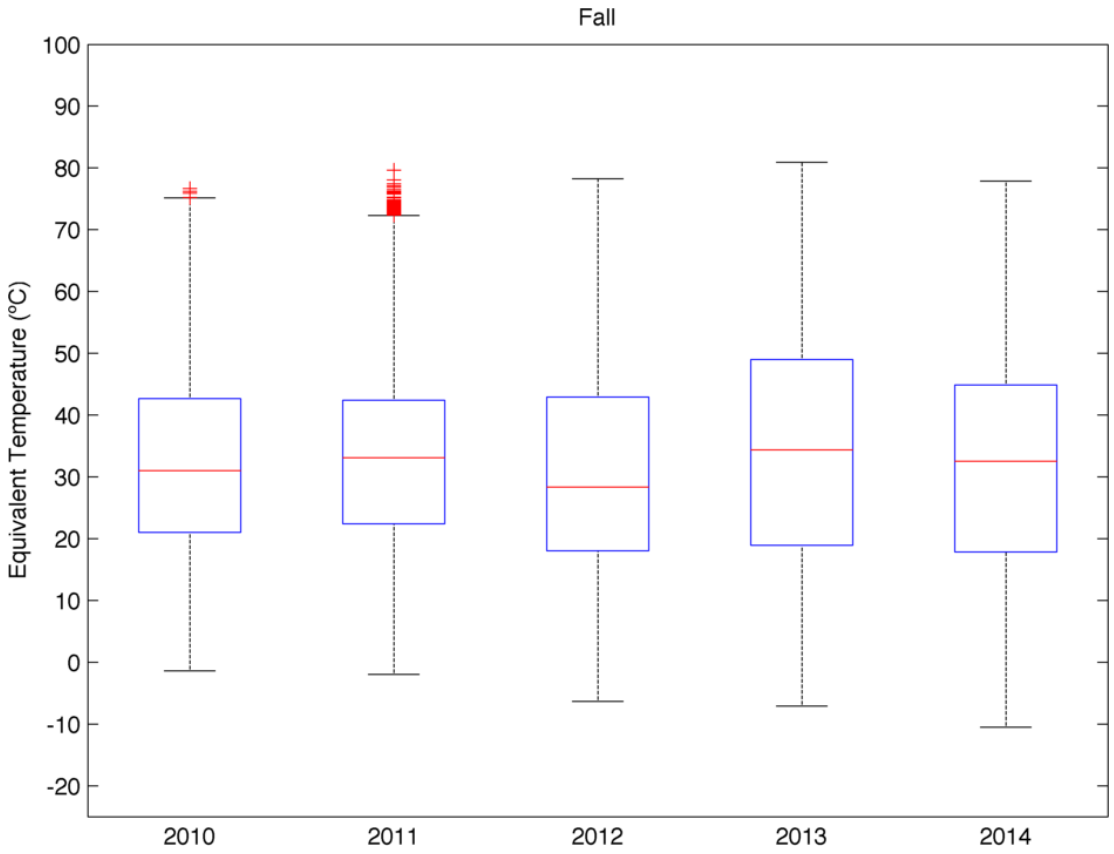

Figure A-11. Boxplots showing the distribution of T_E values during fall for each year. This includes all fall data from every study station in the area.

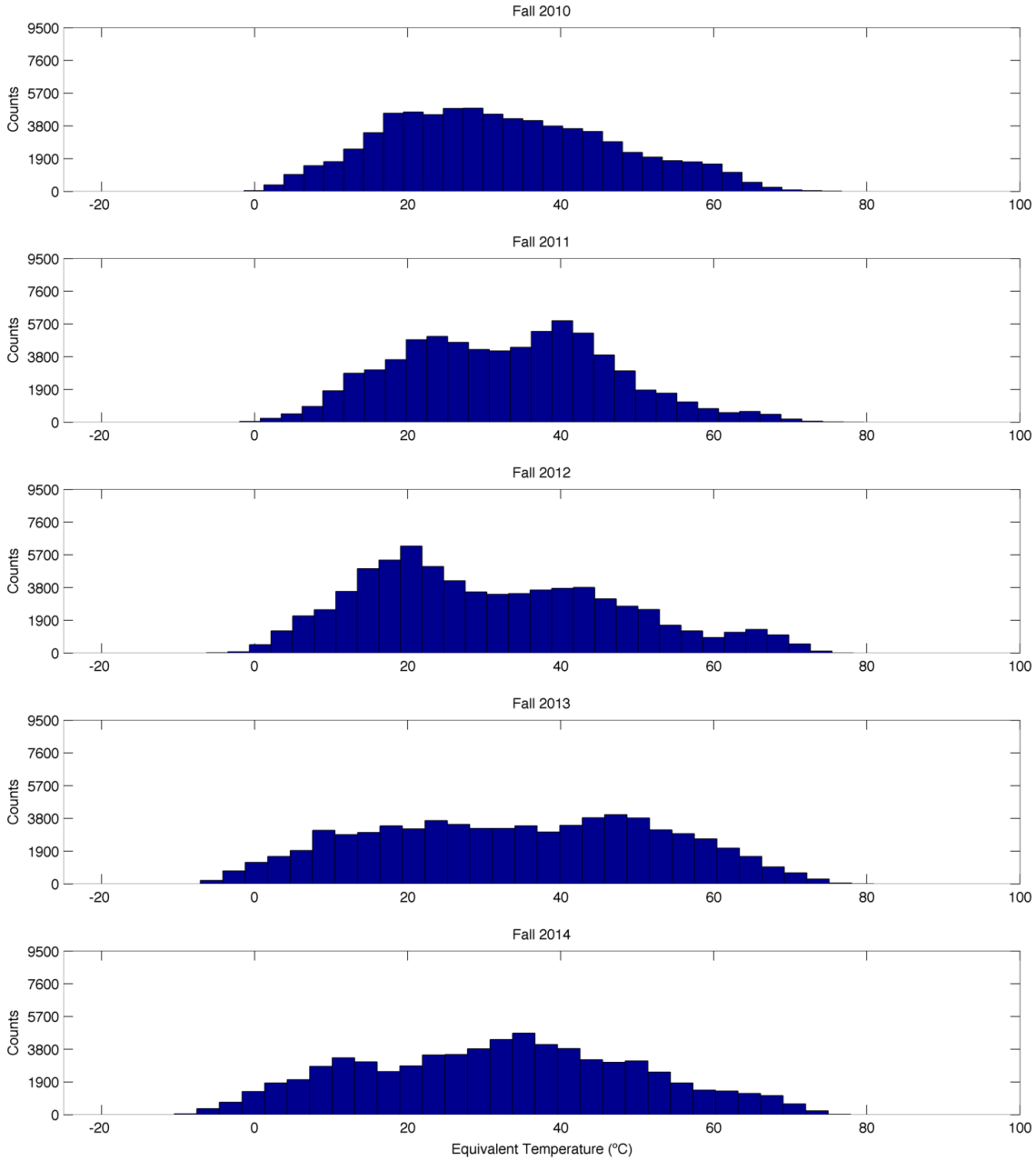

Figure A-12. Histograms (bins = 30) showing the distribution of T_E values during fall for each year. This includes all fall data from every study station in the area.

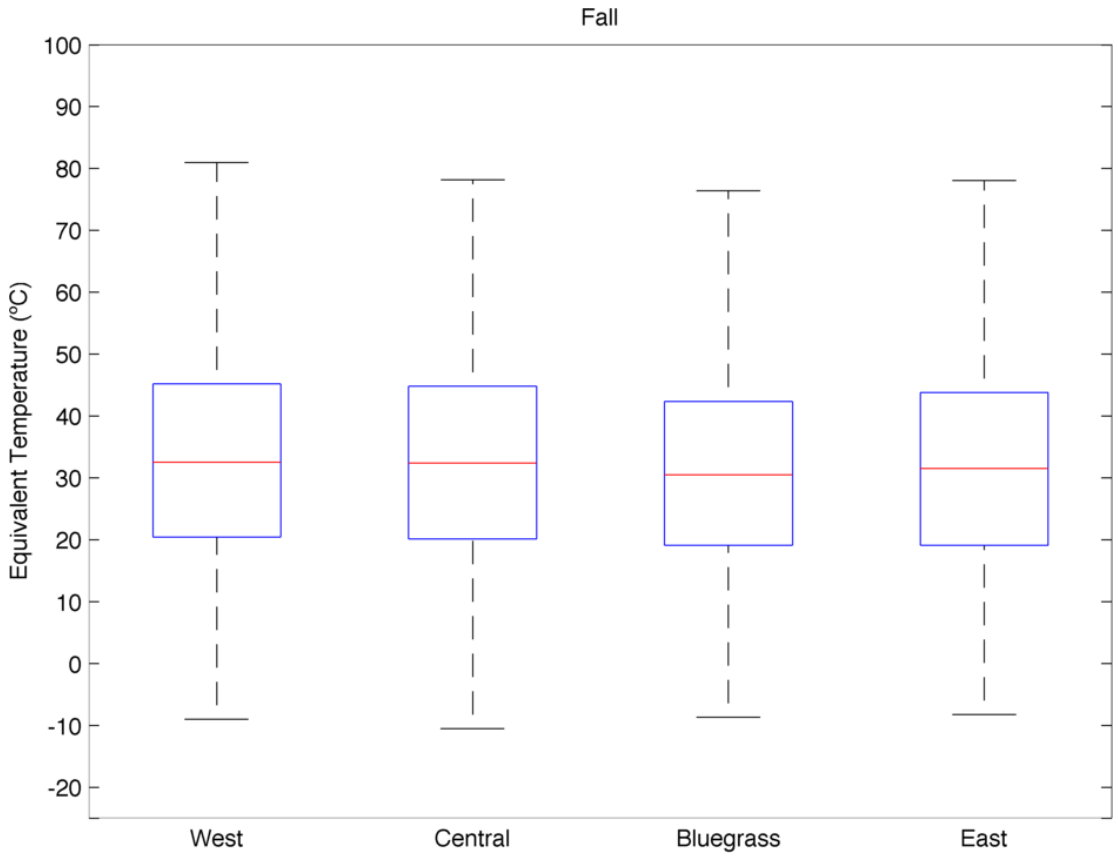

Figure A-13. Boxplots showing the distribution of T_E values during fall for each climate division. This includes all fall data from every study station in each climate division.

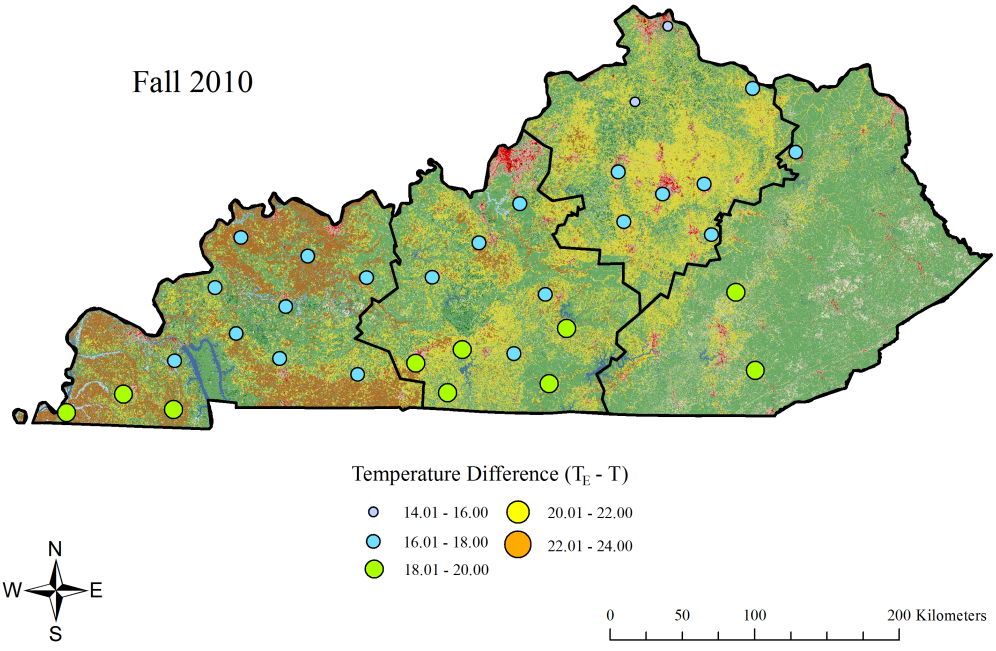

Figure A-14. Average temperature differences (T_E -T) for Fall, 2010.

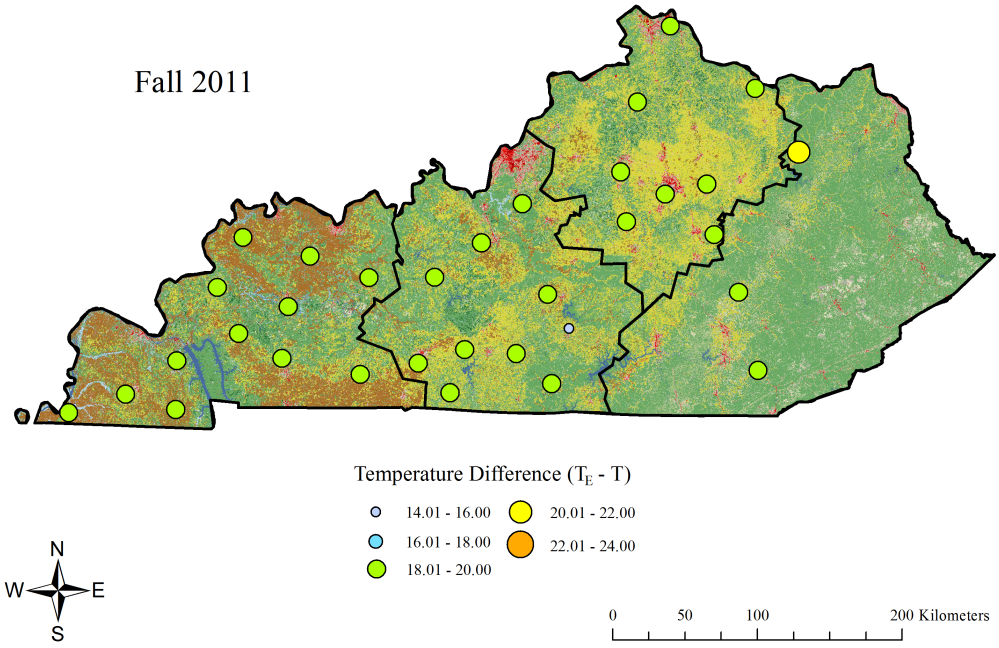

Figure A-15. Average temperature differences (T_E -T) for Fall, 2011.

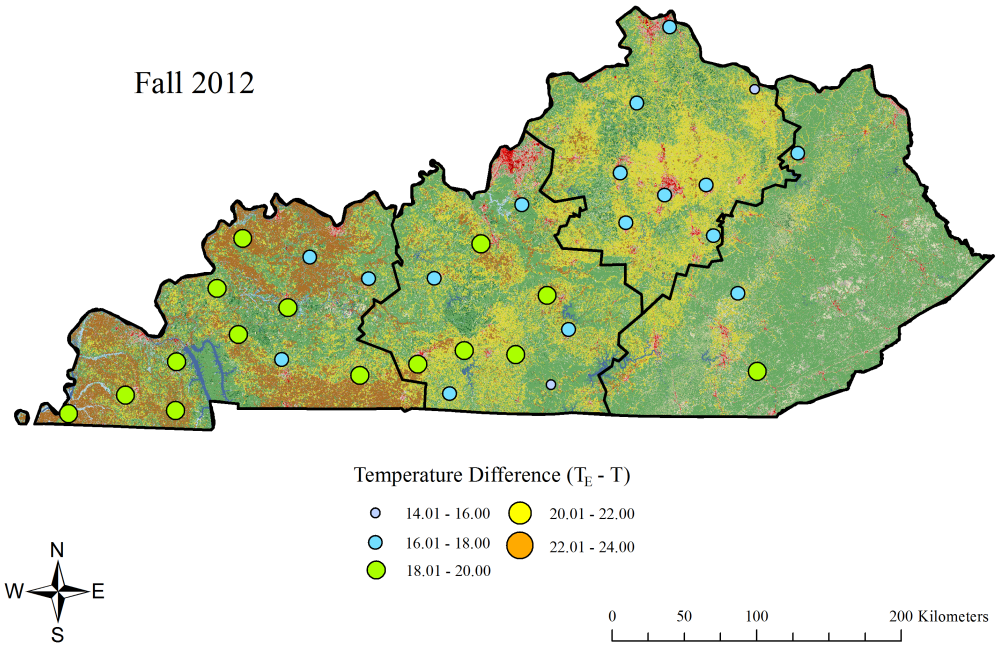

Figure A-16. Average temperature differences (T_E -T) for Fall, 2012.

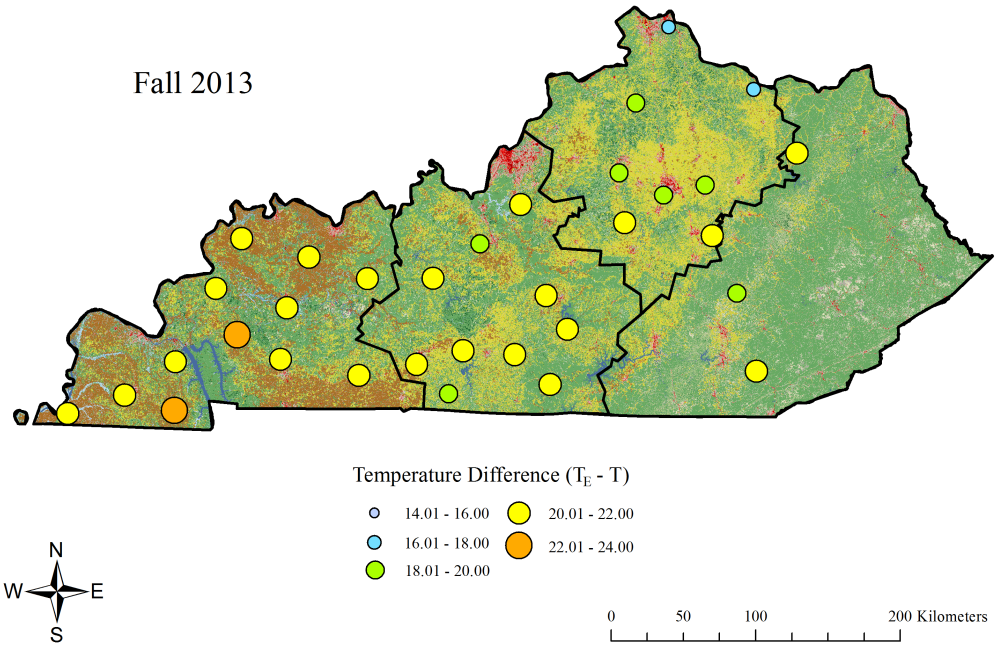

Figure A-17. Average temperature differences (T_E -T) for Fall, 2013.

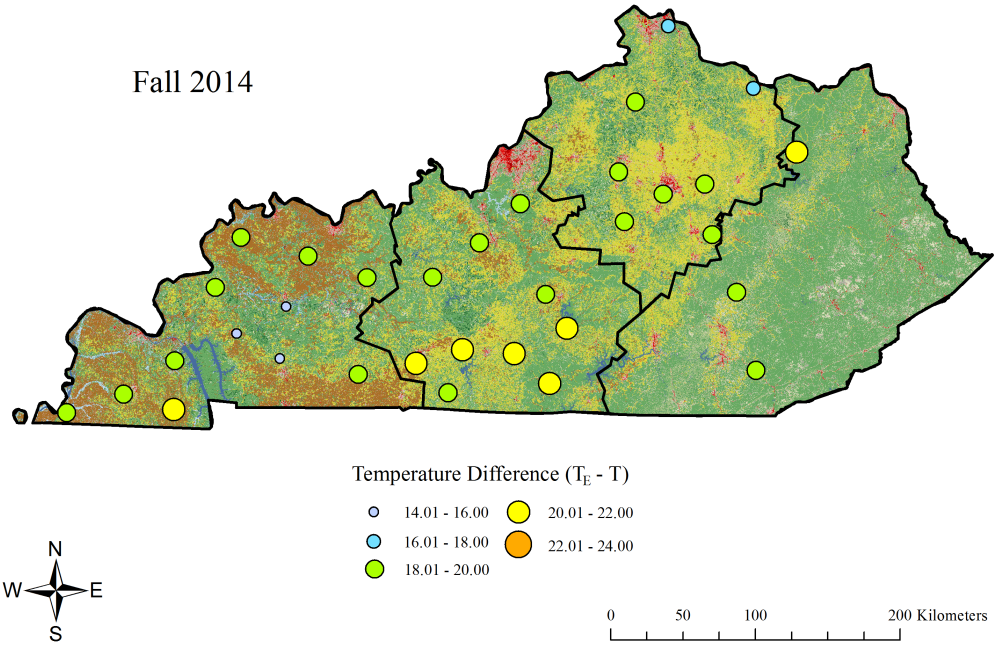

Figure A-18. Average temperature differences (T_E -T) for Fall, 2014.

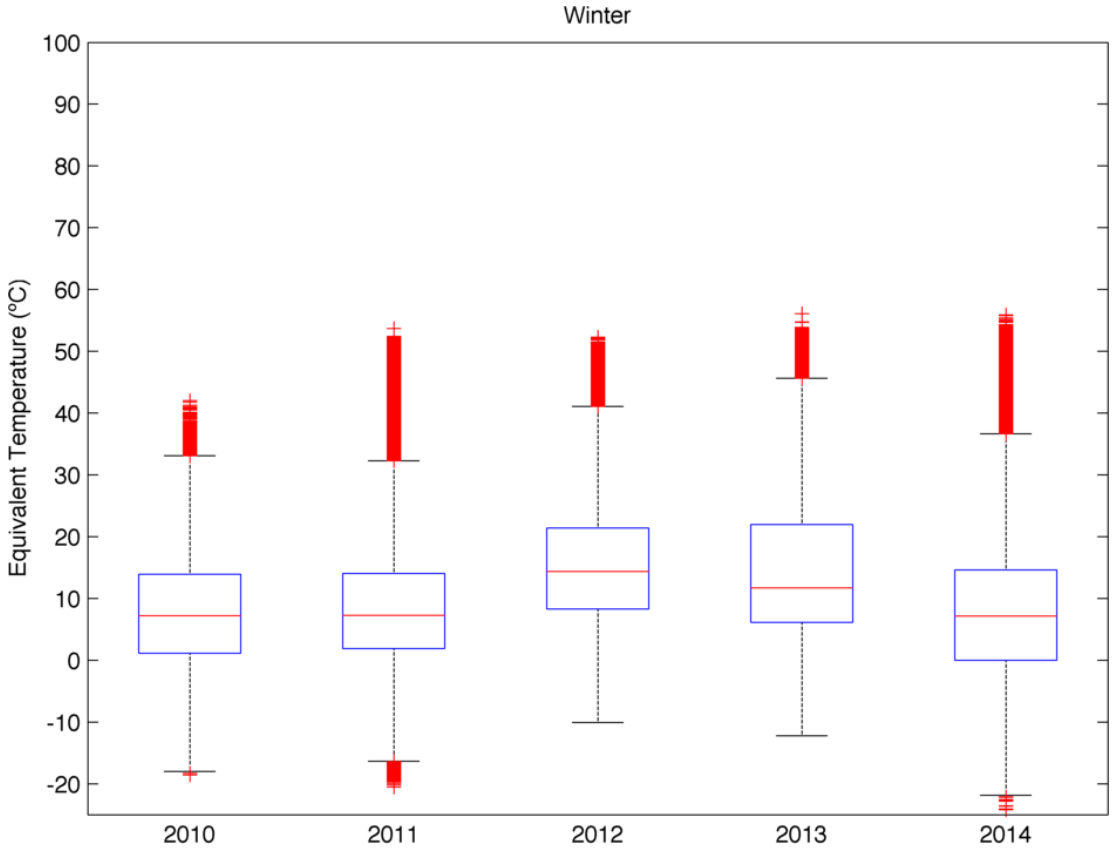

Figure A-19. Boxplots showing the distribution of T_E values during winter for each year. This includes all winter data from every study station in the area.

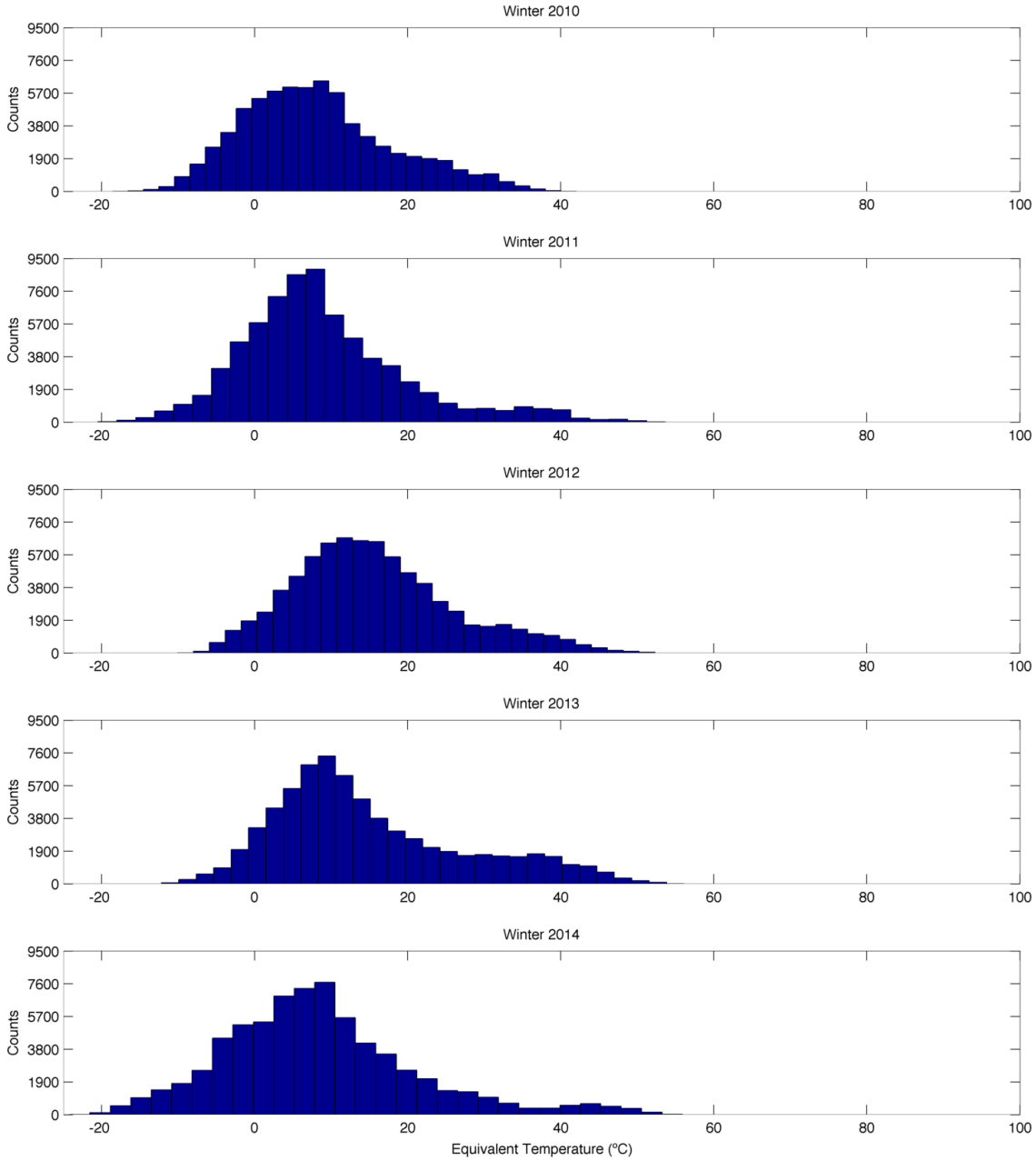

Figure A-20. Histograms (bins = 30) showing the distribution of T_E values during winter for each year. This includes all winter data from every study station in the area.

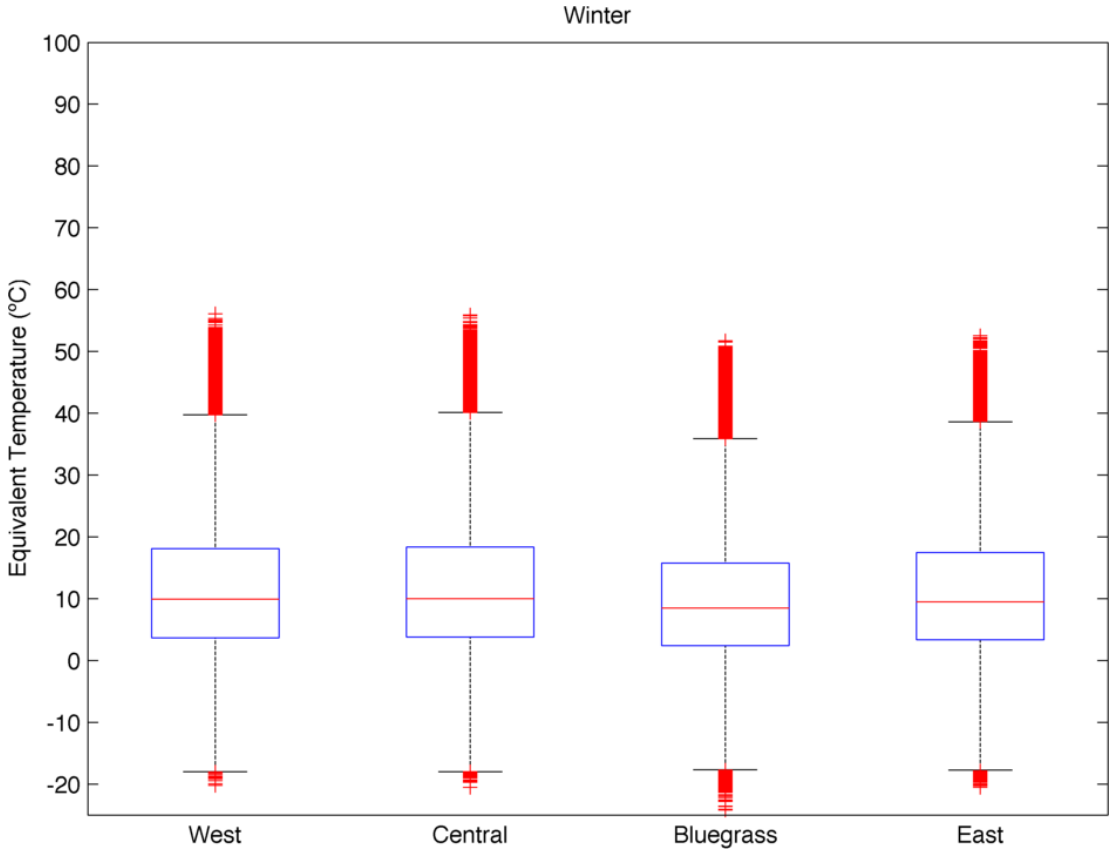

Figure A-21. Boxplots showing the distribution of T_E values during winter for each climate division. This includes all winter data from every study station in each climate division.

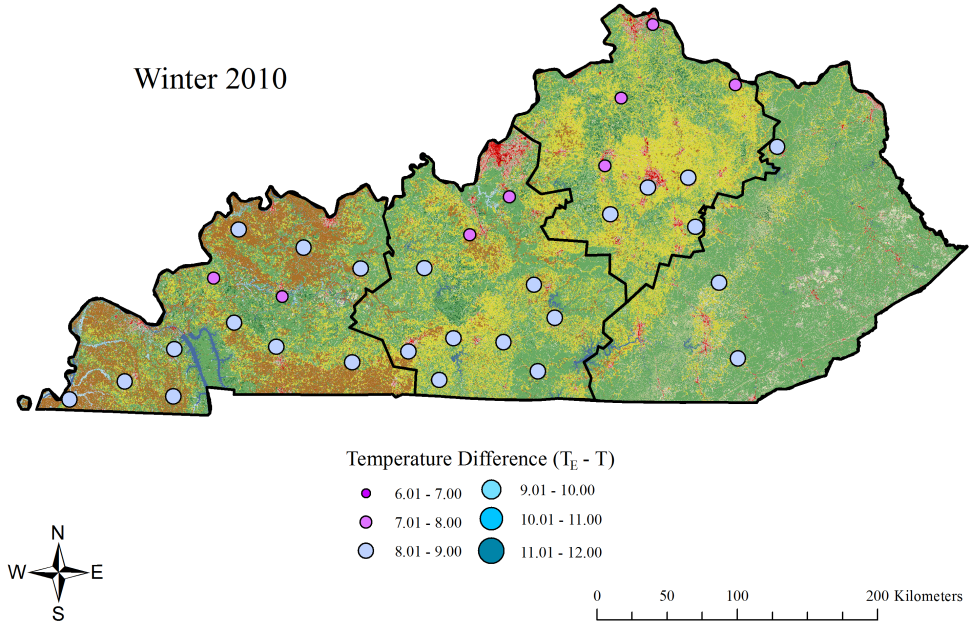

Figure A-22. Average temperature differences (T_E -T) for Winter, 2010.

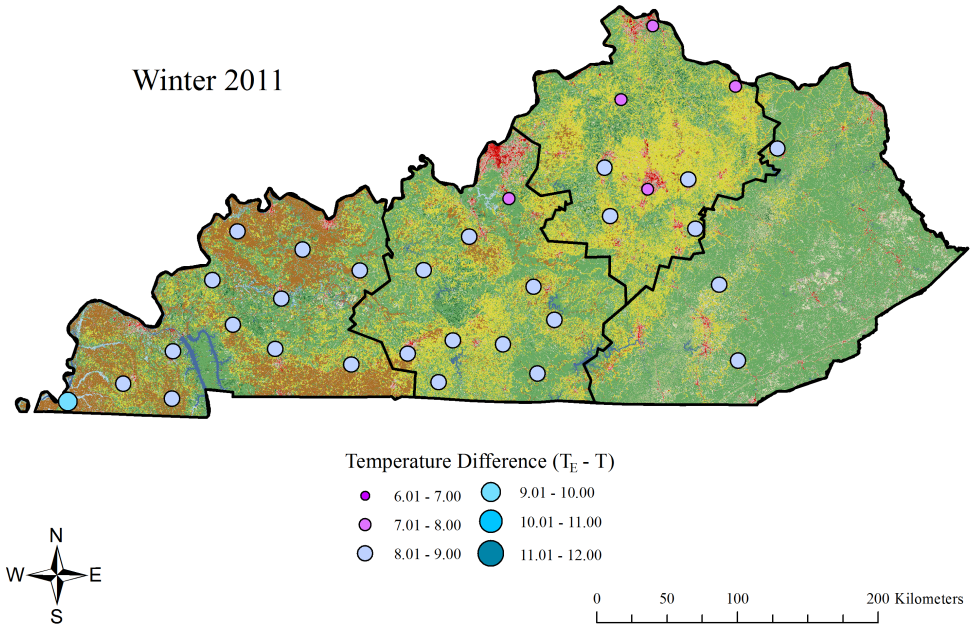

Figure A-23. Average temperature differences (T_E -T) for Winter, 2011.

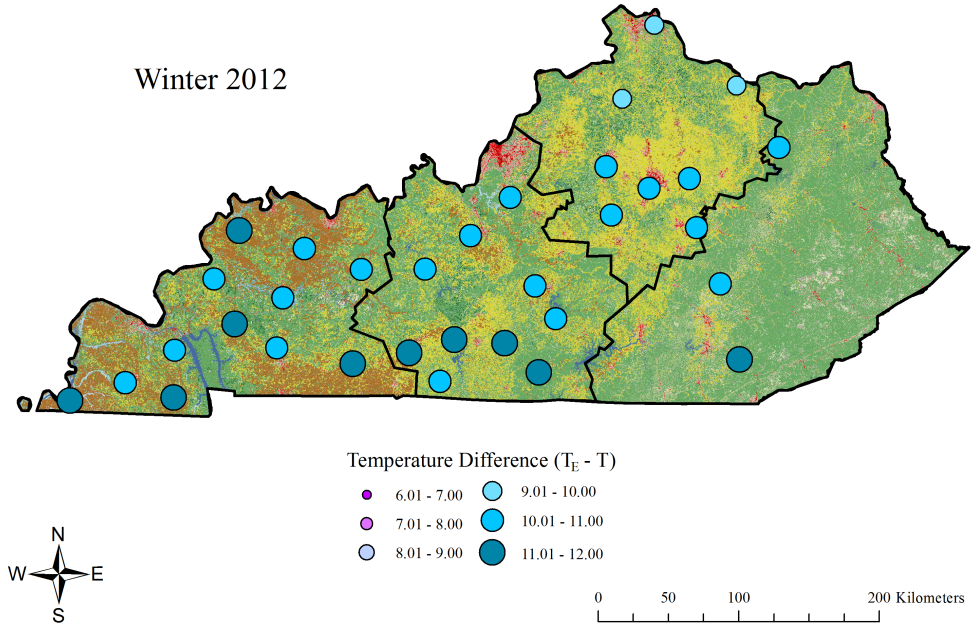

Figure A-24. Average temperature differences (T_E -T) for Winter, 2012.

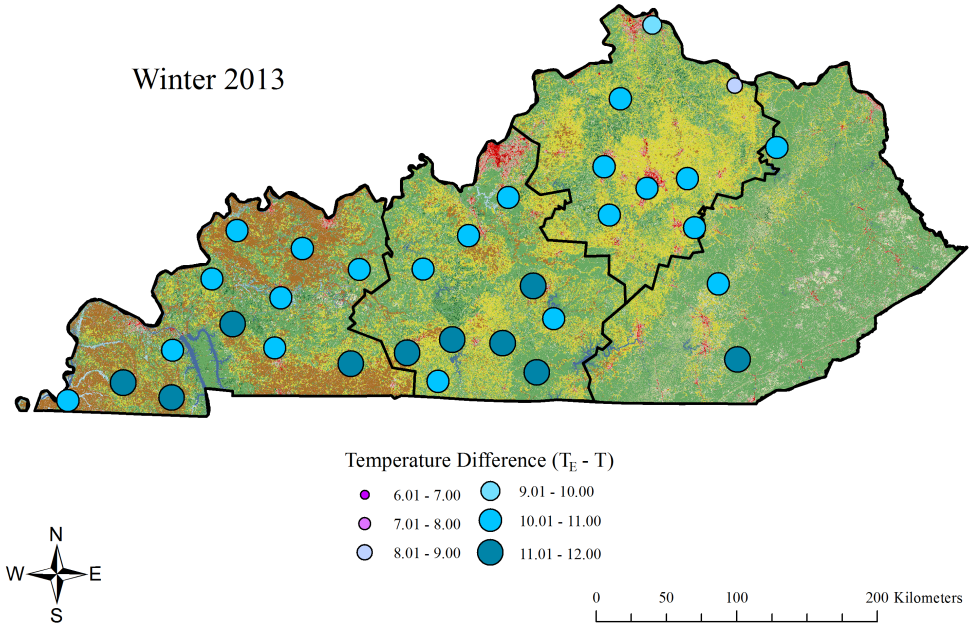

Figure A-25. Average temperature differences (T_E -T) for Winter, 2013.

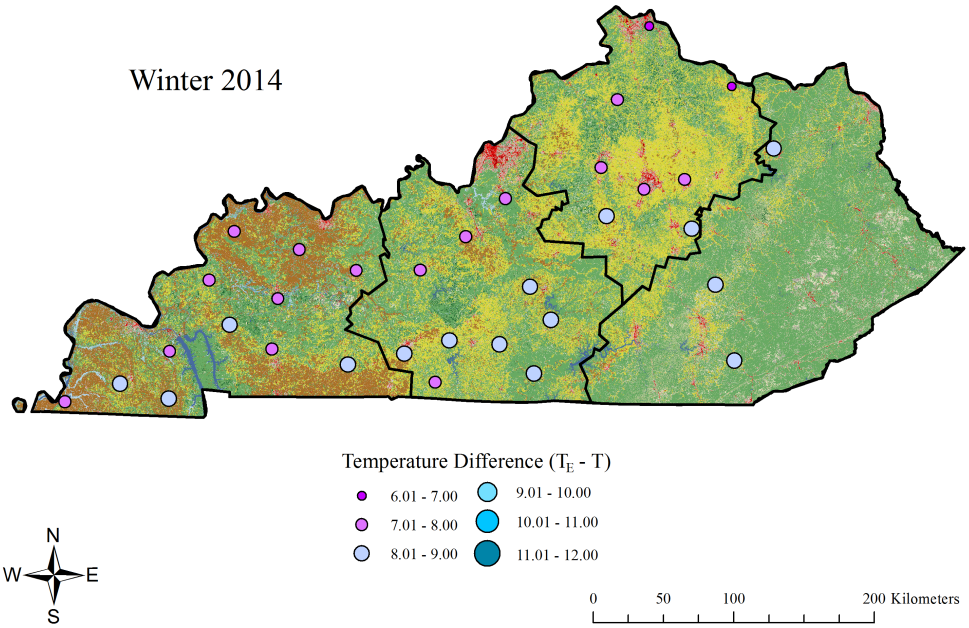

Figure A-26. Average temperature differences (T_E -T) for Winter, 2014.